UNIVERSITI TEKNOLOGI MARA

EFFECT OF RAINWATER INFILTRATION ON A SOIL'S EROSION AT PERMATANG RAWA RIVERBANK

MUHAMMAD FAHMI BIN MUHAMMAD ISKANDAR

MSc

August 2026

UNIVERSITI TEKNOLOGI MARA

EFFECT OF RAINWATER INFILTRATION ON A SOIL'S EROSION AT PERMATANG RAWA RIVERBANK

MUHAMMAD FAHMI BIN MUHAMMAD ISKANDAR

Thesis submitted in fulfilment
of the requirement for the degree of
Master of Science
(Civil Engineering)

Faculty of Civil Engineering

August 2026

CONFIRMATION BY PANEL OF EXAMINERS

I certify that a Panel of Examiners as met on 3rd March 2026 to conduct the final examination on Muhammad Fahmi Bin Muhammad Iskandar of his Master of Science thesis entitled "Effect of Rainwater Infiltration on a Soil's Erosion at Permatang Rawa Riverbank" in accordance with Universiti Teknologi MARA Act 1976 (Akta 1976). The Panel of Examiners recommends that the student awarded the relevant degree. The Panel of Examiners was as follows:

Yee Hooi Min,PhD
Professor
Faculty of Civil Engineering
Universiti Teknologi MARA
(Chairman)

Juhaizad Ahmad,PhD
Senior Lecturer
Faculty of Civil Engineering
Universiti Teknologi MARA
(Internal Examiner)

Mohamad Anuar Kamaruddin,PhD
Associate Professor
Faculty of Civil Engineering
Universiti Sains Malaysia
(External Examiner)

PROF DR HJH ZURAEDA BINTI IBRAHIM
Dean
Institute of Postgraduates Studies
Universiti Teknologi Mara
Date: 14 August 2026

AUTHOR'S DECLARATION

I declare that the work in this thesis was carried out in accordance with the regulations of University Technology MARA. It is original and is the results of my own work, unless otherwise indicated or acknowledged as referenced work. This thesis has not been submitted to any other academic institution or non-academic institution for any degree or qualification.

I, hereby, acknowledge that I have been supplied with the Academic Rules and Regulations for Postgraduate, University Technology MARA, regulating the conduct of my study and research.

Name of Student	:	Muhammad Fahmi Bin Muhammad Iskandar
Student ID No.	:	2024520339
Programme	:	CEEC750
Faculty	:	Civil Engineering
Thesis Title	:	Effect of Rainwater Infiltration on a Soil's Erosion at Permatang Rawa Riverbank

Signature of Student	:	.....
Date	:	August 2026

ABSTRACT

Rainfall-induced hazards such as floods and landslides remain major concerns worldwide and in Malaysia, where seasonal monsoons regularly trigger flooding and cause significant economic losses. The country's tropical climate, with its high rainfall and humidity, further accelerates soil erosion and increases vulnerability, particularly in Pulau Pinang. This study examines the relationship between soil erodibility and seasonal rainfall patterns along the Permatang Rawa riverbank in Bukit Mertajam. Rainfall trends were analyzed using the Mann-Kendall test and Sen's slope estimator, while soil erodibility was assessed with the ROM-scale. The results was also evaluated as a rapid alternative to conventional soil testing. ROM-scale results show that several sections of the riverbank exhibit high erodibility, making them especially prone to rainfall-driven erosion. Rainfall analysis revealed a significant decreasing trend ($p < 0.05$) during Inter-Monsoon 1 (September–October) and a slight, though insignificant, increase ($p > 0.05$) during Inter-Monsoon 2 (March–April). Although the Northeast Monsoon (NEM) showed no significant decline in total rainfall, the frequency of erosive rainfall events during this season continues to present a critical risk. The JKR Probe, however, demonstrated only a weak correlation with the ROM-scale ($R^2 = 0.155$), limiting its immediate applicability for erosion risk assessment. In conclusion, the Permatang Rawa riverbank remains highly vulnerable to erosion due to both soil characteristics and seasonal rainfall. While the JKR Probe shows potential as a rapid field tool, further calibration for local soils is needed. Future work should expand erodibility assessments to a wider stretch of the riverbank and incorporate longer rainfall datasets to improve trend accuracy and strengthen risk evaluation.

Keywords: Rainfall, ROM-Scale, erosion, flood, landslide, Mann Kendall test, Sen's Slope estimator Permatang Rawa River, Pulau Pinang.

ACKNOWLEDGEMENT

I would like to express my deepest gratitude to the Most Gracious and Merciful Allah SWT for His guidance and blessings throughout the course of this research journey. I extend my sincere appreciation to my supervisor, Dr. Anas Bin Ibrahim, for his invaluable guidance, continuous support, and for ensuring that the thesis development process was conducted successfully, smoothly, and in a well-organized manner. I am also grateful to my co-supervisors, Dr. Zul Azmi Bin Mohtar and Dr. Muhammad Faizal Bin Pakir Mohamed Latiff, for their insightful consultations in expanding my methodology and for providing a deeper understanding of statistical analysis.

My heartfelt appreciation goes to my parents, Muhammad Iskandar and [illegible] as well as my wife, Nur Farah Izaty, for their unwavering love, support, and encouragement throughout this endeavor.

Additionally, I would like to thank Sir Azrul and Sir Salahudin for their assistance and support during laboratory work, and my friends Yusof and Aslam for their unwavering support and for sharing valuable information during the process of writing this thesis.

TABLE OF CONTENTS

		Page
CONFIRMATION BY PANEL OF EXAMINERS		**ii**
AUTHOR'S DECLARATION		**iii**
ABSTRACT		**iv**
ACKNOWLEDGEMENT		**v**
TABLE OF CONTENTS		**vi**
LIST OF FIGURES		**ix**
LIST OF TABLES		**xii**
CHAPTER 1: INTRODUCTION		**1**
1.1	Research Background	1
1.2	Problem Statement	2
1.3	Research Objectives	4
1.4	Significant of Study	4
1.5	Scope of Study	5
1.6	Thesis Outline	6
CHAPTER 2: LITERATURE REVIEW		**8**
2.1	Introduction	8
2.2	Soil Stability Testing	9
	2.2.1 Standard Penetration Test	10
	2.2.2 JKR Probe Test	11
	2.2.3 Soil Stability Index	13
2.3	Rainfall Trend in Malaysia	17
	2.3.1 Northeast Monsoon (NEM)	19
	2.3.2 Southwest Monsoon (SWM)	22
	2.3.3 Intermonsoon (IM)	27
2.4	Rainfall Trend in Northern Region	31

2.5 Rainfall Prone Disaster 32
2.5.1 Flood 33
2.5.2 Slope Failure 34
2.6 Rainfall Trend Analysis 35
2.6.1 Mann Kendall Test 35
2.6.2 Sen's Slope Estimator 36
2.7 Rainfall Induced Erosion 37
2.8 Conclusion 41

CHAPTER 3: METHODOLOGY 43
3.1 Introduction 43
3.2 Soil Characterization 45
3.2.1 Soil Sampling 45
3.2.2 Physical Properties 48
3.2.2.1 Sample Preparation (BS 1377: Part 1:1990) 48
3.2.2.2 Moisture Content Test (BS 1377: Part 2: 1990) 49
3.2.2.3 Particle Density Method (BS 1377: Part 2: 1990) 50
3.2.2.4 Liquid Limit (BS 1377: Part 2: 1990) 51
3.2.2.5 Plastic Limit (BS 1377: Part 2: 1990) 51
3.2.2.6 Particle Size Distribution (Sieve Analysis) and Hydrometer Test (BS 1377: Part 2: 1990) 52
3.2.3 Engineering Properties 53
3.2.3.1 JKR Probe 53
3.2.3.2 Standard Penetration Test (SPT) 55
3.3 Seasonal Trend 55
3.3.1 The Descriptive Statistics Analysis 55
3.3.1.1 Minimum and Maximum 56
3.3.1.2 Median 56
3.3.1.3 Mean 57
3.3.1.4 Mode 57
3.3.1.5 Skewness 57
3.3.1.6 Kurtosis 58
3.3.1.7 Variance 59

3.3.1.8 Standard Variation 59
3.3.2 Data Treatment 60
3.3.2.1 Identify Outlier 61
3.3.2.2 Replace Missing Value 63
3.3.2.3 Performance Indicator 65
3.3.3 Time Series Plot 66
3.3.4 Trend Analysis 66
3.3.4.1 Mann Kendall Test (MK) 67
3.3.4.2 Sen's Slope Estimator (SSE) 68
3.4 Soil Erodibility Index 69
3.4.1 Correlation 70

CHAPTER 4: RESULT AND DISCUSSION 71
4.1 Introduction 71
4.2 Soil Characterization 71
4.2.1 Physical Properties 71
4.2.2 Engineering Properties 75
4.3 Rainfall Trend 79
4.3.1 Descriptive Statistic 79
4.3.2 Data Treatment 83
4.3.3 Time Series Plot 89
4.3.4 Trend Analysis 92
4.4 Correlation 94
4.4.1 Soil Erodibility Index 94
4.4.2 ROM Scale and JKR Probe 98
4.4.3 ROM Scale and Rainfall 103

CHAPTER 5: CONCLUSION AND RECOMMENDATIONS 106
5.1 Conclusion 106
5.2 Recommendations and Limitations 107
REFERENCES 109
APPENDICES 120
AUTHOR'S PROFILE 128

LIST OF FIGURES

Figure	Title	Page
Figure 2.1	Standard Penetration Test (SPT)	10
Figure 2.2	Correlation between ROM-Scale and M-values based on SI and Laboratory Testing results.	12
Figure 2.3	Type of Erosion: a) Sheet Erosion, b) Rill Erosion, c) Gully Erosion	15
Figure 2.4	Map of Peninsular Malaysia	18
Figure 2.5	Northeast Monsoon	19
Figure 2.6	Box and Whisker Plot of Monthly Areal Mean Rainfall (1975-2006) in Peninsular Malaysia.	20
Figure 2.7	Plot for Precipitation in December for Alor Setar.	21
Figure 2.8	Average Monthly in October for (1988-1992, 1993-1997, 1998-2002, 2003-2007, 2008-2012, 2013-2017)	22
Figure 2.9	Southwest Monsoon	23
Figure 2.10	Graph for Station Stor JPS Johor Bahru, Johor	23
Figure 2.11	Spatial Distribution of TAR Index Averages (in mm/year) during SWM	25
Figure 2.12	Average Monthly Rainfall in May for (1988-1992, 1993-1997, 1998-2002, 2003-2007, 2008-2012, 2013-2017)	26
Figure 2.13	Rainfall Trend (SWM) of Peninsular Malaysia (1975-2006)	26
Figure 2.14	Location of Rainfall Station	28
Figure 2.15	Monthly Rainfall at each Station	29
Figure 2.16	Average Maximum Daily Rainfall in March for (1988-1992, 1993-1997, 1998-2002, 2003-2007, 2008-2012, 2013-2017)	30
Figure 2.17	Average Maximum Daily rainfall in October for (1988-1992, 1993-1997, 1998-2002, 2003-2007, 2008-2012, 2013-2017)	30
Figure 2.18	Flash Flood events near Relau River Basin, Pulau Pinang.	33

Figure 2.19	a) Landslide at Tanjung Bungah; b) Landslide at Bukit Kukus	34
Figure 2.20	Fournier Index Variability 1983-2012	38
Figure 2.21	Fournier Modified Index Variability 1983-2012	38
Figure 2.22	Flowchart and Research Gap for this study	42
Figure 3.1	Framework of Study	44
Figure 3.2	Soil Characterization Process	45
Figure 3.3	Map of Borehole Test	46
Figure 3.4	a) Hand Auger apparatus b) Sampling activity	48
Figure 3.5	a) Sampling b) Aggregate broken down using Rubber Pestle after oven drying.	49
Figure 3.6	Moisture Content procedure	49
Figure 3.7	a) Weigh for m_2, b) Soil sample in Desiccator	50
Figure 3.8	a) Mixing the sample with Distilled Water, b) Cone Penetration	51
Figure 3.9	a) Mixing the sample with Distilled Water, b) After rolling the sample until it crack	52
Figure 3.10	a) Hydrometer Test, b) Dry Sieving Method	53
Figure 3.11	JKR Probe apparatus	53
Figure 3.12	JKR Probe Testing.	54
Figure 3.13	Location of Rainfall Station	55
Figure 3.14	Normal and Skewed Distribution of the data. (a) Normal Distribution. (b) Positive Skew. (c) Negative Skew.	58
Figure 3.15	Presentation of the different types of Kurtosis.	59
Figure 3.16	Data Treatment process	60
Figure 3.17	Trend Analysis process	67
Figure 4.1	Comparison of Atterberg Limit (2022 to 2025)	74
Figure 4.2	Comparison of Particle Size Distribution (2022 to 2025)	75
Figure 4.3	Time Series Plot for total 10 years 8 months rainfall (monthly)	89
Figure 4.4	Time Series Plot for NEM	90
Figure 4.5	Time Series Plot for SWM	90
Figure 4.6	Time Series Plot for IM1	90

Figure 4.7	Time Series Plot for IM2	91
Figure 4.8	Comparison of ROM Scale (2022 to 2025)	96
Figure 4.9	Correlation of ‘ROM’ Scale and JKR Blow (3.0m)	100
Figure 4.10	Correlation of ‘ROM’ Scale and JKR Blow (1.5m)	101
Figure 4.11	a) Previous SI location, b) Recent SI location.	102
Figure 4.12	Comparison of Erosive Rainfall Frequency at (Bukit Berapit and Permatang Rawa) Rainfall Station	105

LIST OF TABLES

Table	Title	Page
Table 2.1	Difference between JKR Probe and Mackintosh Probe	12
Table 2.2	Consistency of Residual Cohesive Soil of Probe and SPT value	13
Table 2.3	Range of ROM-Scale and the Degree of Soil Erodibility.	16
Table 2.4	Summary of Percentage of Rainfall in Southwest Region	24
Table 2.5	Summary of Mann-Kendall and Sen's Slope result	36
Table 2.6	Rainfall Erosivity Category (ROSE Index)	39
Table 2.7	Ranking of Erosive Rainfall according to month for the period of 1997-2001 (Fraser Hill)	40
Table 3.1	Borehole Coordinate	46
Table 3.2	Erodibility Category	69
Table 4.1	Physical Properties (2022)	72
Table 4.2	Physical Properties (2025)	73
Table 4.3	Result of JKR (J) and SPT (N)	77
Table 4.4	Descriptive Statistic for total 128 Months Rainfall.	79
Table 4.5	Descriptive Statistic for Northeast Monsoon (NEM) Rainfall.	80
Table 4.6	Descriptive Statistic for Southwest Monsoon (SWM) Rainfall.	80
Table 4.7	Descriptive Statistic for Intermonsoon 1 (IM1) Rainfall.	82
Table 4.8	Descriptive Statistic for Intermonsoon 2 (IM2) Rainfall.	82
Table 4.9	Interquartile Range (IQR) Method	83
Table 4.10	Semi Interquartile Range	84
Table 4.11	Robust Skewness (Medcouple)	84
Table 4.12	Missing Value	85
Table 4.13	Performance Indicator for Bukit Berapit (MS) and (MA) Rainfall Data	86
Table 4.14	Performance Indicator for Permatang Rawa (MS) and (MA) Rainfall Data	87
Table 4.15	Trend Analysis for Monthly Sum (MS) and Monthly Average (MA) Rainfall	93
Table 4.16	Soil Erodibility Index (2022)	95

Table 4.17	Soil Erodibility Index (2025)	97
Table 4.18	Table of Erodibility Index and JKR Probe (J)	98
Table 4.19	Ranking of Erosive Rainfall according to month for the period of 2014-2023 (Bukit Berapit)	103
Table 4.20	Ranking of Erosive rainfall according to month for the period of 2014-2023 (Permatang Rawa)	104

CHAPTER 1
INTRODUCTION

1.1 Research Background

The global greenhouse effect is altering global climate patterns, resulting in increased mean global temperatures and changes in rainfall characteristics (Yahaya et al., 2015). This is further evidenced by predictions of rising atmospheric temperatures and more intensive hydrologic cycles, leading to increased rainfall variability (Yahaya et al., 2015). The IPCC's Sixth Assessment Report supports these findings, projecting a 1.5°C temperature increase by 2040 (Hanif et al., 2022). This changing climate is already contributing to a significant rise in extreme weather events and catastrophic natural disasters worldwide (Chen, 2022), Mountainous regions are disproportionately affected by natural disasters, which are increasingly frequent and costly. Over the last two decades, more than 300 such events have occurred annually globally, impacting over four billion people and causing over USD 2.97 trillion in damage, often due to a combination of tectonic, climatic, and human factors.

Southeast Asia, characterized by complex landscapes and climatic conditions as mentioned by Lu et al., (2024), is particularly vulnerable to these hazards. Chin et al., (2023) stated that the region's rapid population growth and urbanization are increasing the demand for land and intensifying the impact of extreme weather events. Flooding, a major global disaster affecting 1.6 billion people between 2000 and 2019 (Manandhar et al., 2023), is becoming increasingly prevalent in urban areas due to increased impermeable surfaces and more frequent intense rainfall events. The region has also experienced a substantial increase in hydro-meteorological disasters over the past two decades highlighting its vulnerability (Yusmah et al., 2020).

Rainfall is a critical factor in triggering landslides, with studies indicating that over 90% of such incidents are precipitation-induced (Lu et al., 2024). High-intensity, short-duration rainfall exceeding 130 mm daily can trigger slope failures (Mukhlisin et al., 2015; Trigo et al.,2005). Prolonged heavy rainfall further saturates the soil, reducing its strength and cohesion. Water-induced soil erosion, a significant threat to soil quality

and agricultural productivity as stated by Chin et al., (2023), is exacerbated by deforestation and other human activities associated with rapid development contributing to increased landslide risk (Abidin & Hassan, 2005).

The observed changes in global climate patterns are significantly impacting Southeast Asia, increasing the frequency and intensity of hydrological hazards. The region's unique geographic characteristics and rapid development exacerbate these risks, highlighting the need for a comprehensive understanding of rainfall patterns and erosion processes to develop effective mitigation strategies. Further research into these complex interactions is crucial for protecting vulnerable communities and infrastructure in the region.

1.2 Problem Statement

Rainfall-induced hazards represent significant global challenges, with floods and landslides among the most pressing concerns. In Malaysia, the seasonal monsoon results in recurrent flooding events that cause substantial economic losses and increase the vulnerability of affected communities (Yusmah et al., 2020). Approximately 29,000 km² of land in Malaysia is prone to flooding, impacting around 4.82 million people and leading to estimated annual economic losses of USD 299 million (Hanif et al., 2022). Despite ongoing adaptation efforts by residents, the rising frequency and intensity of these events emphasize the urgent need for enhanced mitigation strategies.

Landslides, defined as the downward movement of soil and rock under gravitational forces, are another critical hazard, particularly prevalent in Asian regions (Yusof et al., 2024). Globally, between 2004 and 2016, nearly 4,862 landslide incidents resulted in over 55,000 fatalities (Froude and David, 2018). In Malaysia, from 1993 to 2011, 28 major landslide events caused more than 100 deaths and inflicted approximately USD 1 billion in economic losses between 1973 and 2007 (Rahman and Jabil, 2017; Yusof et al., 2024). Erosion-induced landslides continue to pose a significant threat, causing extensive damage to both natural and built environments (Abidin & Hassan, 2005).

Malaysia’s tropical rainforest climate, marked by high humidity and an average annual rainfall exceeding 2,000 mm significantly above the global average (NAHRIM, 2008) renders the country highly susceptible to soil erosion (Abidin et al., 2017). Heavy

rainfall accelerates soil particle detachment, thereby increasing erosion rates. This heightened erodibility underscores the importance of incorporating soil erodibility indices into risk assessments and mitigation planning (Abidin & Hassan, 2005).

Heavy rainfall has been closely associated with increased landslide occurrences, especially in regions with equatorial climates such as Penang Island, Malaysia. Notable incidents include the Tanjung Bungah landslide on 21 October 2017, which resulted in 11 fatalities (The Sun Daily, 2017), followed by another deadly landslide at Bukit Kukus on 19 October 2018, causing nine fatalities (Malay Mail, 2018). Penang Island's climate, characterized by consistently high temperatures and substantial monthly rainfall, creates conditions conducive to geo-hydrological hazards. Research by Othman et al. (2018) revealed that rainfall during the Tanjung Bungah landslide was significantly above average, contributing to slope instability and triggering the event.

In terms of erosion-related challenges, failures of riverbank protection structures have been documented in Southeast Asia. For example, in 2011, the town of Molo in the Philippines experienced severe erosion and flooding due to the vulnerability of the Jalaur Riverbank during intense rainfall (Dekaraja and Mahanta, 2020). Similarly, in 2014, Kuala Krai, Malaysia, suffered one of its worst floods, which destroyed existing riverbank protection structures and caused widespread damage to infrastructure, buildings, and agricultural land (Berita Harian, 2015). These events highlight the critical need to improve erosion control measures.

Positive mitigation efforts have been demonstrated in locations such as Fraser Hill and Genting Highlands, where Abidin and Hassan (2005) implemented effective strategies to address erosion and rainfall-related hazards. This study aims to apply similar methods to the riverbank at Permatang Rawa, seeking to enhance local resilience against erosion.

In conclusion, a comprehensive analysis of rainfall patterns and soil erodibility is essential for understanding and effectively mitigating the risks posed by floods and landslides in Malaysia. Recent research by Derahman et al. (2025) emphasizes the critical role of these factors in hazard prediction and management. Building upon this foundation, the present study seeks to further investigate these key parameters to inform and develop more effective mitigation strategies.

1.3 Research Objectives

To achieve the aim of this study, a set of specific objectives has been formulated to guide the research process. These objectives focus on assessing the characteristics of riverbank soils, analysing local rainfall trends, and evaluating the impact of rainfall variability on soil erodibility. The study is guided by the following three objectives: -

1. To examine the physical and engineering properties of riverbank soils along the Permatang Rawa riverbank area.
2. To analyse the seasonal rainfall trends in the Permatang Rawa sub-district using the Mann-Kendall test and Sen's slope estimator.
3. To evaluate the relationship between seasonal rainfall trends and the soil erodibility index along the Permatang Rawa Riverbank.

1.4 Significant of Study

This study tackles the critical issue of rainfall-induced hazards in the Seberang Perai Tengah district of Malaysia, an area home to approximately 442,985 residents (DOSM, 2024) who are directly affected by such events. Concentrating on the Permatang Rawa locality within this district, the research employs contemporary methodologies aimed at enhancing the prediction and mitigation of hazards related to rainfall. This investigation offers an important foundation for academic institutions to build upon and refine further.

The significance of this research lies in the pivotal influence of rainfall as a primary catalyst for floods and landslides (Yusmah et al., 2020). A thorough understanding of rainfall patterns, especially the seasonal variations characteristic of Malaysia (Muhammad et al., 2020), is vital for the development of robust early warning systems. By integrating a modified soil erodibility formula developed by Roslan and Mazidah (2002) with up-to-date rainfall data, this study seeks to deliver more precise hazard forecasts, thereby enabling the reduction of potential economic losses and safeguarding human lives. Ultimately, the research aims to strengthen community

resilience in Seberang Perai Tengah and contribute valuable knowledge applicable to other regions confronting similar environmental challenges.

Moreover, the insights gained from this study will be of significant value to policymakers and local communities, informing efforts to devise effective strategies for disaster risk reduction and sustainable land management. The findings are expected to provide a scientific basis for informed decision-making, fostering adaptive responses that can mitigate the adverse effects of climate variability and land degradation in Malaysia and comparable settings globally.

The urgency of this research is underscored by the broader context of global climate change. According to the 2024 progress assessment by the United Nations (UN, 2024), the international community is substantially behind in meeting the targets outlined in the 2030 Agenda for Sustainable Development, with numerous climate-related goals deviating markedly from intended paths. The extreme climate events witnessed in 2023 illustrate the pressing and profound impacts of climate change on vulnerable communities worldwide. This study directly supports Sustainable Development Goal 13 (SDG 13) Climate Action, by focusing on the role of rainfall variability in exacerbating erosion and land degradation, thereby contributing to urgent global efforts aimed at climate mitigation and adaptation.

1.5 Scope of Study

This study examines rainfall-induced hazards at the Permatang Rawa Riverbank in Seberang Perai Tengah, Penang. Soil samples were collected using both automated borehole techniques and manual hand augers to analyze their physical properties. Rainfall data were sourced from two nearby rain gauge stations, Bukit Berapit and Permatang Rawa, aligning with the emphasis on localized data in landslide research (Mukhlisin et al., 2015). Subsoil bearing capacity and weak soil layers were identified through cost-effective in-situ JKR Probe testing (Yusof et al., 2017).

Data pre-processing involved outlier detection based on the method by Zhao and Yang (2019), and missing values were addressed using regression imputation as described by Wang and Hu (2022). These processes were facilitated by R programming and the Statistical Package for Social Science (SPSS), respectively. The effectiveness of the data treatment steps was evaluated using performance indicators outlined by Noor

et al. (2015). Following this, non-parametric Mann-Kendall trend tests and Sen's slope estimators (Guo et al., 2018) were employed using R to analyze rainfall trends. These analyses provide valuable insights for climate-related planning (Gocic & Trajkovic, 2013) and serve as early warning indicators for soil erodibility and potential landslides (Fung et al., 2022).

Erosion severity along the riverbank was quantitatively assessed using a modified ROM scale formula developed by Roslan and Mazidah (2002), taking into consideration the significant erosion and sedimentation risks associated with intense rainfall events). Correlation analysis between the erodibility index and JKR Probe data was conducted using SPSS. Additionally, the ranking methodology proposed by Abidin et al. (2005) was applied to evaluate erodibility in conjunction with erosive rainfall, enabling a comprehensive assessment of how rainfall intensity and frequency impact soil erosion processes.

During the sampling process, challenges were encountered, particularly in collecting soil samples at various depths to accurately determine the erodibility index. The use of manual hand augers frequently encountered obstructions such as underground aggregates, likely due to the area's development and certain locations restricting sample collection. These difficulties highlight practical limitations in field sampling within developed or constrained sites.

1.6 Thesis Outline

Chapter 1 introduces the global and local impacts of rainfall-induced hazards, focusing on flooding, landslides, and erosion in Southeast Asia and Peninsular Malaysia. The chapter establishes the context by highlighting the recent socio-economic consequences of these events and clearly defines the scope and objectives of the present study.

Chapter 2 reviews existing literature on rainfall patterns in Peninsular Malaysia's northern region, examining seasonal variations and their influence on flooding and landslides. This review informs the selection of correlation variables for this study, drawing upon the findings of previous research conducted in the region.

Chapter 3 details the research methodology used to address the research questions.. This includes soil sampling and analysis (physical and engineering

properties, in-situ testing) at the Permatang Rawa river site, rainfall trend analysis using Mann-Kendall tests and Sen's slope estimators, and a correlation analysis between the erodibility index and rainfall patterns.

In chapter 4 presents and analyses the results from laboratory testing, in-situ testing, and soil property analyses. The chapter details the data treatment process preceding the application of the Mann-Kendall and Sen's slope tests to identify significant rainfall trends at the study site. The correlation between in-situ testing results, erodibility index, and daily rainfall data is thoroughly discussed.

Lastly, chapter 5 summarizes the key findings and their implications, acknowledging this study’s limitations and proposing avenues for future research. This chapter provides concluding remarks and recommendations for future studies in this field.

CHAPTER 2
LITERATURE REVIEW

2.1 Introduction

The escalating frequency and intensity of extreme rainfall events in Peninsular Malaysia, a phenomenon linked to anthropogenic climate change (Roy 2009; Cheng et al. 2012), are resulting in significant socio-economic consequences. These events, encompassing both high-intensity, short-duration storms and prolonged periods of intense precipitation, are major contributors to widespread flooding and substantial economic losses (Syafrina et al., 2015). While precipitation is the dominant factor in flood generation (Shankar et al., 2023), the interplay of infiltration characteristics, channel conveyance capacity, and groundwater levels significantly modulates flood severity.

Intense rainfall also acts as a primary triggering mechanism for landslides, a prevalent natural hazard in Malaysia, especially during the monsoon season (Ng et al., 2022). The 2017 Kajang landslide, directly following heavy rainfall, serves as a compelling case study. However, it is crucial to acknowledge that inadequate geotechnical site characterization and subsequent design flaws contribute substantially to landslide susceptibility (Rosly et al., 2022). Comprehensive geotechnical investigations are therefore indispensable for robust slope stabilization strategies.

The impact of rainfall extends to soil erosion, a critical geomorphological process exacerbated by intense precipitation. The erosive capacity of rainfall, manifested in the detachment and transport of soil particles (Sholagberu et al., 2016), presents a significant global challenge (Sabri et al., 2022). Identifying areas prone to erosion is paramount for delineating regions with heightened landslide risk (Abidin & Hassan, 2005). A thorough understanding of soil properties is fundamental for effective hazard mitigation techniques such as particle size distribution analysis provide valuable insights into soil erodibility and, consequently, landslide potential (Abidin & Hassan, 2005).

Rainfall is a pivotal factor in the occurrence of both flooding and landslides within Peninsular Malaysia. Integrating analyses of rainfall patterns, erosion processes, and slope stability offers a pragmatic and cost-effective approach to forecasting and mitigating these hazards.

2.2 Soil Stability Testing

Assessing soil stability requires a multifaceted approach, as various methodologies present both advantages and limitations. Software-based assessments, while potentially powerful, often require extensive datasets and parameters, hindering their application in certain situations (Sabri et al., 2022). Direct data collection methods, such as sensor-based monitoring of soil displacement, can be time intensive, typically requiring at least three years of data acquisition to establish correlations between soil instability and rainfall patterns (Khalid et al., 2018).

Geomorphic Rapid Assessment (GRA) techniques, based on channel patterns and other geomorphic features, offer a broader approach. While methods like Rosgen's stream classification system made by Rosgen, (1994) and its extensions by Heeren et al., (2012) provide valuable insights into streambank stability, they require extensive field observations and expert judgment, making them time-consuming and resource-intensive (Abidin et al., 2017). The simplicity of Rapid Geomorphic Assessment (RGA) is appealing, but it too necessitates the collection of numerous parameters, demanding significant time and specialized skills.

To expedite the assessment process, in situ testing and soil sampling offer more efficient alternatives. In situ testing is crucial for obtaining comprehensive soil engineering properties as stated by Tan & Ramli, (2023), while soil sampling provides a direct and straightforward approach to erosion risk assessment, particularly effective for rapid identification of high-risk riverbank sections (Abidin et al., 2017). The choice of methodology should therefore be guided by the specific context, available resources, and desired level of detail.

2.2.1 Standard Penetration Test

The Standard Penetration Test (SPT) as shown in Figure 2.1 stands as a widely recognized and frequently employed in-situ geotechnical testing method (Singh et al., 2017; Yusof & Zabidi, 2018). This dynamic penetration test yields the SPT blow count (N-value), a key parameter for estimating soil stiffness.



Figure 2.1 Standard Penetration Test (SPT)

Source : Standard Penetration Test in Engineering Geological Site Investigations. (Wazoh, 2014)

The SPT N-value's extensive use in empirical geotechnical correlations further enhances its utility, allowing for the estimation of other crucial soil properties, including unit weight, relative density, and internal friction angle (Sivrikaya & Toğrol, 2006). This versatility makes the SPT a valuable tool for characterizing soil behaviour and informing geotechnical design decisions (Tan & Ramli, 2023)

The ROM Scale equation requires soil particle distribution data, making it necessary to conduct physical properties testing to obtain the distribution percentages. Compared to other methods used in Malaysia for analysing soil erodibility, the ROM Scale is less time consuming and more cost effective (Derahman et al., 2022). Despite its efficiency and minimal parameter requirements, previous researchers continue to explore alternative methods that further reduce time consumption and enhance

productivity. In recent years, machine learning techniques have gained prominence as predictive tools, with the ROM Scale also being incorporated into such approaches (Derahman et al., 2025).

According to Yusof & Zabidi. (2018), the Standard Penetration Test (SPT) is a commonly used in-situ test employed to identify soil type and stratigraphy, as well as to measure relative soil strength. However, their study primarily focuses on the reliability of SPT in predicting other soil properties, such as Atterberg limits and shear strength, rather than its use solely for soil classification. While SPT results correlate with soil density and consistency, the test alone does not provide definitive soil type classification, additional methods are necessary for accurate soil characterization.

In contrast, Sarkar et al. (2015) demonstrated that the SPT can be used to predict soil type specifically sand, silt, and clay which serve as primary parameters in estimating the soil erodibility index. Using a General Regression Neural Network (GRNN) model, their study predicted both soil type and SPT (N) values, with SPT data acting as a key input feature. However, the model's accuracy depends heavily on the spatial distribution of borehole data used for training, performing well within the trained area but showing limitations when applied beyond that zone.

While the primary outputs of the SPT are soil strength and consistency, some researchers have attempted to utilize SPT data for soil type identification. Although the SPT does not provide exact percentages of particle size distribution as required by the ROM Scale, it can predict the dominant soil type, such as clay. This is significant because clay content plays a crucial role in determining the erodibility index. Notably, areas with high clay content have shown minimal indications of erosion (Zhang et al., 2023; Abidin et al., 2017).

2.2.2 JKR Probe Test

The Mackintosh Probe (MP) test is a conventional site investigation (SI) method widely used to estimate soil strength. Sabri et al. (2022) established an empirical correlation between the Mackintosh Probe (MP) test's M-value (blows per unit penetration) and the Erodibility Index (ROM) scale value (derived from soil particle size distribution) as show in figure 2.2. This correlation facilitates a more efficient estimation of soil erosion potential. The MP test, therefore, provides a streamlined

alternative to more intricate and time-consuming methods for assessing soil properties relevant to erosion risk assessment, offering a practical approach for evaluating soil susceptibility to erosion.

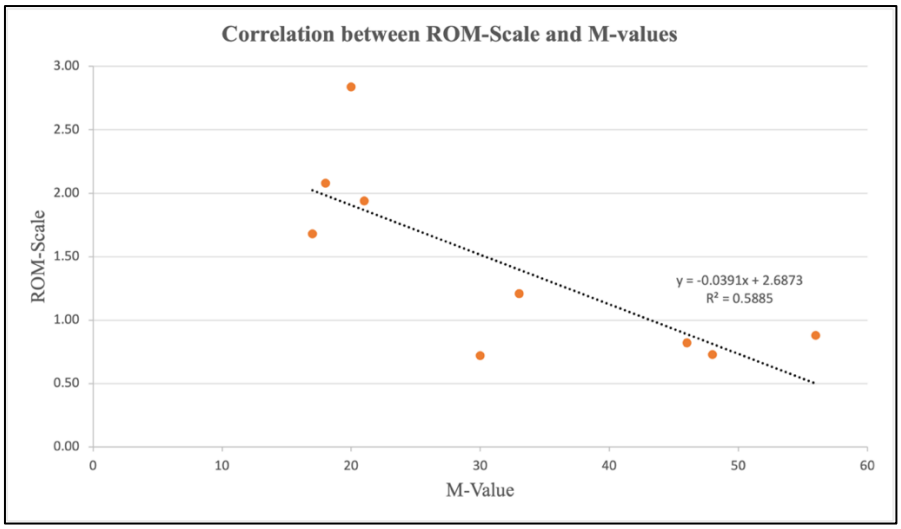

Figure 2.2 Correlation between ROM-Scale and M-Values based on SI and Laboratory Testing results.

Source : Erosion risk index: Correlation of ROM-scale and Mackintosh Probe at Sungai Langat tributary (Sabri et al. 2022)

Table 2.1

Difference between JKR Probe and Mackintosh Probe

Equipment	**Cone angle (°)**	**Diameter of rods (mm)**	**Diameter of coupling (mm)**	**Weight of hammer (kg)**	**Height of hammer fall (mm)**
JKR Probe	60	12	22	5.0	280
Mackintosh Probe	30	13	24	4.5	300

Source : Correlation of JKR Probe with Undrained Shear Strength (Yusof et al., 2017)

Table 2.1 highlights the key distinctions between the JKR and Mackintosh probes. The JKR probe method, a relatively inexpensive and straightforward site investigation technique, is frequently employed in Malaysia, particularly during

preliminary site assessments. Its primary applications include evaluating subsoil layering and assessing soil bearing capacity (Yusof et al., 2017). This simplicity and cost-effectiveness make it a valuable tool for initial site characterization.

Table 2.2

Consistency of Residual Cohesive Soil of Mackintosh Probe and SPT value

Number of Blow/penetrations		**Consistency**
M-value	**SPT, N value**	
<15	<2	Very soft
15-33	2-4	Soft
33-72	4-8	Medium
72-147	8-16	Stiff
147-322	16-30	Very stiff
>322	>30	Hard

Source : Mackintosh Probe as an exploration tool (Sabtan & Shehata, 1994)

The soil consistency can be divided into various sub-groups based on SPT-N values (Table 2.2). Additionally, Sabtan & Shehata, (1994) reported that the M-value also could be regarded as the soil stiffness as shown in Table 2.2. While Table 2.2 is primarily used to predict soil consistency, it also serves to evaluate the consistency of data obtained from both the SPT and Mackintosh test results.

2.2.3 Soil Stability Index

Geotechnical problem, soil erosion in Malaysia commonly occurs in several distinct environments. Mountainous areas experience gradual erosion of their slopes due to flowing water transporting soil particles downstream. Agricultural lands are particularly vulnerable because farming activities disrupt soil structure, increasing susceptibility to rainfall-induced erosion. Riverbanks are continuously eroded by flowing water, which contributes sediment to nearby water bodies. Steep slopes face heightened risks of landslides triggered by erosion processes. Areas with sparse vegetation lack protective ground cover, exposing soil to erosive forces and thus

elevating erosion risk. Regions with high rainfall intensity are prone to both surface erosion and landslides due to the increased water impact. Additionally, deforested areas, where forest cover has been removed, leave soil exposed and highly susceptible to erosion. Finally, soils with a high sand content tend to be less resistant to erosion compared to those with higher clay content (Derahman et al., 2022).

The ROM Scale, recognized as one of the simplest methods for assessing soil erodibility as mentioned by Derahman et al., (2022), is widely applied to various soil types across Malaysia. Among the locations prone to erosion, riverbanks and mountainous areas are the most commonly studied by previous researchers utilizing the ROM Scale methodology.

Figure 2.3 illustrates the three primary types of water erosion, showing a progression in severity and concentration. Sheet erosion, the most common and least damaging form, involves the uniform removal of a thin soil layer across a wide area, resembling a sheet of water flowing over the surface. Rill erosion is more concentrated, forming small channels or rills on the soil surface; it is considered moderate in severity and these channels can typically be smoothed out by normal tillage. Gully erosion is the most severe type, creating large, deep channels that often extend into the subsoil, resulting in significant soil loss and landscape alteration. Overall, the figure visually represents how water erosion intensifies from a relatively mild and uniform process to increasingly focused and destructive forms.

The Langat River is subject to various types of erosion, including sheet, rill, and gully erosion, making it an ideal case study for testing newly developed risk assessment index. Flowing through three districts, Hulu Langat, Sepang, and Kuala Langat the river exhibits differing erosion intensities across these areas, providing a diverse range of conditions for comprehensive analysis. Abidin et al. (2017) applied the ROM Scale method to further evaluate the erodibility index specifically along the riverbanks of the Langat River.

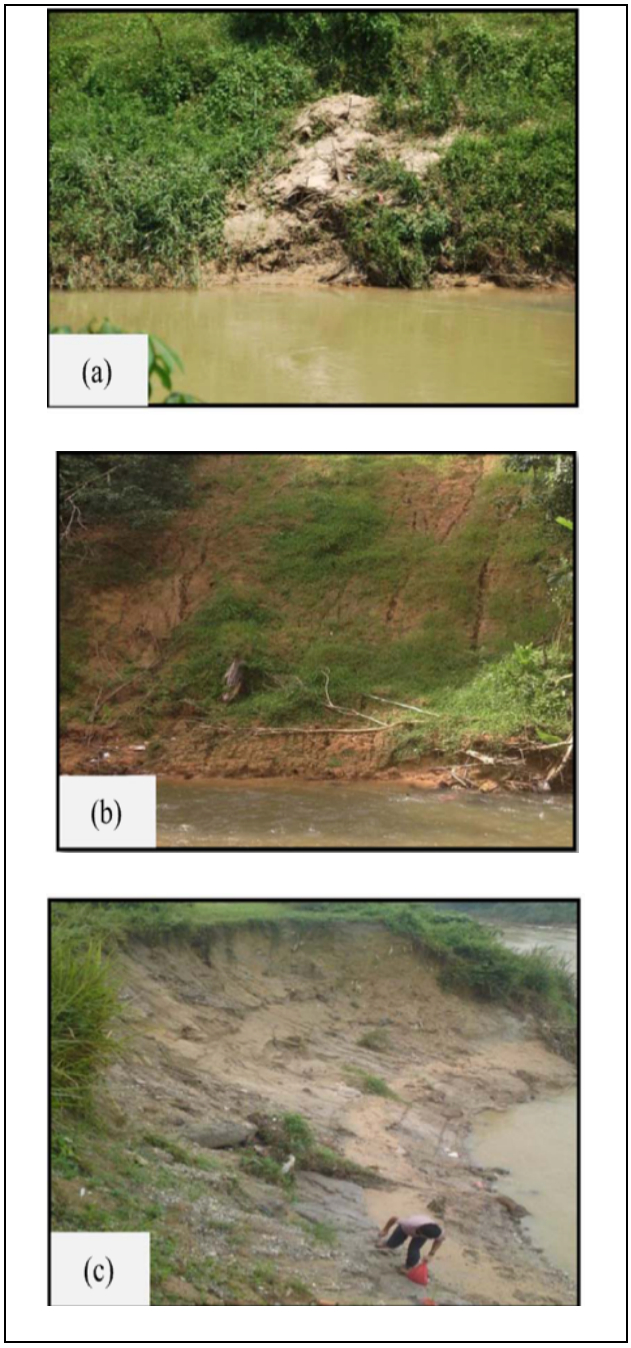

Figure 2.3 Type of Erosion: a) Sheet Erosion, b) Rill Erosion, c) Gully Erosion
Source : Erosion risk assessment: A case study of the Langat River bank in Malaysia. (Abidin et., 2017)

A related study was conducted on a tributary of the Sungai Langat near Universiti Kebangsaan Malaysia in Bangi. This location was selected to facilitate the use of Mackintosh Probe tests alongside the collection of soil samples for ROM Scale evaluation at three distinct points along the riverbank. (Sabri et al., 2022).

In the context of hilly terrain, Fraser's Hill and Genting Highlands two prominent highland resort areas in Malaysia—were chosen for study due to their susceptibility to landslides. The rapid pace of land development and encroachment on steep slopes in these regions exacerbates the risk of slope failure. Abidin and Hassan et al. (2005) employed the ROM Scale methodology to identify potential landslide hazard zones and to predict the likelihood of landslide occurrences in these vulnerable highland areas.

Since this study focuses on riverbank environments, which are inherently prone to erosion as noted by Derahman et al. (2022), the application of ROM Scale in similar contexts such as those studied by Abidin et al. (2017) and Sabri et al. (2022) is theoretically justified. The careful selection of study locations and the integration of appropriate methodologies will contribute valuable insights into soil erodibility and the factors influencing erosion processes in these specific areas.

Foundational work of Bouyoucos (1962), alter by Roslan and Mazidah (2002) developed a modified approach to assess erosion risk within the Malaysian context. This led to the creation of the ROM scale (named after Roslan and Mazidah), presented in Equation 2.1 and Table 2.3. The ROM scale employs a logical predictive calculation to quantify the degree of soil erosion susceptibility, providing a valuable tool for assessing erosion risk in Malaysia.

$$\mathrm{EI}_{\mathrm{ROM}} = \frac{\%\ \text{sand} + \%\ \text{silt}}{2\ (\%\ \text{clay})} \tag{2.1}$$

Table 2.3

Range of ROM-Scale and The Degree of Soil Erodibility.

ROM-scale	Soil erodibility category
<1.5	Low
1.5 – 4.0	Moderate
4.0 – 8.0	High
8.0 – 12.0	Very high
>12.0	Critical

Source : Establishment of Soil Erosion Scale With Regards to Soil Grading Characteristic. (Roslan & Mazidah., 2002)

The (ROM) scale provides a rapid and efficient method for identifying slopes and riverbanks susceptible to erosion-induced landslides. Knowledge of the soil's textural composition (sand, silt, and clay content) allows for a direct and expeditious determination of the erodibility index, significantly reducing assessment time while maintaining accuracy (Derahman et al., 2022). This streamlined approach makes the ROM scale a valuable tool for prioritizing areas requiring immediate attention and implementing effective mitigation strategies.

The erodibility index formula (ROM) scale offers a practical approach to assessing soil erodibility, particularly in smaller areas prone to landslides. Its simplicity and speed compared to methods like USLE or RUSLE make it suitable for identifying high-risk zones (Derahman et al., 2022). This rapid assessment capability is important for prioritizing areas requiring immediate attention.

2.3 Rainfall trend in Malaysia

Peninsular Malaysia (PM), geographically situated between 1° and 7° North latitude and 99° to 105° East longitude (Figure 2.4), covers an area of 131,587 km² (Mohtar et al., 2014). Its diverse topography, encompassing highlands, floodplains, and coastal zones, is significantly shaped by the Titiwangsa mountain range, which stretches approximately 480 km from southern Thailand, effectively dividing the peninsula into distinct eastern and western regions. This varied topography plays a crucial role in influencing the distribution and intensity of rainfall across the region.

Fung et al., (2022) facilitate analysis of regional rainfall variations in Peninsular Malaysia, (Figure 2.2) the peninsula is divided into four distinct regions. The Northern Region (Perlis, Kedah, Pulau Pinang, and Perak), the East Coast Region (Pahang, Kelantan, and Terengganu), the Central Region (Selangor, Negeri Sembilan, and Melaka), and the Southern Region (Johor). This regional classification allows for a more detailed analysis of differing rainfall trends across the peninsula during various seasonal periods.

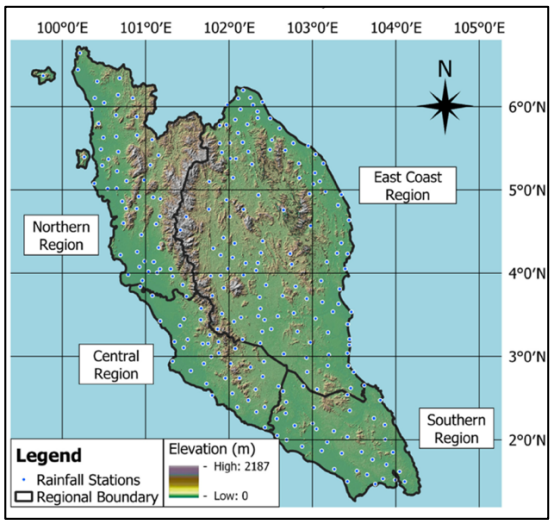

Figure 2.4 Map of Peninsular Malaysia

Source : Evaluation of spatial interpolation methods and spatiotemporal modeling of rainfall distribution in Peninsular Malaysia. (Fung et al., 2022)

The annual rainfall in PM is characterized by significant seasonal variability. While an average annual rainfall of approximately 2440 mm is often cited (Tan, 2018), with supporting evidence suggesting a range of 2000-3000 mm analysed by Saimi et al., (2020), the actual amount varies considerably across different regions. This variation is largely attributed to the influence of the northeast (NEM) and southwest monsoons, which are the primary drivers of the seasonal rainfall patterns. The warm and humid tropical climate, with temperatures ranging from 21°C to 32°C (Mohtar et al., 2014; Sa'adi et al., 2024), further contributes to the region's susceptibility to intense rainfall events.

The period of the monsoon seasons, and thus the periods of peak rainfall, remain a subject of ongoing discussion within the scientific community. One prevailing model identifies two primary rainy seasons: the southwest monsoon (May-September) and the northeast monsoon (November-March) (Mohtar et al., 2014; Sa'adi et al., 2024). However, a contrasting perspective emphasizes the northeast monsoon (November-February) and southwest monsoon (May-August) as dominant periods, with heavier rainfall typically affecting the eastern and southern regions during the northeast monsoon and intense convective rainfall impacting the west coast during the inter-monsoon periods (March-April and September-October) (Syafrina, 2017). Furthermore, April is often highlighted as a transitional month with substantial rainfall (Fung et al., 2022).

2.3.1 Northeast Monsoon (NEM)

Malaysia's rainfall regime is substantially influenced by the Northeast Monsoon (NEM). The precise timing of the NEM remains a topic of ongoing discussion within the research community, with the period from November to February generally considered dominant (Syafrina et al., 2015; Sa'adi et al., 2024; Pour et al., 2020). The nation's geography, comprising Peninsular Malaysia (West Malaysia) and East Malaysia (Sabah and Sarawak) separated by the South China Sea, contributes to regional differences in rainfall characteristics during the NEM. Figure 2.5 provides a visual representation of these rainfall patterns and their correlation with the monsoon system.



Figure 2.5 Northeast Monsoon

Source : Floods in Malaysia : Historical Reviews, Causes, Effects and Mitigations Approach. (Toriman & Gasim, 2014)

The geographical division of Malaysia into Peninsular Malaysia and East Malaysia, separated by the South China Sea, results in distinct meteorological conditions and consequently, varying rainfall responses to the NEM. The Northeast Monsoon (NEM) is a dominant climatic feature significantly impacting rainfall patterns in Peninsular Malaysia (Ali et al., 2022; Hamed et al., 2022a; Jasmin et al., 2020). Its influence extends across various sectors, including agriculture, water resource management, and disaster preparedness (Sa'adi et al., 2024). The NEM's importance

stems from its contribution to the nation's water resources, with a substantial portion of the annual rainfall occurring during this period.

Intense or prolonged rainfall associated with the NEM can lead to severe flooding, causing significant damage to infrastructure, disrupting transportation networks, and posing considerable risks to human life. The devastating floods of December 2014 serve as a stark example, highlighting the vulnerability of certain regions, particularly Kelantan (Hai et al., 2017; Sa'adi et al., 2024). The high variability in rainfall during the NEM, exceeding that observed during the Southwest Monsoon (SWM), further underscores its significance (Wong et al., 2018).

November typically exhibits the highest mean monthly rainfall, reaching 311 mm, representing approximately 13% of the mean annual rainfall (Wong et al., 2018). A substantial portion of Peninsular Malaysia receives a significant proportion of its annual rainfall (50-70%) during the NEM (Yik et al., 2015; Pour et al., 2020). This underscores the NEM's crucial role in replenishing water resources across a large area of the country (Pour et al., 2014). Figure 2.6 visually supports these findings, demonstrating that November, falling within the NEM period, experiences the highest rainfall amounts. This observation reinforces the established understanding that this season is a primary contributor to the country's significant annual precipitation.

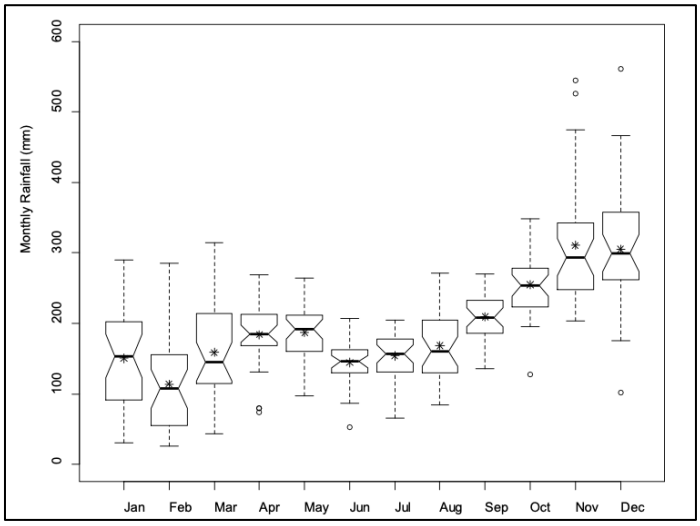

Figure 2.6 Box and Whisker Plot of Monthly Areal Mean Rainfall (1975-2006) in Peninsular Malaysia.

Source : Trend of Daily Rainfall and Temperature in Peninsular Malaysia Based on Gridded Data Set. (Wong et al., 2018)

Figure 2.7 presents the precipitation pattern observed in Alor Setar, Kedah, for the month of December. The data indicates a relatively low amount of rainfall during this period when compared to other months, aligning with the broader climatic trends previously discussed. Although the data points exhibit some variability, the overall trend remains relatively flat, with a slight upward inclination. This analysis suggests that Kedah experiences a lower volume of rainfall during the Northeast Monsoon, reflecting a distinct regional variation within the context of Malaysia's monsoonal climate.

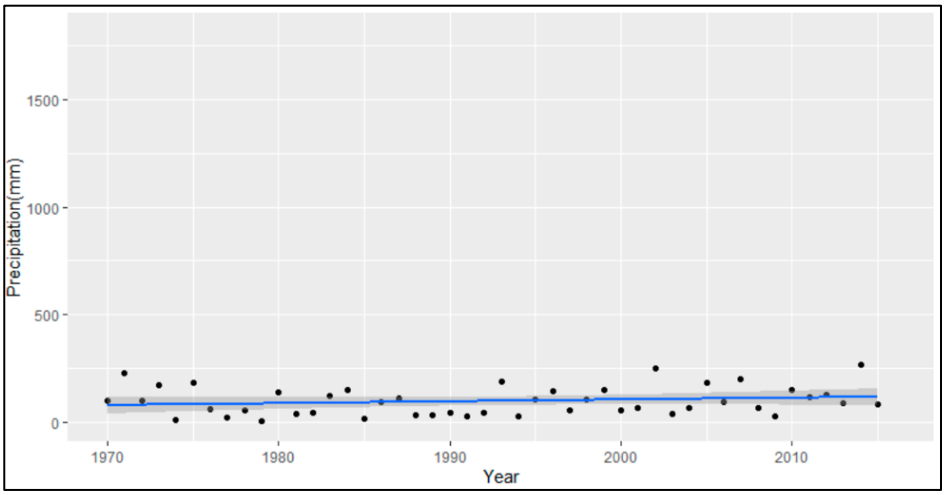

Figure 2.7 Plot for Precipitation in December for Alor Setar.

Source : Trend and Linearity Analysis of Meteorological Parameters in Peninsular Malaysia. (Saimi et al., 2020)

Analysis of the data presented in Figure 2.8 reveals a contrasting pattern during the onset of the Northeast Monsoon (NEM) in October. Specifically, the northern region and the northern portion of the east coast experienced comparatively higher monthly rainfall than other areas of Peninsular Malaysia. This observation contrasts with findings by Saimi et al. (2020), who reported an insignificant rainfall trend in the northern region during the NEM. However, this discrepancy may be explained by the study of Fung et al. (2020), which highlights the importance of monitoring rainfall patterns during the pre-NEM period (October), particularly during the first intermonsoon period (IM1), a topic further elaborated in the intermonsoon section of this study.

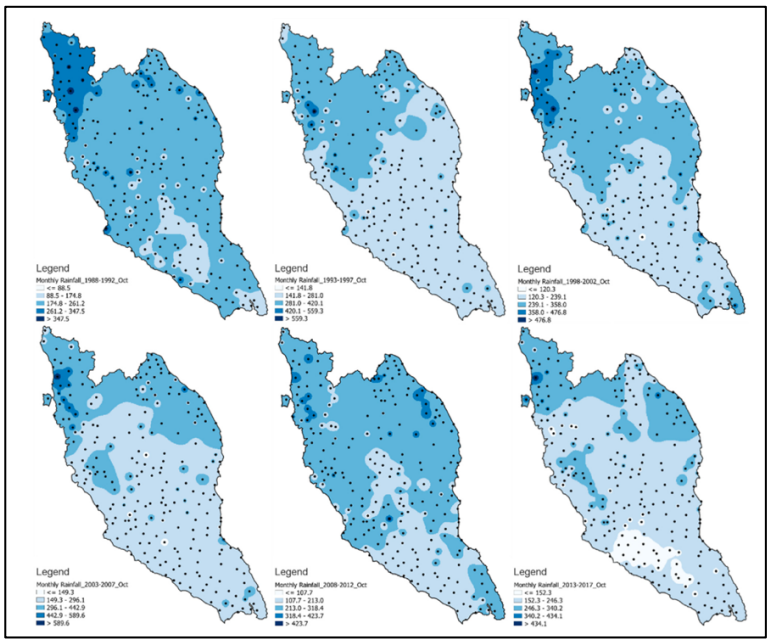

Figure 2.8 Average Monthly in October for (1988-1992, 1993-1997, 1998-2002, 2003-2007, 2008-2012, 2013-2017)

Source : Evaluation of spatial interpolation methods and spatiotemporal modeling of rainfall distribution in Peninsular Malaysia. (Fung et al., 2022)

2.3.2 Southwest Monsoon (SWM)

In contrast to the Northeast Monsoon (NEM), the Southwest Monsoon (SWM) exhibits less variability in the scholarly literature regarding its precise temporal occurrence. A consistent finding across multiple studies (Syafrina et al., 2015; Fung et al., 2022; Pour et al., 2020; Wong et al., 2018) indicates that the SWM typically manifests between May and August. Figure 2.9 illustrates the rainfall patterns associated with the SWM and their relationship to the overall monsoonal climate system.

Figure 2.10 illustrates study by Mohtar et al., (2014) the rainfall patterns in Johor state during the Southwest Monsoon (SWM) period (May-August) for the years 2010-2012. The data reveals consistently high rainfall amounts during the SWM in 2010 and 2011. However, a significant decrease in rainfall is observed during the SWM of 2012. This reduction may be attributed to the effects of climate change, potentially increasing the vulnerability of the region to drought and subsequent haze events resulting from forest fires.



Figure 2.9 Southwest Monsoon

Source : Floods in Malaysia : Historical Reviews, Causes, Effects and Mitigations Approach. (Toriman & Gasim, 2014)

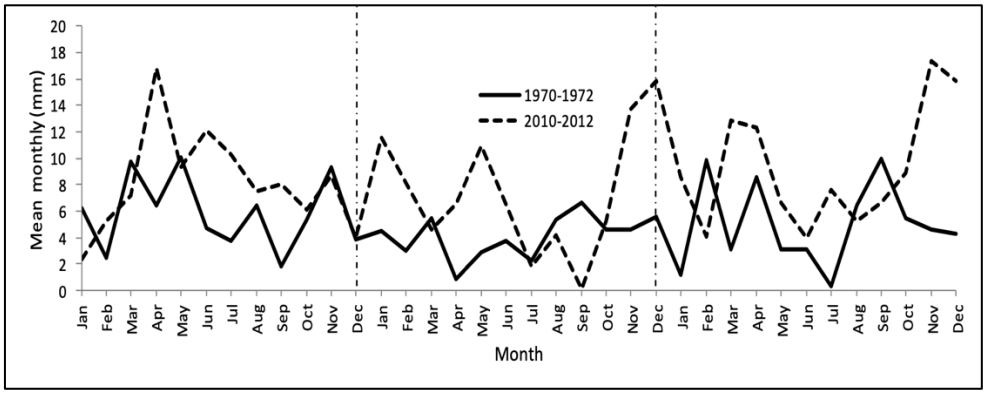

Figure 2.10 Graph for Station Stor JPS Johor Bahru, Johor

Source : Trends for Daily Rainfall in Northern and Southern Region of Peninsular Malaysia. (Mohtar et al., 2014)

Finding by Mohtar et al., (2014) are support by Vincent and Yusoff (2022) study, where it utilizing data from 2011 to 2020, indicates that the southwest region of Peninsular Malaysia experiences drought conditions during the Southwest Monsoon (SWM). Table 2.4 shows that July and August are the months with the highest risk, with over 95% of rainfall amounts categorized as low (<90 mm).

Table 2.4

Summary of Percentage of Rainfall in Southwest Region

Rainfall Station	Percentage		Risk Month
	Low (<90)	Moderate (90-120)	
Empangan Sg. Machap	97.42	2.58	August
Stor JPS. Johor Bahru	95.45	4.55	August
Empangan Sg. Sembrong	96.48	3.52	July August

Source : Trends In Peninsular Malaysia Rainfall During The Southwest Monsoon Using Degree Of Rainfall Amount (DORA). (Vincent & Yusoff., 2022)

Analysis of Figure 2.11 reveals the spatial distribution of average Total Annual Rainfall (TAR) indices during the Southwest Monsoon (SWM) season, based on data collected between 1975 and 2004. The data shows the highest TAR indices concentrated in the northwestern region, specifically in inland areas. These areas exhibit average TAR values exceeding 680 mm, with maximum values approaching 980 mm. Similar elevated TAR indices were observed at stations located in the far north of the western region.

This spatial pattern of high rainfall is likely attributable to the geographical characteristics of these locations, as suggested by Wong et al. (2018). The stations recording the highest TAR values are situated in foothills and sheltered by mountain ranges. This orographic effect is consistent with established climatological principles, where maximum rainfall is typically observed in foothills and adjacent lowlands rather than at higher altitudes (Dale, 1959). Consequently, the higher rainfall observed in these northwestern areas during the SWM season is explained by their unique geographical context within the western Peninsular Malaysia.

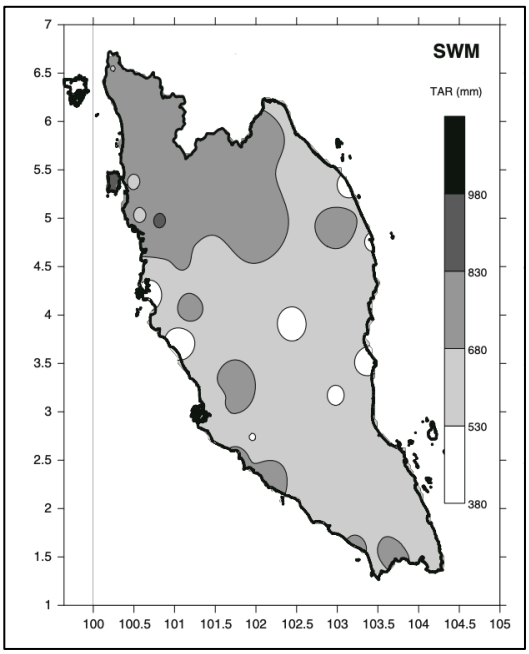

Figure 2.11 Spatial Distribution of TAR Index Averages (in mm/year) during SWM
Source : Spatial patterns and trends of daily rainfall regime in Peninsular Malaysia during the southwest and northeast monsoons: 1975-2004. (Suhaila et al., 2010)

Supporting Suhaila et al., (2010) finding. Figure 2.12 reveals that the Northern region of Peninsular Malaysia experiences relatively high average monthly rainfall in May, marking the onset of the Southwest Monsoon (SWM), across several sub-periods: 1988–1992 (146.7–250.0 mm), 1993–1997 (151.6–226.3 mm), 2003–2007 (154.8–231.3 mm), 2008–2012 (159.1–237.7 mm), and 2013–2017 (200.9–268.2 mm). This suggests a consistent trend of higher rainfall at the beginning of the SWM in the northwest region.

In contrast to previous findings, Wong et al. (2018) report a declining trend in rainfall during the Southwest Monsoon (SWM) in Peninsular Malaysia, as depicted in Figure 2.13, at a rate of -1.7 mm/season/year. However, this trend is not statistically significant at the 95% confidence level. Wong et al. (2018) suggest that the interannual variability in rainfall is likely influenced by topographic features and local/regional conditions, superimposed upon larger-scale weather patterns. This conclusion aligns with the findings of Vincent and Yusoff (2022).

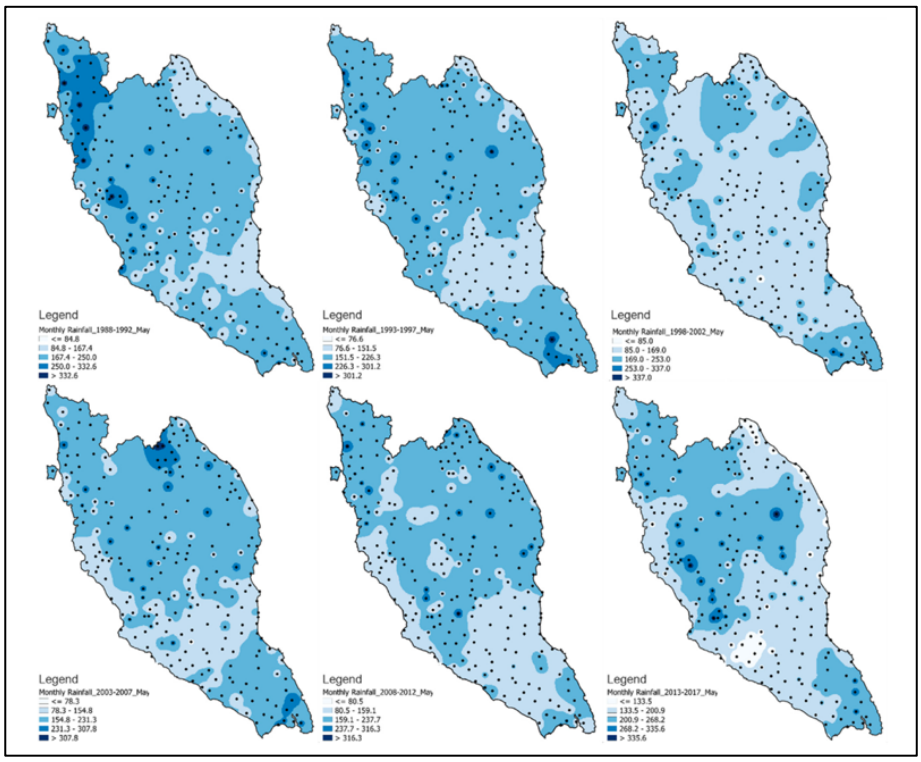

Figure 2.12 Average Monthly Rainfall in May for (1988-1992, 1993-1997, 1998-2002, 2003-2007, 2008-2012, 2013-2017)

Source : Evaluation of spatial interpolation methods and spatiotemporal modeling of rainfall distribution in Peninsular Malaysia. (Fung et al., 2022)

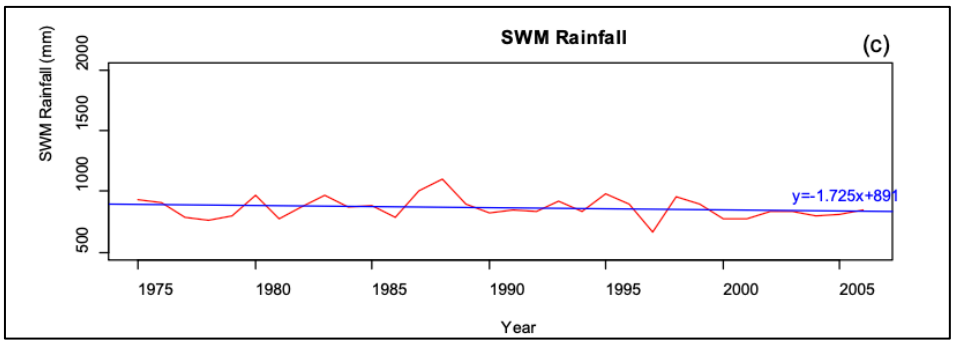

Figure 2.13 Rainfall Trend (SWM) of Peninsular Malaysia (1975-2006)

Source : Trend of Daily Rainfall and Temperature in Peninsular Malaysia Based on Gridded Data Set. (Wong et al., 2018)

Recent research by Vincent and Yusoff (2022) focusing on the northern region of Peninsular Malaysia corroborates the findings of Wong et al. (2018) regarding declining rainfall trends during the Southwest Monsoon (SWM). Their study reveals that June experiences the lowest rainfall within the SWM season, while August exhibits the highest. Furthermore, the northwest region demonstrates the fewest rainfall days compared to other regions. Employing Degree of Rainfall Amount (DORA) analysis, Vincent and Yusoff (2022) identified increasing drought trends and a higher risk of forest fires in this region, classifying it as experiencing low rainfall amounts throughout the SWM season. These findings highlight the complex and regionally variable impacts of the SWM on rainfall patterns in Peninsular Malaysia.

2.3.3 Intermonsoon (IM)

The First Intermonsoon (FIM) and Second Intermonsoon (SIM) periods are generally defined as March–April and September–October, respectively (Suhaila et al., 2010). This timeframe aligns with observations by Syafrina et al. (2015), who also identify these months as periods of intense convective rainfall along the western coast of Peninsular Malaysia. However, some variation exists in the literature; Muhammad et al. (2020) suggest April and October as the key months, while Fung et al. (2022) identify only April as a transitional period with substantial rainfall.

Given the varied perspectives on intermonsoon timing, this study adopts a definition based on the temporal boundaries of the Northeast (NEM) and Southwest (SWM) monsoons. The intermonsoon seasons are thus defined as the periods between the NEM and SWM, approximately spanning March–April and September–October, as proposed by Suhaila et al. (2010) and Syafrina et al. (2015).

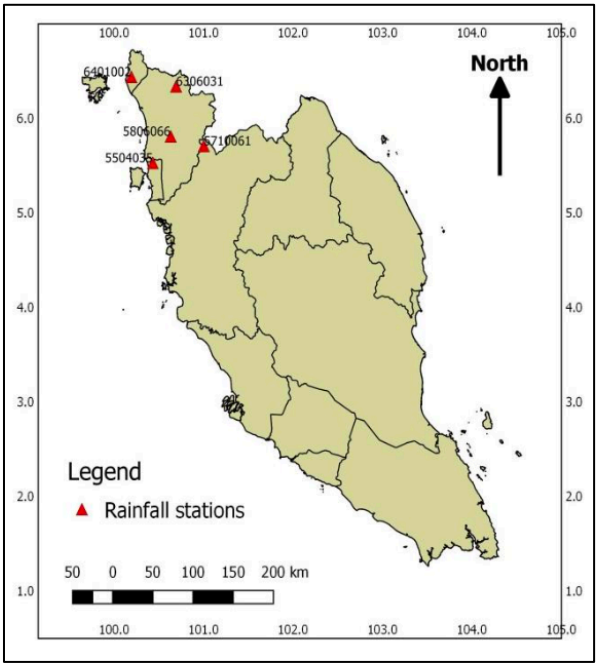

Figure 2.14 Location of Rainfall Station

Source : Rainfall analysis in the northern region of Peninsular Malaysia. (Syafrina et al, 2017)

Figure 2.14 presents the rainfall analysis conducted by Syafrina (2017), focusing specifically on the northern region of Peninsular Malaysia (Pulau Pinang, Perlis, Kedah, and Perak). The figure displays the selected rainfall stations and the corresponding data period (1975–2005) used in the subsequent analysis.

Figure 2.15 illustrates the rainfall patterns in the northern region of Peninsular Malaysia, revealing a bimodal annual distribution. A pronounced peak in rainfall occurs during the first intermonsoon (IM1) period in October (300–500 mm). Rainfall subsequently decreases to a minimum during the Northeast Monsoon (NEM) from November to February (mean rainfall of 50 mm), before increasing again in April/May (250–350 mm) at all stations. The primary rainfall peak in October (IM1) significantly surpasses that of the second intermonsoon (IM2). A sharp decline in rainfall is observed in January, followed by a gradual increase from March/April (IM2) continuing through the Southwest Monsoon (SWM) period (May–August), culminating in the maximum rainfall in October.

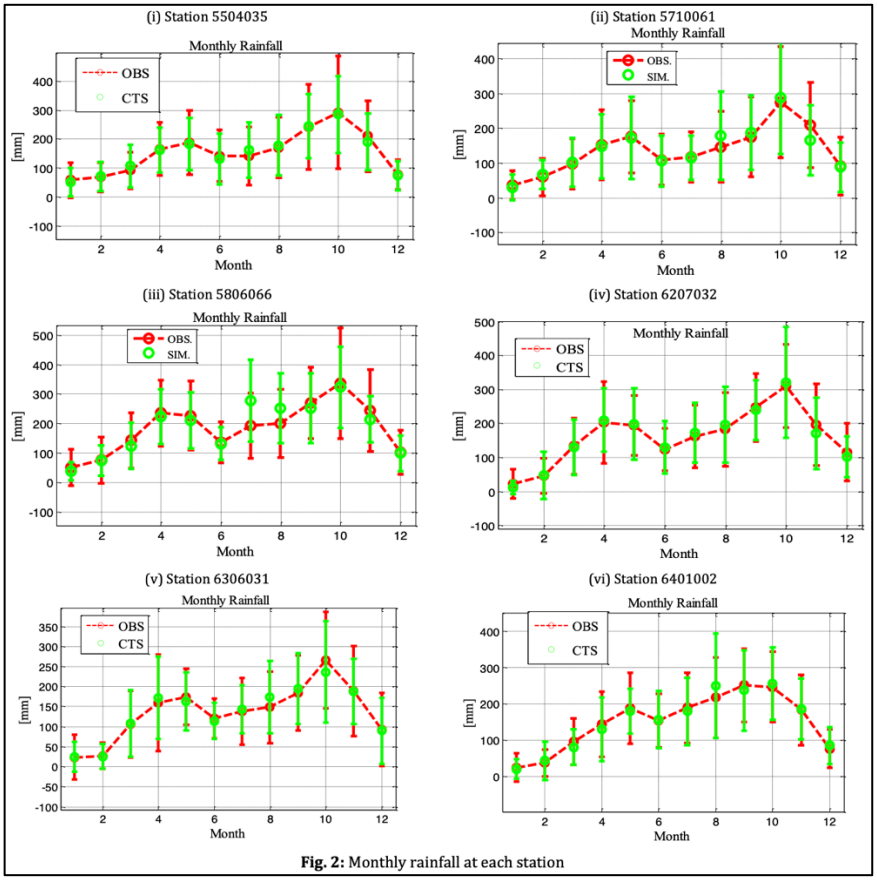

Figure 2.15 Monthly Rainfall at each station

Source : Rainfall analysis in the northern region of Peninsular Malaysia. (Syafrina et al, 2017)

Figure 2.16 presents finding by Fung et al., (2022) the Maximum Daily Rainfall (MDR) in the northern East Coast region during the intermonsoon period (March) across several sub-periods. Observed MDR values were less than 24.5 mm (1988–1992), 32.6–48.7 mm (1993–1997), 47.9–71.7 mm (1998–2002), 43.5–65.0 mm (2003–2007), 69.7–138.8 mm (2008–2012), and less than 36.4 mm (2013–2017). These data suggest an overall increase in monthly rainfall, number of wet days, and MDR in the northern East Coast region across the observed sub-periods. The relatively low monthly rainfall observed during 1988–1992 and 2013–2017 may be attributed to the strong 1991/92 and very strong 2015/16 El Niño events, which induced sea surface temperature anomalies resulting in reduced rainfall.

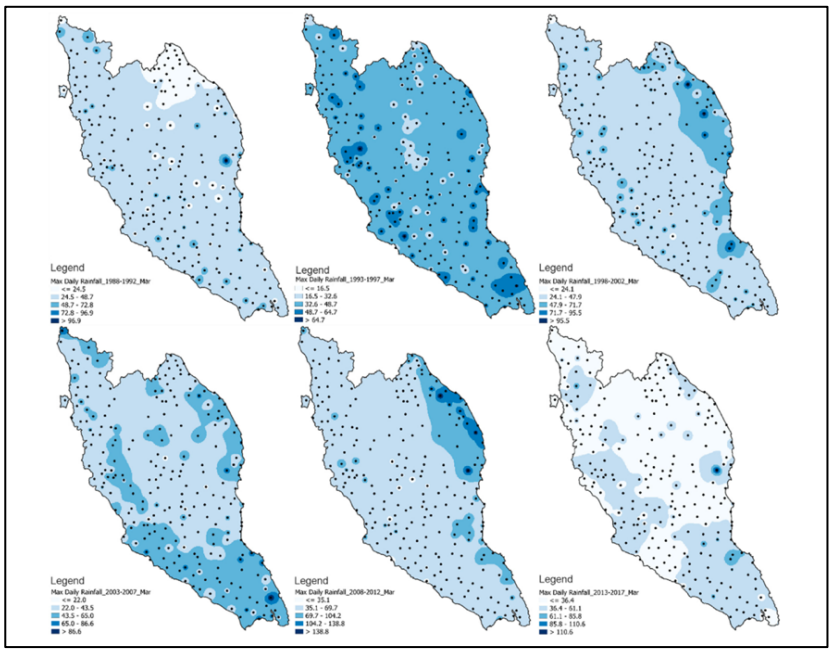

Figure 2.16 Average Maximum Daily Rainfall in March for (1988-1992, 1993-1997, 1998-2002, 2003-2007, 2008-2012, 2013-2017)

Source : Evaluation of spatial interpolation methods and spatiotemporal modeling of rainfall distribution in Peninsular Malaysia. (Fung et al., 2022)

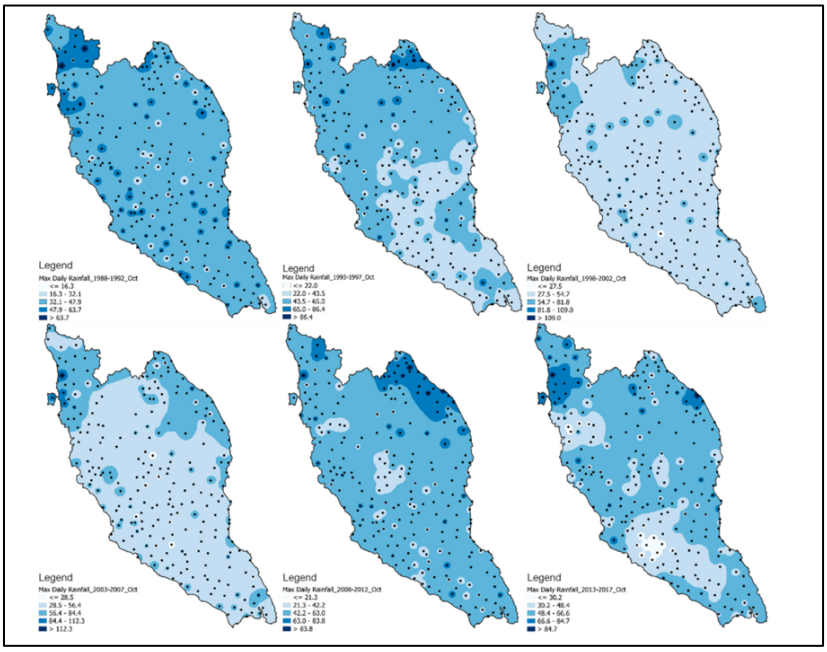

Figure 2.17 Average Maximum Daily Rainfall in October for (1988-1992, 1993-1997, 1998-2002, 2003-2007, 2008-2012, 2013-2017)

Source : Evaluation of spatial interpolation methods and spatiotemporal modeling of rainfall distribution in Peninsular Malaysia. (Fung et al., 2022)

In contrast to the March intermonsoon period, October's Maximum Daily Rainfall (MDR) in the northern Peninsular Malaysia, as depicted in Figure 2.17, ranged from 32.1–47.9 mm (1988–1992), 43.5–65.0 mm (1993–1997), 27.5–54.7 mm (1998–2002), 28.5–56.4 mm (2003–2007), 41.2–63.0 mm (2008–2012), and 48.4–66.6 mm (2013–2017). While the northern and northeast coastal regions exhibited relatively higher monthly rainfall, no significant changes in average monthly rainfall were observed across the sub-periods. However, a decrease in the number of wet days coupled with an increase in MDR indicates a rise in rainfall intensity across the northern Peninsular Malaysia. Consequently, despite insignificant changes in total rainfall amount, these regions may experience a higher frequency of flood events due to this increased rainfall intensity.

While Fung et al. (2022) reported higher monthly rainfall in March compared to October, Figure 2.15 reveals a slight downward trend in March rainfall during the 2013–2017 period. This suggests that October may exhibit a greater propensity for higher rainfall in the future. This conclusion is supported by Syafrina et al. (2017), whose findings indicate higher rainfall in October across all six stations studied in the northern region, representing a peak value for the year.

2.4 Rainfall Trend in Northern Region

A review of existing literature reveals contrasting rainfall patterns across Peninsular Malaysia's various monsoon seasons. Studies by Fung et al. (2022) and Syafrina et al. (2017) indicate that the northern region experiences significant rainfall during the First Intermonsoon (IM1) period (September-October). However, rainfall patterns differ across other seasons. For example, while Saimi et al. (2020) report relatively low rainfall in Alor Setar, Kedah during December (within the Northeast Monsoon, NEM), Syafrina et al. (2017) observed decreased rainfall in December during the NEM, but other months had higher amounts.

During the Southwest Monsoon (SWM), Johor experienced consistently high rainfall in 2010 and 2011 as studied by Mohtar et al., (2014), while May showed relatively high average monthly rainfall in the northern region (Fung et al., 2010). Conversely, the northwest region exhibited the fewest rainfall days during the SWM (Vincent & Yusoff et al., 2022), a finding consistent with Syafrina et al.'s (2017)

observation of May as the month with the highest rainfall during the SWM. Overall, the SWM exhibits intermediate rainfall levels.

In summary, the NEM represents the driest period, increasing the region's vulnerability to drought. Conversely, the IM1 (September-October) period shows the highest rainfall in the northern region, necessitating further investigation to mitigate the risk of associated disasters such as flooding, erosion, and landslides (Yusof et al., 2024). The identification of potential erosion sites, as emphasized by Abidin and Hassan (2005), is crucial for determining landslide-prone areas, a topic that will be further explored in the following section.

2.5 Rainfall Prone Disaster

Hydrological disasters, particularly floods and flash floods associated with extreme rainfall events, pose significant challenges to Peninsular Malaysia, causing substantial economic and societal damage (Varikoden et al., 2011). Flash floods are of particular concern. However, a contrasting perspective is offered by Vincent and Yusoff (2022), who identify the Southwest Monsoon (SWM) as the season most vulnerable to drought, with a discernible increasing trend in drought severity observed in the southern region. This heightened drought risk is further compounded by climate change, resulting in hotter and drier conditions.

Monsoon rainfall exerts a significant influence on pore water pressure (PWP) within slopes. Increased PWP, resulting from monsoon precipitation, reduces matric suction, thereby contributing to slope instability (Saadatkhah et al., 2015). This effect is particularly pronounced in slopes composed of fine-grained soils, which exhibit lower permeability and higher water retention capacity, making them more susceptible to failure during prolonged rainfall events (Gofar et al., 2008). Furthermore, rainfall-induced erosion can destabilize landscapes, leading to states of unstable equilibrium and resulting in various forms of land degradation, including landslides and mudslides (Bellocchi & Diodato, 2020).

2.5.1 Flood

Climate change is identified as a primary factor contributing to the increased frequency and intensity of extreme rainfall events, directly impacting the occurrence of natural disasters such as floods and landslides (Syafrina, 2017). While flooding is a major natural hazard in Malaysia, the northern region, despite experiencing relatively lower overall rainfall, remains vulnerable due to significant rainfall variability.

Intense rainfall during the intermonsoon and northeast monsoon seasons substantially elevates flood risk in this region (Syafrina, 2017). The devastating floods in the northeast region of Peninsular Malaysia in December 2014 serve as a compelling case study (Pour et al., 2020). This extreme rainfall event resulted in record-breaking flood levels, necessitating the evacuation of 100,000 people and causing substantial economic losses due to widespread damage and disruption of water supply in the capital city and surrounding areas for over a month.



Figure 2.18 Flash Flood events near Relau River Basin, Pulau Pinang.
Source : Analysis of the Flash Flood Event and Rainfall Distribution Pattern on Relau River Basin Development, Penang, Malaysia. (Saad et al., 2023)

The September 2017 flood event in Seberang Perai Tengah, illustrated in Figure 2.18, resulted from intense rainfall exceeding river capacity, causing substantial property damage (Saad et al., 2023). This flash flood impacted several hundred residents across 14 villages, including Taman Guar Perahu, Kubang Semang, Padang Ibu, and Sungai Permatang Rawa (New Strait Times, 2025). Furthermore, the significant contribution of soil erosion to increased flood risk should be considered; approximately 60% of eroded soil is transported into waterways, thereby exacerbating flood potential (Chin et al., 2023).

2.5.2 Slope Failure

The significant landslide events in Penang Island, Malaysia, highlight the region's vulnerability to such disasters. Figure 2.19(a) depicts the Tanjung Bungah landslide (October 21, 2017), resulting in 11 fatalities and attributed to human activities and development. Figure 2.19(b) shows the Bukit Kukus landslide (October 19, 2018), causing 9 deaths, and occurring just one year after the Tanjung Bungah event, underscoring the persistent landslide risk. The frequency of these events is significant, with approximately 28 major landslides recorded in Malaysia between 1993 and 2011.



Figure 2.19 a) Landslide at Tanjung Bungah b) Landslide at Bukit Kukus
Source : Assessing the impact of RCP4.5 and RCP8.5 scenarios on landslide susceptibility mapping using support vector machine: A case study of Penang Island, Malaysia. (Yusof et al., 2024)

Increased water bodies resulting from elevated rainfall contribute to erosion and slope instability, further exacerbating landslide risk (Yusof et al., 2024). This susceptibility to soil erosion and landslides necessitates improved soil and land management practices Atika et al., (2023). Furthermore, water infiltration alters soil properties over time, impacting particle size distribution through the migration and deposition of fine particles (Zhang et al., 2023).

The erodibility index formula (ROM) scale offers a practical approach to assessing soil erodibility, particularly in smaller areas prone to landslides. Its simplicity and speed compared to methods like USLE or RUSLE make it suitable for identifying

high-risk zones (Derahman et al., 2022). This rapid assessment capability is important for prioritizing areas requiring immediate attention.

2.6 Rainfall Trends Analysis

Several methodologies exist for analysing rainfall trends, each possessing inherent limitations. The Degree of Rainfall Amount (DORA) method, as utilized by Vincent and Yusoff (2022), is primarily suited for classifying rainfall intensity but lacks the capacity for robust trend prediction. Similarly, descriptive statistical analyses, encompassing calculations of mean, standard deviation, skewness, kurtosis, minimum, and maximum rainfall values used by Mohtar et al., (2014), can only superficially indicate trend presence without establishing statistical significance. Both approaches fall short in quantifying the magnitude of any detected trends, a limitation overcome by the Mann-Kendall test and Sen's slope estimator.

Alternative approaches include the application of linear regression combined with the Mann-Kendall test for statistically rigorous trend assessment (Syafrina et al., 2015; Khyber et al., 2021). The Mann-Kendall test has also been independently employed (Wong et al., 2018). A more comprehensive approach involves the combined use of the Mann-Kendall test and Sen's slope estimator used at Serbia (latitude 44° 48', longitude 20° 28') providing a more nuanced understanding of both the presence and magnitude of rainfall trends (Gocic & Trajkovic, 2013; Agarwal et al., 2021). This integrated methodology offers a significant advancement in the analysis of rainfall data.

2.6.1 Mann Kendall Test

The Mann-Kendall test stands as a widely employed non-parametric statistical method for evaluating the significance of trends within hydro-meteorological time series data (Gocic & Trajkovic, 2013). Its robustness and applicability to the analysis of temporal trends make it a particularly valuable tool for identifying monotonic patterns within time-series datasets (Agarwal et al., 2021). Specifically designed for the examination of trends in time-series data, the Mann-Kendall test offers a powerful non-parametric approach to discerning directional changes over time (Hashim et al., 2021). This non-parametric nature renders it particularly useful when dealing with data that

may not adhere to assumptions of normality or other distributional characteristics often required by parametric tests. The test's capacity to detect monotonic trends, whether increasing or decreasing, makes it a versatile instrument for analysing a wide range of hydro-meteorological phenomena.

2.6.2 Sen's Slope Estimator

Sen's slope estimator serves as a valuable tool for quantifying the magnitude of change within a water quality trend, providing a measure of the rate of increase or decrease over time (Hashim et al., 2021). This estimator is specifically designed to identify the presence of trends within time-series datasets (Agarwal et al., 2021), offering a robust method for assessing the significance of directional changes. Its widespread application in the analysis of hydro-meteorological time series data highlights its effectiveness in determining the magnitude of observed trends (Gocic & Trajkovic, 2013; Agarwal et al., 2021). The ability to quantify the rate of change, rather than simply detecting the presence of a trend, enhances the analytical power of Sen's slope estimator, providing a more comprehensive understanding of temporal variations in water quality parameters.

Table 2.5

Summary of Mann-Kendall and Sen's Slope result

Station	Kendall's Tau	p-value	Sen's slope
Ldg. Kuala Balah	0.0521	0.3554	0.0113
Kg. Gemang Bahru	0.0093	0.8697	0.0014
Kg. Jeli	-0.1412	0.0121	-0.0272
Kg. Ayer Lanas	-0.0538	0.3395	-0.0538

Source : Rainfall trend analysis using the Mann-Kendall test with pyMannKendall: a case study of Jeli, Kelantan. (Muhammad et al., 2024)

Table 2.5 presents exemplary findings from a prior study by Muhammad et al. (2024) illustrating the application of Mann-Kendall and Sen's slope analyses to rainfall

patterns in an east coast region. The synergistic application of these two non-parametric statistical methods provides a robust approach to identifying and quantifying rainfall trends. Specifically, the Mann-Kendall test establishes the statistical significance of any detected trend (i.e., whether a trend is present), while Sen's slope estimator quantifies the magnitude of that trend (i.e., the rate of change). This combined approach allows for a more comprehensive assessment of rainfall patterns, thereby enhancing the predictive capabilities of the model for forecasting future rainfall behaviour. Muhammad et al. (2024) study leverages the Python programming language, incorporating the 'trend' package, to facilitate efficient and accurate analysis of the rainfall data. Computational approach streamlines the analytical process, allowing for a more focused examination of the results and their implications for future rainfall projections.

2.7 Rainfall Induced Erosion

The amount and intensity of rainfall are critical factors influencing soil erosion, with higher rainfall volumes and more intense rainfall events significantly increasing erosion risk. Several studies have demonstrated a positive correlation between rainfall trends and soil erosivity.

To quantify rainfall erosivity, the Fournier Index and the Modified Fournier Index were calculated using monthly average rainfall data. Mohtar et al. (2015) applied these indices to assess soil erosion potential in Bukit Berapit (05° 22' 32” and longitude 100° 26' 52) and Johor Bahru (latitude 01° 28' 15" and longitude 103° 45' 10"). Their findings, illustrated in Figures 2.20 and 2.21, indicate that soil erosion occurrence in Bukit Berapit is generally low, whereas Johor Bahru experiences years with increased soil erosion risk, which may lead to landslides.

Specifically, the Fournier Index results (Figure 2.20) reveal a relatively small occurrence of soil erosion in Bukit Berapit. In contrast, Johor Bahru exhibits certain years with moderate to severe erosion potential. The Modified Fournier Index (Figure 2.21) further supports these findings, showing that for Johor Bahru, the highest impact category is moderate, accounting for 73.33% of the studied years. Conversely, Bukit Berapit recorded no instances of very high impact, with the majority of years classified as low to moderate impact.

Additionally, the correlation between rainfall trends and soil erosivity was examined using statistical methods, including the Mann-Kendall test and Sen's slope estimator. The study concluded that there is a significant positive correlation between increasing rainfall trends and soil erosivity, reinforcing the importance of rainfall characteristics in soil erosion risk assessments.

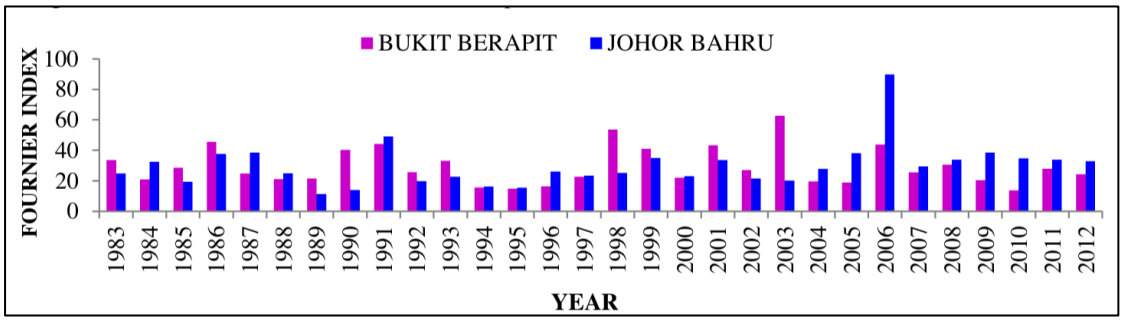

Figure 2.20 Fournier Index Variability 1983-2012

Source : Rainfall erosivity estimation for Northern and Southern peninsular Malaysia using Fourneir indexes. (Mohtar et al., 2015)

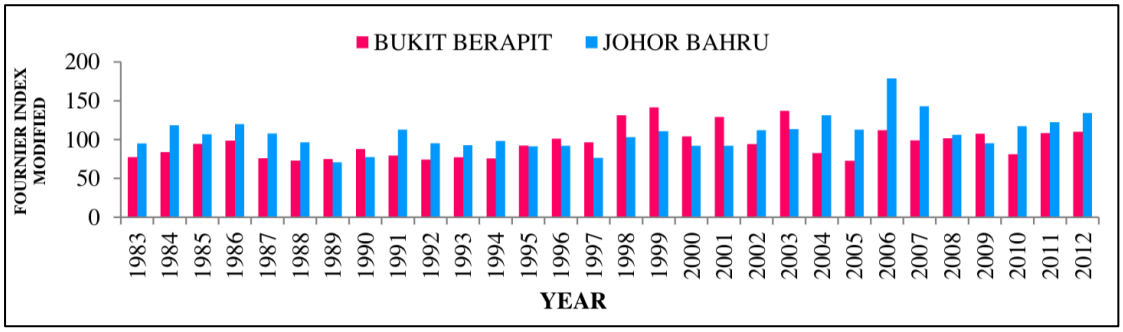

Figure 2.21 Fournier Modified Index Variability 1983-2012

Source : Rainfall erosivity estimation for Northern and Southern peninsular Malaysia using Fourneir indexes. (Mohtar et al., 2015)

While, Atika et al. (2023) calculated the 30-minute maximum rainfall intensity (I_{30}) and rainfall kinetic energy (E) values to estimate the monthly rainfall erosivity factor (R-factor) for each study location and year. Subsequently, they assessed soil erosion risk using the ROSE index, which categorizes erosion risk levels based on the calculated R-factor values, providing a practical framework for evaluating erosion potential.

The study area exhibited high monthly rainfall erosivity (R-factor) values, particularly during months with daily rainfall exceeding 20 mm, consistent with the methodology established by Abidin & Hassan (2005). The calculated R-factor values frequently classified these locations within the "extremely high" and "critical" risk categories of the ROSE index (Table 2.6), underscoring the significant erosion risk in these regions.

Table 2.6

Rainfall Erosivity Category (ROSE Index)

ROSE Index (MJ.mm (ha.h)$^{-1}$	**Category**
<5000	Low
5000-10,000	Moderate
10,000-15,000	High
15,000-20,000	Very High
>20,000	Critical

Source : Soil Erosion Risk in Relation To Rainfall Erosivity in Gunung Alab and Inobong of Crocker Range Park in Sabah, Malaysia. (Atika et al., 2023)

Another method by Abidin and Hassan, (2005) employed to investigate the relationship between rainfall and erosion involves analysing the frequency of erosive rainfall events. Table 2.7 presents the ranking of months with erosive rainfall for Fraser Hill during the period 1997–2001. The data reflect the number of days within each month where daily rainfall exceeded 20 mm, a threshold commonly used to define erosive rainfall.

A key finding from Abidin and Hassan (2005) is the identification of September and November as the months with the highest landslide risk in Fraser Hill. This temporal analysis, integrated with spatial assessment of soil erodibility using the ROM scale, provides critical insights for predicting and mitigating landslide hazards within the study areas.

By correlating the monthly frequency of erosive rainfall events, defined by rainfall exceeding 20 mm per day with the spatial distribution of soil erodibility, able to pinpoint periods and locations exhibiting the greatest combined risk of erosion and landslide occurrence. Specifically, September and November emerged as peak months

for erosive rainfall in Fraser Hill, which, when considered alongside soil susceptibility data, indicated a heightened probability of landslides during these times. A comparable analysis was conducted for Genting Highlands, reinforcing the utility of combining temporal rainfall patterns with soil erodibility assessments to accurately evaluate landslide risk.

Table 2.7

Ranking of Erosive Rainfall according to month for the period of 1997-2001 (Fraser Hill)

Ranking no.	**Month**	**Erosive rainfall frequency**
1	September	24
2	November	23
3	April	19
4	October	17
5	December	17
6	June	16
7	May	14
8	August	13
9	February	12
10	March	12
11	July	10
12	January	8

Source : 'ROM' Scale for Forecasting Erosion Induced Landslide Risk on Hilly Terrain. (Abidin & Hassan, 2005)

There are several methods available to analyze the relationship between rainfall and soil erosion, including the Fournier Index, Modified Fournier Index, and the ROSE Index. Abidin and Hassan (2005) employed a simpler approach by calculating the number of days with rainfall exceeding 20 mm, a threshold derived from previous studies, to identify and analyze rainfall-induced erosion risk.

This method is straightforward and easy to implement, yet it produces results comparable to those obtained from more complex indices. By avoiding intricate

formulas, this approach minimizes potential mathematical errors during analysis while still effectively capturing the critical relationship between rainfall intensity and erosion risk.

2.8 Conclusion

The analysis of Malaysia's rainfall patterns elucidates the impact of the three main monsoon seasons, the northeast monsoon, southwest monsoon, and inter-monsoon. Notably, the inter-monsoon period significantly affects the northern region, particularly the study area of Pulau Pinang, specify on March and October, as indicated by (Syafrina et al, 2017). The weather conditions during this period play a pivotal role in shaping various incidents that can affect the local population. Statistical data from Department of Statistics Malaysia (DOSM., 2024) reveals that approximately 442,985 individuals in the study state area (Seberang Perai Tengah) are susceptible to these weather-related incidents. These findings reinforce the necessity of highlighting key elements for further study and the implementation of suitable mitigation strategies to address the potential risks associated with the intermonsoon season.

Consideration of the implications of rainfall-induced floods and the importance of soil stability, a focused examination of rainfall trend at Permatang Rawa emerges as an important component in providing advance notice to authorities. By leveraging statistical analysis (Mann Kendall and Sen’s Slope), this study can enhance the accuracy of data interpretation and decision-making processes. Through regression analysis, researchers can predict and model rainfall patterns, soil stability, and trend analysis in Permatang Rawa. This predictive modelling can assist in anticipating flood risks, evaluating soil erosion vulnerabilities, and forecasting water flow rates to enable proactive measures in mitigating potential flood impacts.

Furthermore, correlation analysis, can unveil intricate relationships between rainfall patterns, and soil properties, and erodibility index. Correlation analysis can help identify critical variables that contribute to flood risks, and erodibility rates, facilitating informed decision-making and targeted mitigation strategies. This methodical analysis facilitates a profound comprehension of the intricate interplay between rainfall patterns and environmental elements in Permatang Rawa, the flowchart in Figure 2.22 herein

outlines a simplified approach to the literature review, clarifying how this study will bridge the existing gap in scholarly knowledge.

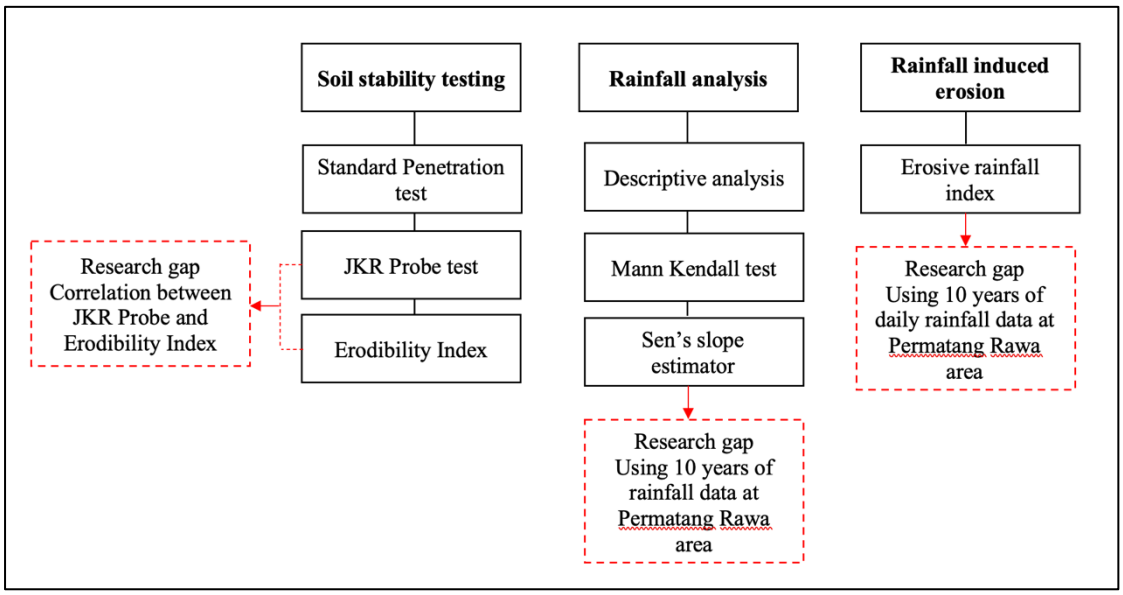

Figure 2.22 Flowchart and Research Gap for this study

CHAPTER 3
METHODOLOGY

3.1. Introduction

This chapter presents the methodology employed in this study, which aimed to investigate the effect of rainfall on soil erodibility along Permatang Rawa Riverbank. The methodology draws upon a combination of established research methods, adapting them to the specific objectives and location suitability of this study. This approach ensures a comprehensive and robust investigation of the relationship between rainfall and the soil erodibility index.

This study aims to determine the soil physical properties, analyse seasonal rainfall trends, and evaluate the relationship between seasonal rainfall and the soil erodibility index along the Permatang Rawa Riverbank. To achieve these objectives, the methodology incorporates several key components, in-situ testing, soil sample collection and analysis of secondary data, and statistical analysis using specialized software. In-situ testing was chosen to provide direct measurements of soil properties and rainfall affect at the study site location. The collection of secondary data, daily rainfall data for 10 years (2014-2024) provided by (Department of Irrigation and Drainage) give a valuable contextual information and allowed for a broader understanding of the study area. Finally, the use of statistical software enabled the analysis of large datasets and the identification of potential relationships between rainfall and soil erodibility index.

This methodology leverages established research practices while incorporating innovative elements to enhance the study's effectiveness. The integration of in-situ testing, secondary data analysis, and statistical software analysis provides a comprehensive and multifaceted approach to investigating the impact of rainfall on soil physical properties at the Permatang Rawa River.

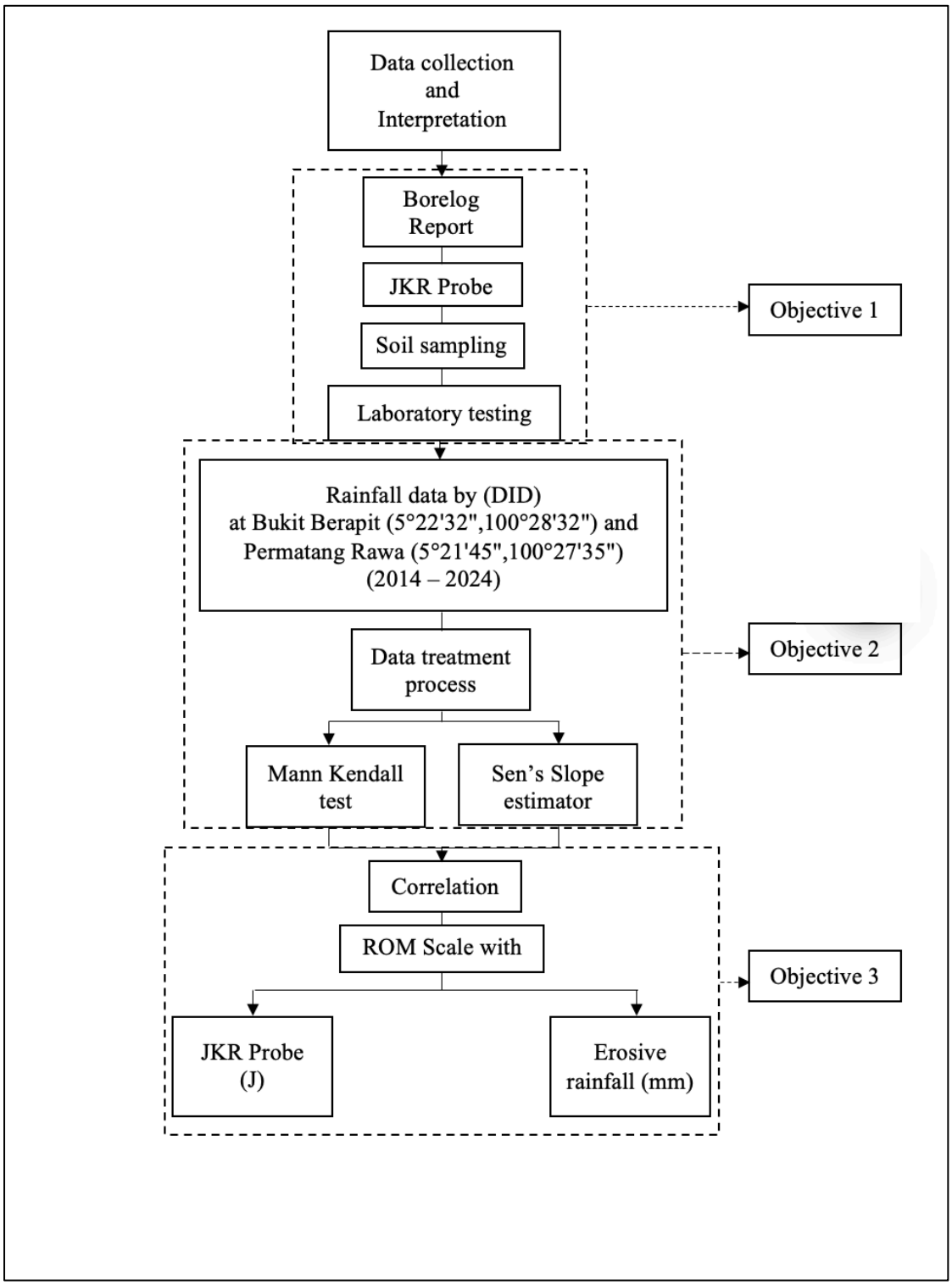

Figure 3.1 Framework of study

3.2 Soil characterization

Figure 3.1 presents the overall framework for achieving the objectives of this study, which will be elaborated upon in the following subtopics. The framework outlines the methodologies applied to address Objectives 1 through 3. Specifically, Figure 3.2 details the process for accomplishing Objective 1, beginning with the sampling and in-situ testing conducted at the study site along the Permatang Rawa riverbank. Upon completion of sampling, the soil samples underwent four types of laboratory tests to analyze their physical properties, including Atterberg limits, particle density, sieve analysis and hydrometer testing. Concurrently, two types of in-situ tests were performed to evaluate soil consistency, JKR Probe and Standard Penetration test (SPT). The results from these tests were then used to correlate the JKR Blow count (J) with the ROM Scale, with the aim of assessing the suitability of the JKR probe tool as an alternative method for predicting ROM Scale values.

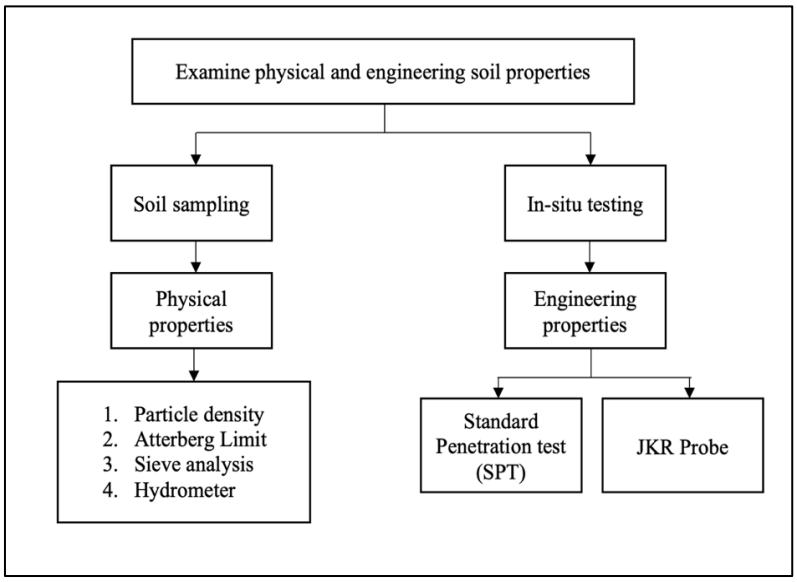

Figure 3.2 Soil Characterization Process

3.2.1 Soil sampling

Manually soil sampling merge with borehole technique in soil sampling following the guidelines of MS1056 (2005), encompassed various tests including Moisture Content, Specific Gravity, Liquid Limit, Plastic Limit, Plasticity Index,

Standard Penetration test and Particle Size Distribution (Hydrometer Analysis). Figure 3.3 show the borehole map at the area and the coordinates for the borehole location listed on Table 3.1.



Figure 3.3 Map of Borehole Location

Table 3.1

Borehole Coordinate

Borehole (BH)	Latitude	Longitude
BH1	5°23'1.90"	100°28'32.10"
BH2	5°23'3.30"	100°28'23.24"
BH3	5°22'48.28"	100°28'11.19"
BH4	5°23'05.4"	100°28'13.6"
BH5	5°23'3.04"	100°28'10.54"
BH6	5°23'02.6"	100°28'09.1"
BH7	5°23'2.88"	100°28'7.71"
BH8	5°23'3.58"	100°28'6.60"
BH9	5°23'0.81"	100°28'5.92"
BH10	5°23'0.74"	100°28'3.97"

Referred by Abidin et al., (2017) methodology, soil sample had been taken along Permatang Rawa riverbank at 10 different location on 2022. To make an additional of

the particle size distribution data, this study chose to conduct physical size distribution analysis at the same location (1m away) from the borehole point. The sampling method employed a hand auger (refer to the figure 3.4a) to extract soil samples for subsequent physical properties analysis at the UiTM laboratory. Sampling was conducted at 0.5m intervals up to a depth of 3.0m, resulting in a total of 6 samples per borehole location (Figure 3.4b). As Abidin et al., (2017) only limit the depth of sampling until 1m depth, this study merge with Zhang et al., (2023) finding where 2-3m depth was also consider as erosion area by rainwater runoff.

Limitations were encountered during subsurface investigation due to unexpected geological conditions. At four borehole locations (2, 4, 6, 7), sampling attempts were unsuccessful, even at 0.5 m depth. At three further locations (8, 9, 10), sampling depths were limited to 1.0 m, 0.5 m, and 0.5 m respectively, likely due to the presence of large aggregate material hindering deeper penetration of the manual hand auger. Only boreholes 1, 3, and 5 achieved the planned 3.0 m sampling depth. As Table 3.1 show quantity of sample that successfully extracted.

The research conducted by Abidin et al. (2017), focusing on erosion analysis by assessing soil physical properties within a 1-meter depth, serves as a fundamental justification for limiting the borehole data collection to a depth of 1.5 meters. However this study will enhance the understanding by exceed the depth of soil sample up to 3.0m. This will further understanding different between 1.5m and 3.0m depth regarding erosion analysis

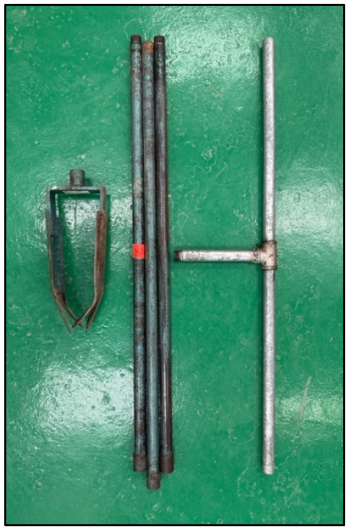

(a)



(b)

Figure 3.4 a) Hand Auger apparatus b) Sampling activity

3.2.2 Physical properties

Each one of the experimental tests was carried out in accordance with the recommendations of BS 1377 (1990). The physical properties of the soil sample were determined to identify and classify.

3.2.2.1 Sample preparation (BS 1377: Part 1:1990)

Collected samples were stored in sealed containers (Figure 3.5a). Disturbed samples were oven-dried to constant mass at 105-110°C. Dried sample were carefully broken down using a rubber pestle (Figure 3.5b) to avoid crushing individual particles, ensuring that sieving retained only individual particles on the specified test sieve.

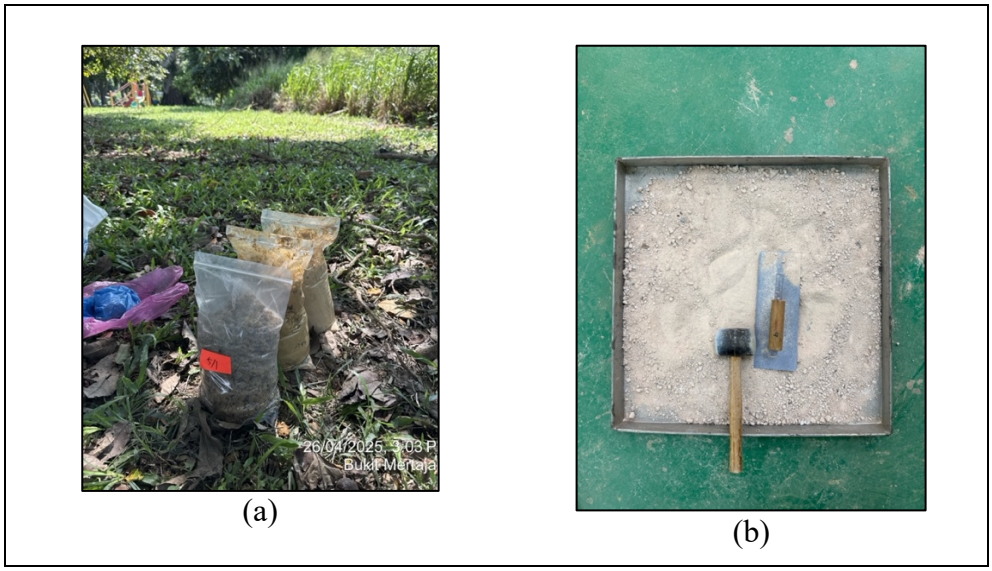

(a) (b)

Figure 3.5 a) Sampling b) Aggregate broken down using Rubber Pestle after oven drying.

3.2.2.2 Moisture content test (BS 1377: Part 2: 1990)

A clean, dry metal container was weighed (m_1) to the nearest 0.01 g (Figure 3.6). Approximately 30 g of soil was added, and the combined weight (m_2) was recorded. The sample was oven-dried at 105-110°C for 24 hours, allowed to cool, and reweighed (m_3). Moisture content (w) was calculated as a percentage of the dry soil mass using the following equation:

$$w = \frac{m_2 - m_3}{m_3 - m_1} \times 100 \quad (3.1)$$



Figure 3.6 Moisture Content Procedure

3.2.2.3 Particle Density method (BS 1377: Part 2: 1990)

The small pycnometer method determines the density of fine-grained soils (<2 mm). Approximately 100 g of soil was sampled, and three 5-10 g subsamples were used. A clean, dry pycnometer (density bottle) and stopper were weighed (m_1). A sample was added, and the weight recorded (m_2) (Figure 3.8a). Distilled water was added to cover the soil, the bottle was then evacuated in a desiccator to remove trapped air (Figure 3.7b). After filling to capacity with air-free water, the bottle was equilibrated in a constant-temperature bath and weighed (m_3). The procedure was repeated with the pycnometer filled only with water (m_4). Density (ρ_s) was calculated using the recorded weights:

$$\rho_s = \frac{\rho_L(m_2 - m_1)}{(m_4 - m_1) - (m_3 - m_2)} \tag{3.2}$$

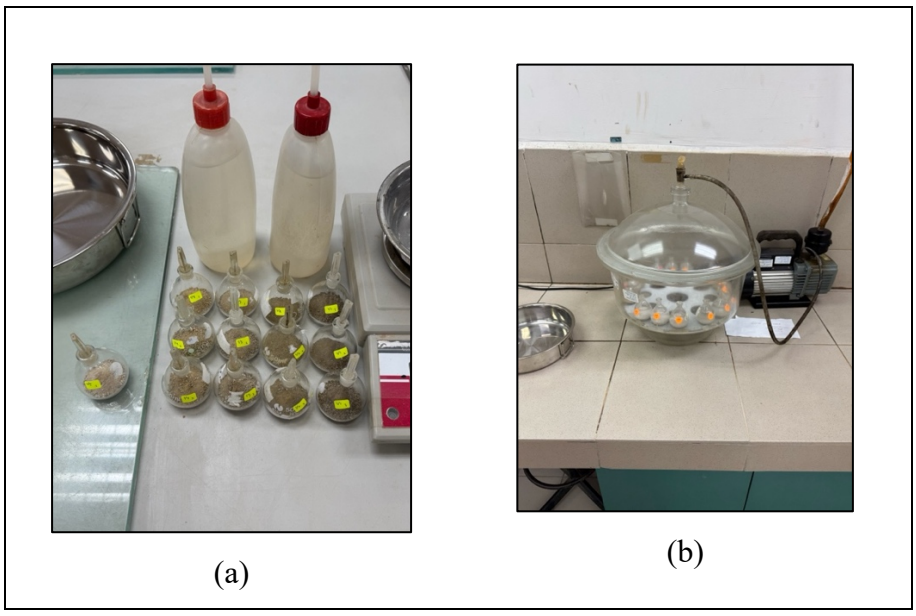

(a) (b)

Figure 3.7 a) Weigh for m_2, b) Soil Sample in Desiccator

3.2.2.4 Liquid Limit (BS 1377: Part 2: 1990)

Soil samples passing 425 µm were oven-dried for at least two hours before testing. A soil paste was prepared, mixing for at least 10 minutes, adding distilled water as needed (Figure 3.8a) to achieve a 10-12 mm initial cone penetration. The paste was placed in the cup, leveled, and the initial cone penetration reading recorded. The cone was released for 5 ± 1 seconds (Figure 3.8b), then removed and cleaned. A moisture content sample (30 g) was taken from the penetrated area. This procedure was repeated five times, adding incremental amounts of distilled water to the same soil sample between each penetration until cone penetration reading reach max 30mm.

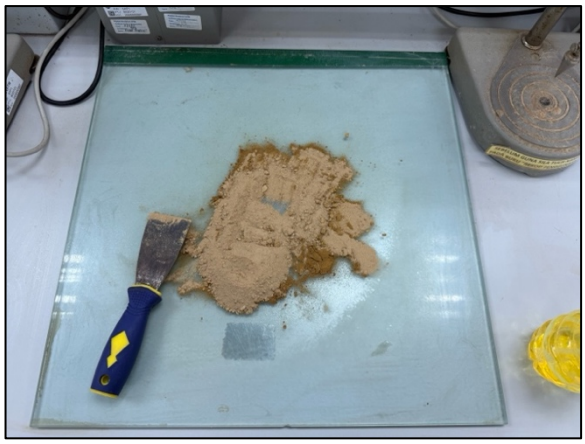

(a)



(b)

Figure 3.8 a) Mixing the sample with Distilled Water, b) Cone Penetration

3.2.2.5 Plastic Limit (BS 1377: Part 2: 1990)

The plastic limit was determined using a soil sample passing 425 µm. Approximately 100 g of soil was mixed with distilled water (Figure 3.9a) until it became plastic. The soil was then rolled into a 6 mm diameter thread, repeatedly rolled until a 3 mm diameter as shown in Figure 3.9b was achieved using consistent pressure. The crumbled thread was collected, and the moisture content (minimum 30 g) was determined to the nearest whole number, representing the plastic limit.

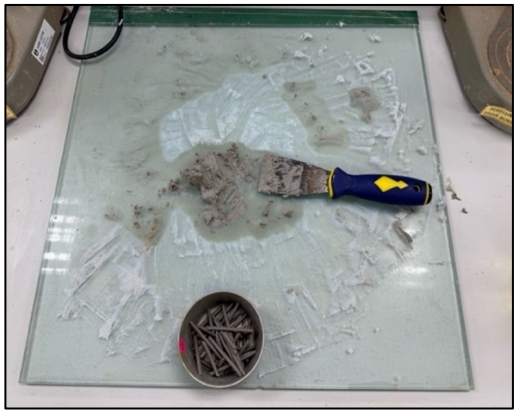

(a)



(b)

Figure 3.9 a) Mixing the sample with Distilled Water
b) After rolling the sample until it crack

3.2.2.6 Particle Size Distribution (Sieve Analysis) and Hydrometer Test (BS 1377: Part 2: 1990)

Procedure for hydrometer test start with, a 100 g soil sample was dispersed in 100 mL of dispersant solution overnight. The suspension was sieved (63 µm), and the material retained was oven-dried (105-110°C), re-sieved (using dry sieve method), and weighed. The material passing the 63 µm sieve was added to a 1 L cylinder (Figure 3.10a) and filled to volume with distilled water. After equilibration in a constant-temperature bath, the suspension was shaken vigorously and hydrometer readings were taken at 0.5, 1, 2, 4, 8, 15, 30, 60, 120, 240, 480, and 1440 minutes. The hydrometer was rinsed from 8 minutes until 1440 minutes readings.

Next, for dry sieving method, the soil sample was sieved using a nested set of sieves (Figure 3.10b), starting with the largest appropriate size. The sample was agitated to allow particles to pass through the sieve under gravity alone; particles were only allowed to pass if they fell through unaided. The mass retained on each sieve was recorded to the nearest 0.1%. This process was repeated sequentially with progressively smaller sieves.

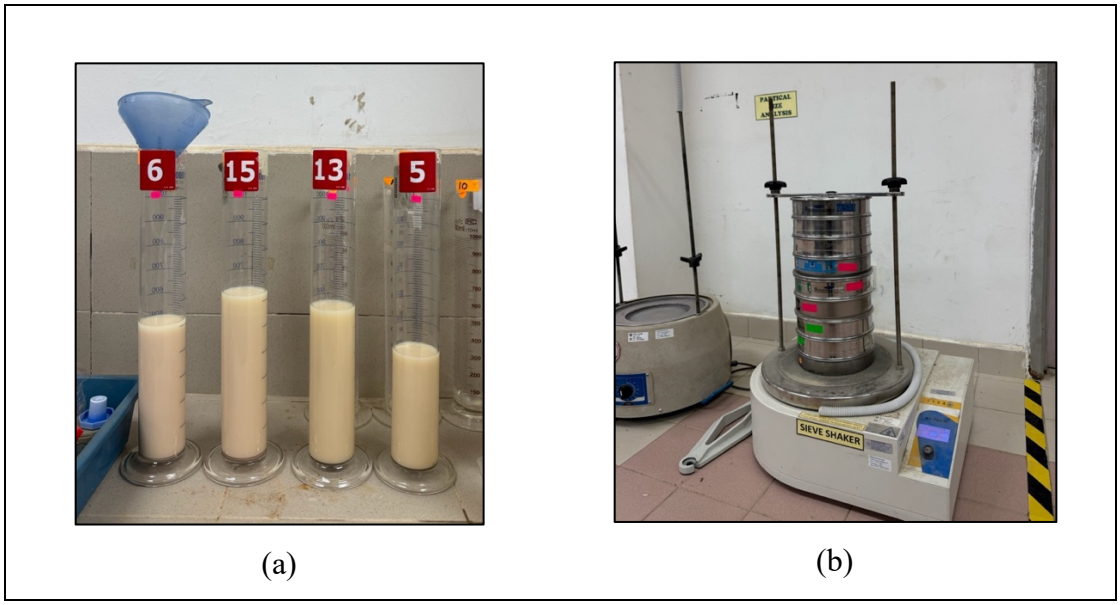

(a) (b)

Figure 3.10 a) Hydrometer Test b) Dry Sieving Method

3.2.3 Engineering Properties

3.2.3.1 JKR Probe

Adapt from Mackintosh probe test to align with the local (Malaysia) soil conditions for determining the bearing capacity. The testing locations will be conduct at 1-2 meters away from 10 borehole location. Figure 3.11 illustrate the apparatus will be use during conduct that In-situ testing.



Figure 3.11 JKR Probe Apparatus

In preparation for the test, the equipment is meticulously assembled, with the cone diameter being measured in the SI unit system. The boring rods and hammer are securely joined using rod couplings, ensuring stability during testing, and grease is applied to facilitate easy disassembly at a later stage. Subsequently, 0.3 meters is precisely measured and marked on the rod from the tip of the cone before positioning the equipment on the ground for testing.



Figure 3.12 JKR Probe Testing.

The operational phase commences with the hammer being raised to its maximum height and then released to drive the cone into the soil (Figure 3.12). The number of blows required for each 0.3-meter penetration is carefully recorded in the data sheet to track the progress accurately. The rod is continuously extended until either the number of blows exceeds 400 for a 0.3-meter penetration or the depth reaches 15 meters, indicating the completion of the test (MS2038:2006). Referred from (Sabri et al., 2022), depth of probe only reach until 1.5m. For this study, depth of probe reached until 3.0m to correlate with sampling depth, thus correlation between JKR probe and soil erodibility obtained.

3.2.3.2 Standard Penetration Test (SPT)

The in-situ testing was carried out in 2022 for analysing soil strength, which will subsequently be utilized as a variable to investigate its correlation with the erodibility index. It was an additional data in comparison to JKR probe blow (J).

3.3 Seasonal Trend

Rainfall data from the years 2014 until 2024 was obtained from Department of Irrigation and Drainage for stations 0070021RF (Kolam Air Bukit Berapit) and 0070031RF (Permatang Rawa). Location for those two locations is illustrated in Figure 3.13.

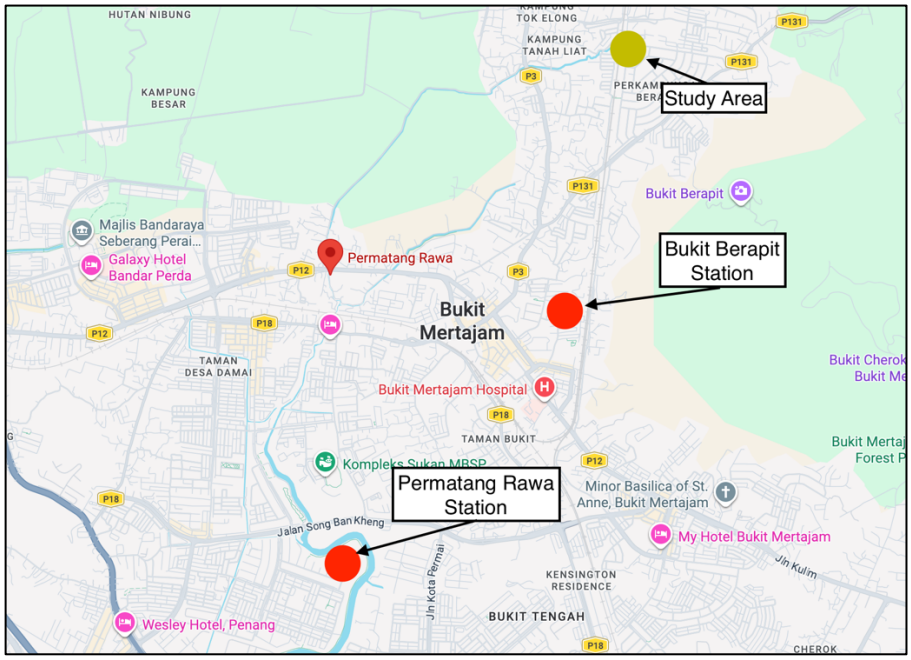

Figure 3.13 Location of Rainfall Station

3.3.1 The Descriptive Statistics Analysis

Descriptive statistics play a vital role in this study by providing essential insights into the data. These statistics offer concise summaries of both the sample and the

measurements, forming the cornerstone of quantitative data analysis alongside graphical representations. They serve as brief descriptive measures that summarize a given dataset, whether it represents the entirety or a sample of a population. Descriptive statistics are categorized into measures of central tendency, such as the mean, median, and mode, and measures of variability, including the standard deviation, variance, minimum and maximum values, as well as kurtosis and skewness. Statistical Product and Services Solution (SPSS 29) software was utilized to derive these statistical descriptions. The descriptive statistics employed in this study encompass maximum, minimum, median, mean, mode, variance, standard deviation, skewness and kurtosis.

3.3.1.1 Minimum and Maximum

The minimum value represents the smallest value within the dataset, being significantly lower than or equal to all other values present. On the other hand, the maximum value denotes the largest value of the variable, surpassing or equalling all other values within the dataset (Piliposyan, 2018).

3.3.1.2 Median

The median is characterized as the middlemost observation when data are organized in either ascending or descending order of magnitude. Consequently, it represents one of the observations occupying a central position within the data distribution. Referred to as the positional average, the median remains unaffected by extreme values (outliers) (Mishra et al., 2019).

$$\text{If n is odd, median} = X_{\left[\frac{(n+1)}{2}\right]} \tag{3.3}$$

$$\text{If n is even, median} = X_{\left[\frac{\left(\frac{n}{2}\right)+\left(\frac{n}{2}+1\right)}{2}\right]} \tag{3.4}$$

3.3.1.3 Mean

The mean represents the arithmetic average value derived from a dataset. Computed by summing all observations and dividing by the total number of observations, it stands as a widely used and easily calculable measure. Being a singular value for a particular group, it provides a distinct and definitive answer, particularly beneficial for group comparisons. In mean calculation, all observations are considered in the process (Mishra et al., 2019).

$$\bar{x} = \frac{\sum_{i=1}^{n} x_i}{n} \tag{3.5}$$

3.3.1.4 Mode

The mode signifies the value that appears most frequently within a set of observations, denoting the observation with the highest frequency (Mishra et al., 2019). To determine the mode, data is organized and tallied to ascertain the frequency of each outcome. The value with the highest frequency is identified as the mode of the dataset (Yahaya et al., 2008).

3.3.1.5 Skewness

Skewness measures the extent of asymmetry within a distribution, indicating the degree to which it is skewed either to the left or right (Bono et al., 2019). It evaluates the symmetry of a variable's distribution, identifying whether the distribution leans towards the right or left tail. Such distributions are described as skewed if they exhibit pronounced stretching towards one tail of the distribution (Hair et al, 2017).

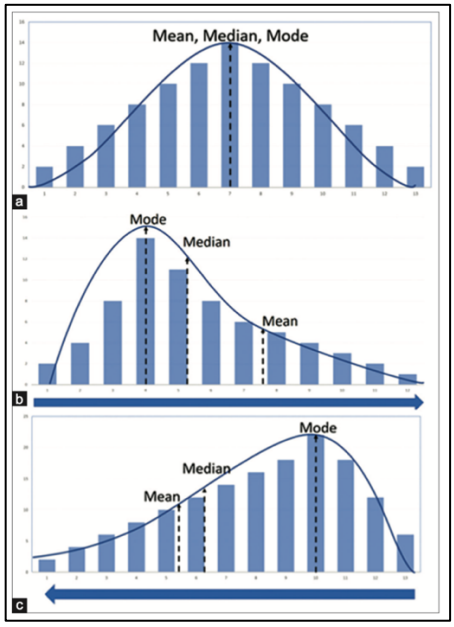

Figure 3.14 Normal and Skewed Distribution of the data. (a) Normal Distribution. (b) Positive Skew. (c) Negative Skew.
Source: Descriptive Statistics. (Kaur et al, 2018)

As previously demonstrated, the shape of the data distribution can impact the measures of central tendency. In a symmetrical distribution (resembling a "bell-shaped" curve), the mean, median, and mode all align at the center [Figure 3.14(a)]. In cases of positive skew where the distribution leans towards lower values, the mode retains its position as the most frequent value, the median remains in the middle, but the mean shifts towards the right tail of the distribution [Figure 3.14(b)]. Conversely, in instances of negative skew where the distribution tilts towards higher values, the mean shifts towards the left tail of the distribution [Figure 3.14(c)] (Kaur et al, 2018).

$$S = \frac{1}{n-1}\sum_{i=1}^{n}\left(\frac{x_i - \bar{x}}{s}\right)^3 \tag{3.6}$$

3.3.1.6 Kurtosis

Kurtosis pertains to the characteristics of distribution tails, encompassing their length and weight (Bono et al., 2020). Furthermore, kurtosis involves comparing the distribution of a dataset to that of a normal distribution. High or positive kurtosis

indicates data with heavier tails or outliers, while low or negative kurtosis suggests lighter tails without outliers (Figure 3.15) (Kaur et al, 2018).

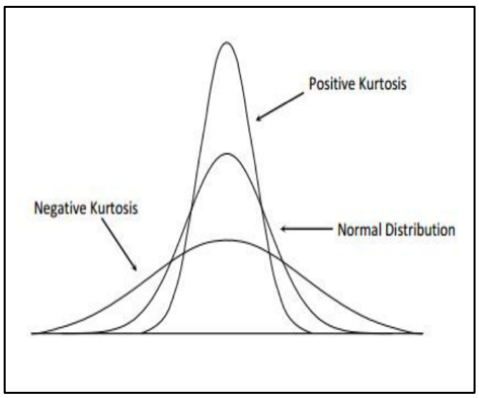

Figure 3.15 Presentation of the different types of Kurtosis.
Source: Normality Testing Methods and The Importance of Skewness and Kurtosis in Statistical Analysis (Hatem et al., 2022)

$$K = \frac{1}{n-1}\sum_{i=1}^{n}\left(\frac{x_i - \bar{x}}{s}\right)^4 \tag{3.7}$$

3.3.1.7 Variance

Variance utilizes data from each individual within the sample to evaluate the dispersion of scores concerning the sample mean. It gauges the average squared deviation of each score from the sample mean (Cooksey, 2020).

$$S^2 = \frac{\sum_{i=1}^{n}(x_i - \bar{x})^2}{n-1} \tag{3.8}$$

3.3.1.8 Standard Deviation

The standard deviation, frequently denoted as SD, sd, or Std. Dev., stands as the most commonly cited indicator of variability due to its meaningful interpretation and its association with sample mean reports. Variance and standard deviation are closely intertwined metrics, as the standard deviation is derived by taking the square root of the variance (Cooksey, 2020).

$$S = \sqrt{\frac{\sum_{i=1}^{n}(x_i - \bar{x})^2}{n-1}} \tag{3.9}$$

3.3.2 Data Treatment

From figure 3.16, show how this study go through data treatment process. For detection on outlier will be through boxplot method with three different type of interval calculation, Interquartile range (IQR), Semi Interquartile Range (SIQR) and lastly, Robust skewness using Medcouple (MC). From each of this process after neglect the outiler will be go through three different method of replacing missing value, Regression Imputation, Mean Method and Linear Interpolation. Selection of good data is based on the performance indicator as (Comparison of Linear Interpolation Method and Mean Method to Replace The Missing Values in rainfall data Set) did. With the lowest MAE and RMSE, and highest R2 are consider as most suitable data for further analysis with less biased and good performance. Data used for this process is monthly sum (MS) and monthly average (MA) for 128 months or 10 years 8 months at two different rainfall station, Bukit Berapit and Permatang Rawa.

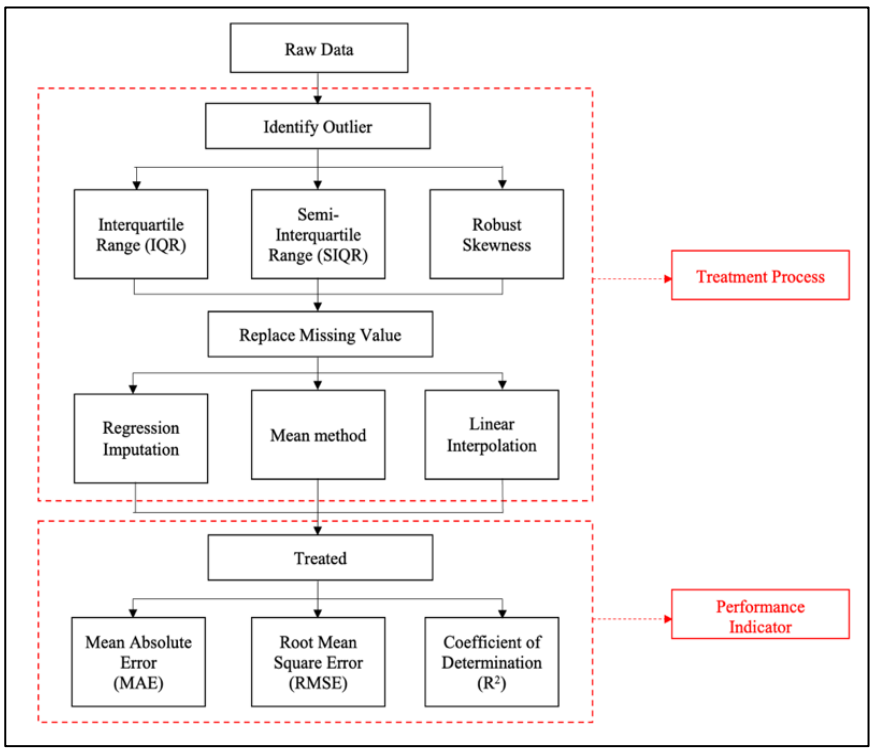

Figure 3.16 Data Treatment Process

3.3.2.1 Identify Outlier

Outliers, defined as data points significantly distant from the rest of the dataset, can exert a substantial influence on the analysis outcomes (Dash et al., 2023). The utilization of outlier detection methods aids in uncovering overlooked characteristics that traditional statistical and mathematical models may miss. Particularly in the examination of rainfall data, outlier detection techniques play a pivotal role in scrutinizing the dataset and identifying extreme values that could impact result accuracy (Hael & Yuan, 2020). Among the frequently employed nonparametric approaches for detecting outliers in univariate datasets is the utilization of boxplots as a foundational concept (Zhao & Yang, 2019). Those are methods was used in identify outlier:

i. Interquartile Range (IQR)

If an observation falls outside the range defined by the lower (q1 - 1.5*IQR) and upper (q3 + 1.5*IQR) quartiles, it is deemed a "potential" abnormal data point. Here, q1 and q3 represent the first and third quartiles, respectively (Zhao & Yang, 2019).

$$IQR = q_3 - q_1 \tag{3.10}$$

$$Lower = (q_1 - 1.5(IQR)) \tag{3.11}$$

$$Upper = (q_3 + 1.5(IQR)) \tag{3.12}$$

ii. Semi-Interquartile Range (SIQR)

In practice, real hourly rainfall observations often exhibit non-normal or asymmetric distributions. When utilizing the standard boxplot for these observations, the proportion of data points falling outside the conventional boxplot fence tends to be unacceptably high. To address this issue, various adjusted boxplot techniques have been introduced specifically for skewed data distributions. Kimber (1990) proposed employing the semi-interquartile range (SIQR) in place of the IQR, where the SIQR boxplot's fence is defined as q1 - 3 * (q2 - q1) and q3 + 3 * (q3 - q2). The application of the SIQR boxplot has proven beneficial in analysing real hourly rainfall data (Zhao & Yang, 2019).

$$Lower = (q_1 - 3(q_2 - q_1) \quad (3.13)$$

$$Upper = (q_3 + 3(q_3 - q_2) \quad (3.14)$$

iii. Robust Skewness (Medcouple)

Zhao and Yang (2019) introduced a novel boxplot methodology designed to be resilient against outliers while maintaining sensitivity to skewness. To enhance accuracy and reduce the potential for human error in calculations, the analysis was conducted using R programming. Specifically, the "robustbase" package was utilized for Medcouple calculation, showcasing the software's capability in handling complex statistical computations.

$$MC = \underset{p_i \le m \le p_j}{med} h(p_i, p_j) \quad (3.15)$$

$$h(p_i, p_j) = \frac{(p_j - m) - (m - p_i)}{(p_j - p_i)} \quad (3.15a)$$

m = Median

$p_i \& p_j$ = The observations in the dataset

$$p_i < m < p_j \quad (3.15b)$$

$$q\alpha = q_{0.0035} \quad (3.16)$$

$$q\beta = q_{0.9965} \quad (3.17)$$

Manual Calculation:

$$ln(\frac{2}{3}\frac{q_1 - q_\alpha}{IQR}) \approx gMC \quad (3.18)$$

$$ln(\frac{2}{3}\frac{q_\beta - q_3}{IQR}) \approx fMC \quad (3.19)$$

Research conducted by Zhao and Yang (2019) determined that the exponential function provides the highest level of accuracy when incorporated into the development of a novel boxplot methodology.

$$f_l(MC) = 1.5e^{gMC} \quad (3.18a)$$

$$f_u(MC) = 1.5e^{fMC} \quad (3.19a)$$

$$Lower = (q_1 - f_l(MC) * IQR) \quad (3.20)$$

$$Upper = (q_3 - f_u(MC) * IQR) \quad (3.21)$$

3.3.2.2 Replace Missing Value

The presence of missing data poses a common challenge in hydrological studies, underscoring the critical need for data reconstruction to leverage all available resources, even with incomplete records. Hamzah et al. (2021) highlight that missing data can significantly impact statistical analysis outcomes, leading to unpredicted variability in the dataset. Addressing this issue is crucial as incomplete datasets may introduce bias through systematic disparities between observed and unobserved data, emphasizing the importance of accurately estimating missing values for ensuring data quality (Noor et al., 2015). In their research, Hamzah et al. (2021) demonstrated that regression imputation yielded the lowest Root Mean Square Error (RMSE) and Mean Absolute Percentage Error, prompting the adoption of this method for handling missing values. Moreover, while Noor et al. (2015) previously employed mean series and linear interpolation for replacing missing values, this study intends to utilize a combination of three methods, regression imputation, mean method, and linear interpolation to address missing data comprehensively.

i. Regression Imputation (Wang & Hu, 2022).

$$\bar{y} = \beta_0 + \beta_1(Y_b) + \beta_2(Y_j) + \varepsilon \quad (3.22)$$

$\bar{y}$ = The imputed value

β_0 = The intercept term of the regression model.

β_1 = The coefficient for the baseline value (Yb).

β_2 = The coefficient for the last on-treatment

Y_b = The baseline value of the primary endpoint

Y_j = The value of the primary endpoint at the last on-treatment visit.

ε = The random error term.

ii. Series of mean (Yahaya et al., 2005)

$$\bar{y} = \frac{1}{n}\sum_{i=1}^{i=n} y_i \tag{3.23}$$

$\bar{y}$ = The imputed data

n = The number of data point

y_i = The value of ith value

iii. Linear interpolation (Chapra and Canale, 1998)

$$f(x) = f(x_0) + \frac{f(x_1) - f(x_0)}{x_1 - x_0}(x - x_0) \tag{3.24}$$

$f(x)$ = The value of the function at the point x.

$f(x_0)$ & $f(x_1)$ = The known values of the dependent variable at x0 and x1, respectively.

x = The independent variable.

x_0 & x_1 = The known values of the independent variable.

3.3.2.3 Performance indicator

Multiple performance indicators were employed to evaluate the effectiveness of imputation methods, as studied by Hamzah et al. (2021) and Noor et al. (2015). A comparison between theoretical and observed data was conducted to identify the optimal approach for estimating missing values. The assessment utilized three key performance metrics: mean absolute error (MAE), root mean squared error (RMSE), and coefficient of determination (R2). The method yielding the lowest MAE and RMSE, along with the highest R2 value, was deemed most suitable for trend analysis.

i. Mean Absolute Error (Junninen et al., 2002)

$$MAE = \frac{1}{N}\sum_{I=1}^{N}|P_i - O_i| \tag{3.25}$$

N = The number of imputations

P_i = The imputed data point.

O_i = The observed data points

ii. Root Mean Squared Error (Junninen et al., 2002)

$$RMSE = \left(\frac{1}{N}\sum_{i=1}^{N}[P_i - O_i]^2\right)^{\frac{1}{2}} \tag{3.26}$$

N = The number of imputations

P_i = The imputed data point.

O_i = The observed data points

iii. Coefficient of Determination (R^2) (Junninen et al., 2002)

$$R^2 = \left[\frac{1}{N}\frac{\sum_{i=1}^{N}[(P_i - \overline{P})(O_i - \overline{O})]}{\sigma_P \sigma_O}\right]^2 \quad (3.27)$$

N = The number of imputations

P_i = The imputed data point.

O_i = The observed data points

$\overline{P}$ = The average of imputed data.

$\overline{O}$ = The average of observed data.

σ_p = The standard deviation of the imputed data.

σ_o = The standard deviation of the observed data.

3.3.3 Time Series Plot

A time series plot is a graphical representation where time serves as the unit on the x-axis, commonly designated as the time-axis. The y-axis corresponds to the variable under examination, with data points plotted and typically linked by straight lines, facilitating the analysis of the generated graph. In a recent investigation, the total rainfall data spanning from January 2014 to August 2024 across two stations was utilized for this plot. Specifically, the plot aimed to monitor the monthly cumulative rainfall pattern in Seberang Perai Tengah, Pulau Pinang. To enhance clarity and insights, regression lines were incorporated into the plot for further analysis.

3.3.4 Trend Analysis

Figure 3.17 shows the trend analysis process, to minimize mathematical errors, the study will incorporate R programming, utilizing the Mann-Kendall and Sen's Slope estimator (trend) packages to automatically compute the trend values based on the processed rainfall data. Transitioning from the conventional method of Microsoft Excel to R Programming will enhance the accuracy and efficiency of trend analysis.

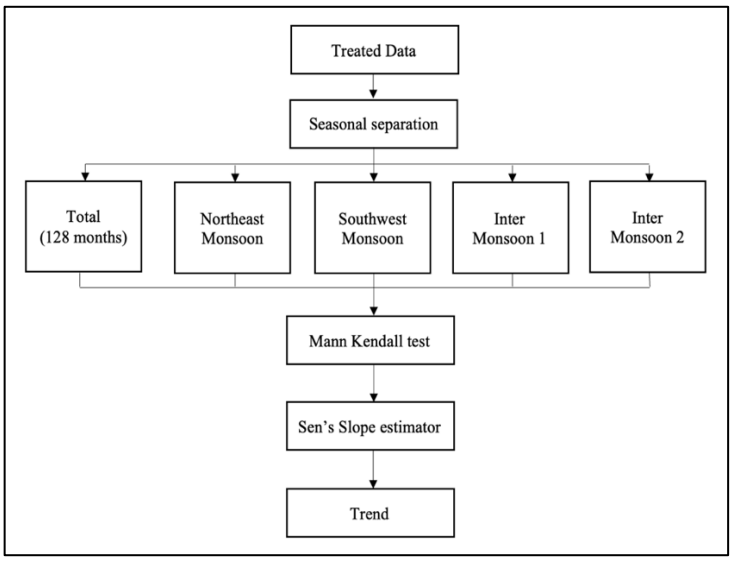

Figure 3.17 Trend Analysis Process

3.3.4.1 Mann Kendall Test (MK)

The Mann-Kendall (MK) test is a robust method for analysing trends in time series data, particularly effective in detecting monotonic trends. Despite the presence of outliers, often associated with extreme rainfall events, the test relies on the analysis of positive or negative signs, making it suitable even for random variables. To detect trends in time series data, the MK statistic (S) is calculated as follows.

$$S = \sum_{i=1}^{n-1} \sum_{j=i+1}^{n} \text{sign}(x_i - x_j) \tag{3.28}$$

'x_j & x_j' are sequential data for i^{th} and j^{th} terms

'n' is the sample size

$$\text{sign}(x_i - x_j) = \{+1, \text{if}(x_i - x_j) > 1\} \tag{3.28a}$$

$$\text{sign}(x_i - x_j) = \{0, \text{if}(x_i - x_j) = 0\} \tag{3.28b}$$

$$\text{sign}(x_i - x_j) = \{-1, \text{if}(x_i - x_j) < 1\} \tag{3.28c}$$

Variance (S) is:

$$\mathrm{Var(S)} = \frac{1}{18}[[\mathrm{n(n-1)(2n+5)}] - \sum_{\mathrm{p=1}}^{\mathrm{n}} \mathrm{t_p(t_p-1)(2t_p+5)}] \tag{3.29}$$

q & t_p are the tied group numbers

p^{th} is group data value numbers

The Z-statistic is computed as

$$\mathrm{Z} = \frac{\mathrm{S-1}}{\sqrt{\mathrm{Var\ (S)}}} \tag{3.30}$$

$$\mathrm{Z} = 0 \tag{3.31}$$

$$\mathrm{Z} = \frac{\mathrm{S+1}}{\sqrt{\mathrm{Var\ (S)}}} \tag{3.32}$$

If the calculated Z-statistic is negative, the trend is considered decreasing, while a positive Z-statistic indicates an increasing trend. The trend is determined based on whether the computed Z-statistic surpasses or falls below the critical z-value corresponding to the 5% significance level. In the scenario where the computed Z-statistic equals zero, it signifies the absence of any discernible trend.

3.3.4.2 Sen's Slope estimator (SSE)

In analysing trends within specific time series datasets, a slope estimator (m_{ij}) is utilized, representing the median across all dataset combinations. A positive value of (m_{ij}) signifies an upward trend, while a negative value indicates a downward trend. The calculation of the slope (m_{ij}) is determined by the following formula.

$$M_i = \frac{(Yj - Yi)}{(J - 1)} \tag{3.33}$$

Y_j & Y_i are the time values at time 'j' and 'i' (j>i)

The Sen's estimator slope is the median of these 'N' values of 'm_{ij}'. The Sen's slope is calculated using the following equation

$$m = m[\frac{N + 1}{2}] \tag{3.34}$$

$$m = \frac{1}{2}[\frac{N}{2} + \frac{N + 1}{2}] \tag{3.35}$$

3.4 Soil erodibility index

The acquired physical properties data, obtained through secondary data collection methods, will serve as inputs for the analysis of soil stability index using the ROM Scale equation. Size distribution parameters, will provide valuable insights into the stability of the soil under investigation.

$$EI_{ROM} = \frac{\%sand + \%silt}{2(\%clay)} \tag{3.36}$$

Table 3.2
Erodibility Category

'ROM' Scale	Soil erodibility category
<1.5	Low
1.5 – 4.0	Moderate
4.0 – 8.0	High
8.0 – 12.0	Very high
>12.0	Critical

Source: Establishment of Soil Erosion Scale With Regards to Soil Grading Characteristic. Roslan & Mazidah (2002)

For analyse the erodibility index, this study utilise formula made by Roslan and Mazinah (2002) who was a local researcher that had produced ROM scale formula to calculate the erodibility index. Table 3.2 as indicator to categorize the erodibility level. The formula as above.

3.4.1 Correlation

In examining the relationship between two variables, this study employs the Pearson correlation coefficient. Adler (2009) demonstrated that this method is the most accurate for assessing such relationships.

$$r = \frac{\sum(R_i - R_{av}) * (G_i - G_{av})}{\sqrt{\sum(R_i - R_{av})^2 * \sum(G_i - G_{av})^2}} \quad (3.37)$$

r = Pearson correlation coefficient

R_i = Value of independent variables

R_{av} = Average value of independent variables

G_i = Value of dependent variables

G_{av} = Average value of dependent variables

In this study, the analysis focused on exploring the relationship between Erodibility Index (EI) with JKR Probe (J).

CHAPTER 4

RESULT AND DISCUSSION

4.1 Introduction

This chapter integrates the findings of preceding chapters, commencing with an analysis of rainfall patterns across seasonal periods, derived from data collected at two distinct rainfall stations. Soil physical properties, determined through laboratory testing conducted in 2022 and 2025, are incorporated into the analysis, supplemented by in situ measurements obtained via Standard Penetration Tests (SPTs) and JKR probe tests.

The second research objective is addressed through a rigorous statistical analysis of ten years of rainfall data. This analysis encompasses data pre-processing, trend identification, and the evaluation of significant temporal variations. The concluding section investigates the correlations between the erodibility index with JKR probe values, and further contextualizing these relationships with rainfall data.

4.2 Soil characterization

This section presents the results obtained from the analysis of physical and mechanical properties, including laboratory testing, in situ testing, and the calculation of soil erodibility using the ROM scale formula.

4.2.1 Physical Properties

The data presented from (2022) in the table 4.1 indicates that locations BH4 and BH10 exhibit the highest percentage of clay content, highlighting the significant presence of clay as a predominant element influencing erosion activity in these areas, stated previous study by (Abidin et al., 2017). The clay content is greatest, yet indications of erosion are minimal (Zhang et al., 2023). Clay, known for its cohesive properties, plays a crucial role in soil erosion processes due to its ability to form a dense network that can impede water infiltration and exacerbate surface runoff. Conversely,

locations BH2, and BH7 display the lowest clay percentage among the observed sites. This lower clay content in these locations suggests a contrasting scenario where the soil may be more susceptible to erosion due to the reduced cohesive properties of clay.

Table 4.1

Physical Properties (2022)

No.	Depth (m)	MC (%)	Specific Gravity	Atterberg Limit (%)			Particle size distribution (%)		
				LL	PL	PI	Clay	Sand	Silt
BH1	1.5	18	2.58	52	22	30	16	64	10
	3.0	-	-	46	22	24	26	52	15
BH2	1.5	21	2.6	17	12	5	1	97	2
	3.0	-	-	30	16	14	1	98	1
BH3	1.5	19	2.56	50	21	29	23	67	9
	3.0	-	-	68	27	41	20	69	9
BH4	1.5	29	2.57	59	26	33	44	32	24
	3.0	-	-	65	28	37	42	29	29
BH5	1.5	-	-	88	37	51	26	63	10
	3.0	-	-	79	33	48	23	64	10
BH6	1.5	20	2.6	86	35	51	21	66	10
	3.0	-	-	-	-	-	21.6	64.38	10
BH7	1.5	-	-	25	20	5	2	81	3
	3.0	-	-	22	15	7	4	84	2
BH8	1.5	-	-	18	16	2	7	81	10
	3.0	31	2.57	36	24	12	55	13	32
BH10	1.5	-	-	75	19	56	49	24	27
	3.0	21	2.58	39	19	20	46	26	28

Table 4.2 explain the variety of physical properties after sampling activity in 2025. It shows deeper depth have high percentage of moisture content because of existing of water table underground, even some result show upper level has higher moisture content may because of rate of rainfall seep into the soil. In comparison with previous lab testing (Table 4.1) have some significant different in term of particle size

distribution that play a crucial role in identifying the erodibility index, for example borehole 5 at depth 1.5m, in 2022 in contains 26% of clay but recent testing it decrease the amount of clay (6.49%). As mentioned, hydraulic erosion, which can modify soil characteristics such as particle size distribution(Zhang et al., 2023).This different it can be relate to the rainfall pattern throughout 3 years that made the soil degradation.

Table 4.2

Physical Properties (2025)

No.	Depth (m)	MC (%)	Specific Gravity	Atterberg Limit (%)			Particle size distribution (%)		
				LL	PL	PI	Clay	Sand	Silt
BH1	0.5	10.01	2.49	39	20	13	2.6	58.17	5.49
	1.0	20.76	2.49	44	28	16	33.18	51.81	6.84
	1.5	15.03	2.44	32	22	10	22.03	51.24	10.74
	2.0	15.78	2.56	40	23	17	25.94	56.41	7.18
	2.5	34.26	2.52	46	26	20	21.48	54.15	6.99
	3.0	28.57	2.53	41	23	18	16.38	61.45	2.99
BH3	0.5	27.47	2.4	43	24	18	23.91	66.47	5.95
	1.0	27.29	2.4	43	23	19	22.26	60.93	7.08
	1.5	30.79	2.37	45	24	21	31.11	56.33	6.33
	2.0	24.45	2.53	40	21	19	23.13	69.27	3.51
	2.5	31.38	2.44	42	22	19	28.47	60.72	8.09
	3.0	31.79	2.41	56	29	27	30.67	62.68	4.50
BH5	0.5	23.16	2.46	46	24	22	24.91	24.66	50.43
	1.0	29.21	2.51	50	15	35	18.53	68.81	12.66
	1.5	32.62	2.6	49	27	22	6.49	41.34	52.22
	2.0	34.53	2.54	52	30	23	8.13	40.13	51.75
	2.5	49.59	2.5	58	34	24	12.78	30.23	56.99
	3.0	40.91	2.49	63	37	26	28.61	62.93	8.46
BH8	0.5	20.06	2.27	60	36	24	50.02	32.22	6.67
	1.0	18.89	2.32	29	18	11	20.41	52.13	18.01
BH9	0.5	20.49	2.26	41	28	13	14.35	52.61	16.05
BH10	0.5	12.59	2.38	33	20	13	11.93	51.11	18.69

As noted in the methodology section, limitations encountered during the sampling process prevented the comparison of all borehole (BH) locations between the years 2022 and 2025. Specifically, at depths of 1.5 m and 3.0 m, only boreholes BH1, BH3, and BH5 could be reliably compared. Figures 4.1 and 4.2 present the comparative analysis of Atterberg limits, and Particle size distribution, respectively, for these boreholes at the specified depths over the two sampling years.

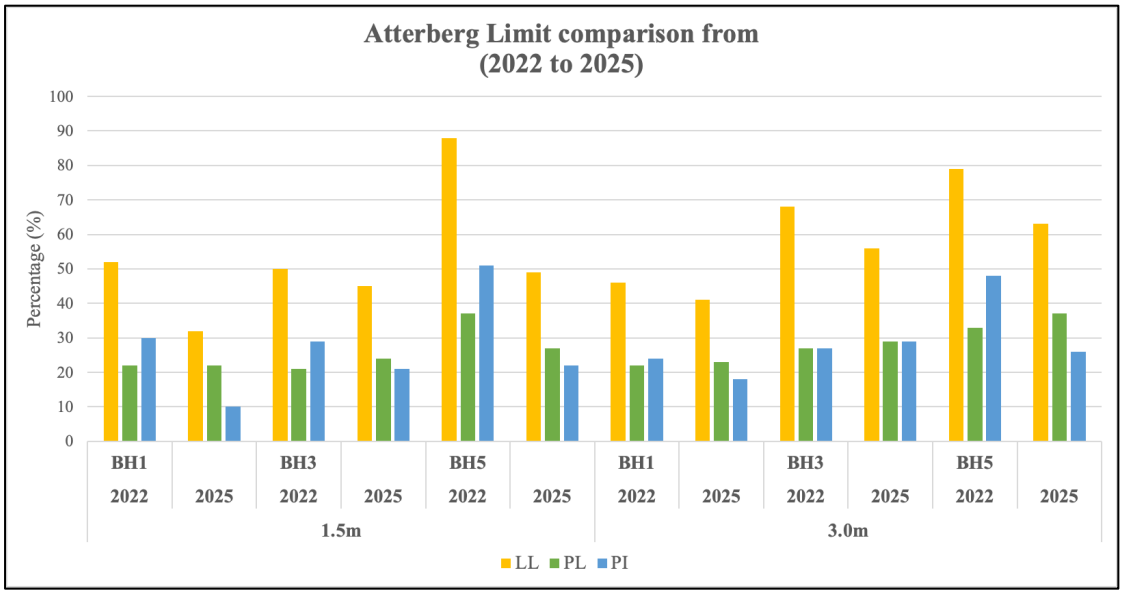

Figure 4.1 Comparison of Atterberg Limit (2022 to 2025)

From Figure 4.1, it can be observed that the Plastic Limit (PL) exhibits minimal variation over the three-year period, whereas the Liquid Limit (LL) and Plasticity Index (PI) show significant differences between 2022 and 2025. These changes may be attributed to the migration of soil particles, as indicated by the particle size distribution trends presented in Figure 4.2. This observation aligns with the findings of Zhang et al. (2023), who reported a high likelihood of erosion occurring at depths between 0 and 3.0 meters due to the infiltration of fine particles into pore spaces. Consequently, this process has influenced the Atterberg limits and particle size distribution over the period from 2022 to 2025.

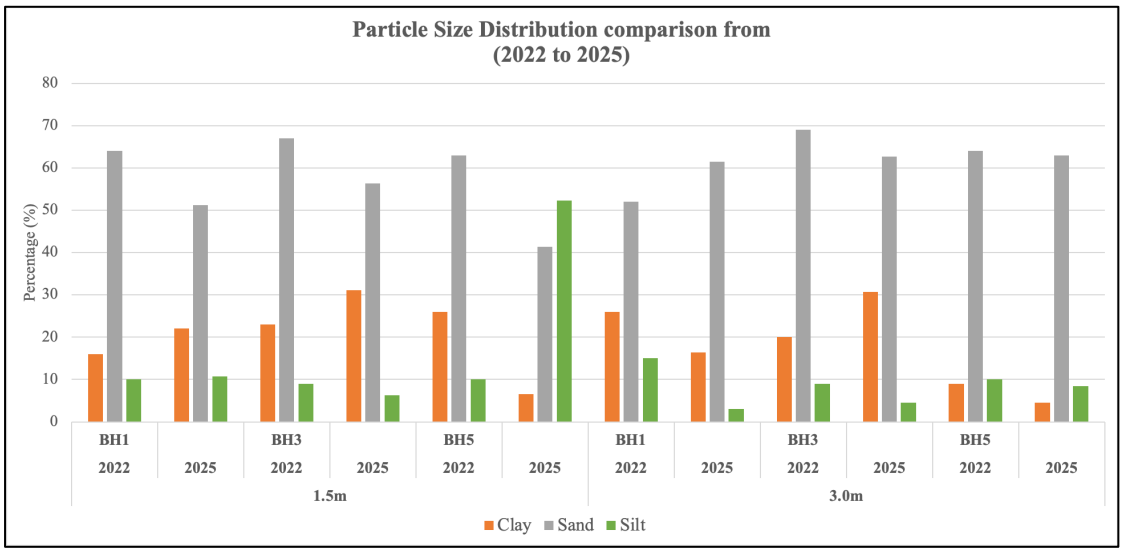

Figure 4.2 Comparison of Particle Size Distribution (2022 to 2025)

4.2.2 Engineering Properties

The results presented in Table 4.3 indicate notable differences as highlighted in the number of blows recorded between two in situ testing methods, JKR Probe (J) and Standard Penetration Test (SPT) (N) at several borehole (BH) locations. For instance, at BH3, the soil consistency assessed by the JKR Probe was classified as soft, whereas the SPT indicated stiff soil conditions. Similar discrepancies were observed at BH4 (at depths of 1.5 m and 3.0 m), as well as at BH7 and BH8 (at 3.0 m and 1.5 m depths, respectively). These variations suggest that the two methods may yield different results even within close proximity. Such differences may be attributed to the distinct operational characteristics of each testing method. The JKR Probe is performed manually and may be influenced by factors such as slight variations in the testing location (within approximately 1 meter) and the presence of underground aggregates. These factors can affect the blow count (J), as manual application may introduce inconsistencies in the impact force and angle of penetration. In contrast, the SPT employs machinery that provides a more uniform and controlled blow impact, which helps preserve the consistency of the test results. This mechanized approach likely accounts for the observed discrepancies between the two methods.

The table 4.3 data highlights that BH4 shows the lowest number of blows (N), suggesting exceptionally soft soil conditions at both 1.5m and 3.0m depths. Conversely,

BH1, particularly at the 3.0m depth, exhibits the highest number of blows (N), indicating the presence of a notably harder layer compared to the other BH locations.

Analysis of the collected data revealed some inconsistencies between JKR probe blow and Standard Penetration Test (SPT) results, particularly at specific depths and locations. For example, at BH1, a depth of 1.5 meters yielded conflicting soil classifications, with the JKR probe suggesting stiff soil and the SPT indicating medium soil. This discrepancy is likely due to procedural differences, specifically the manual blow application in the JKR probe versus the mechanical blow in the SPT. Moreover, the high concentration of aggregates at this particular site, as previously mentioned, is a potential factor affecting the manual testing outcome.

Table 4.3

Result of JKR (J) and SPT (N)

No. of Borehole	Depth	JKR (J)	SPT (N)	Consistency (J)	Consistency (N)
BH1	0.5m	58	-	Medium	-
	1.0m	97	-	Stiff	-
	1.5m	134	7	Stiff	Medium
	2.0m	95	-	Stiff	-
	2.5m	61	-	Medium	-
	3.0m	93	9	Stiff	Stiff
BH2	0.5m	296	-	Very stiff	-
	1.0m	86	-	Stiff	-
	1.5m	48	5	Medium	Medium
	2.0m	51	-	Medium	-
	2.5m	51	-	Medium	-
	3.0m	85	5	Stiff	Medium
BH3	0.5m	56	-	Medium	-
	1.0m	16	-	Soft	-
	1.5m	17	8	Soft	Stiff
	2.0m	22	-	Soft	-
	2.5m	42	-	Medium	-
	3.0m	134	7	Stiff	Medium
BH4	0.5m	225	-	Very stiff	-
	1.0m	84	-	Stiff	-
	1.5m	107	3	Stiff	Soft
	2.0m	31	-	Soft	-
	2.5m	178	-	Very Stiff	-
	3.0m	181	4	Very Stiff	Soft
BH5	0.5m	104	-	Stiff	-
	1.0m	51	-	Medium	-
	1.5m	24	5	Soft	Medium
	2.0m	25	-	Soft	-
	2.5m	128	-	Stiff	-

	3.0m	136	6	Stiff	Medium
BH6	0.5m	180	-	Very stiff	-
	1.0m	94	-	Stiff	-
	1.5m	64	5	Medium	Medium
	2.0m	12	-	Very soft	-
	2.5m	68	-	Medium	-
	3.0m	51	8	Medium	Stiff
BH7	0.5m	100	-	Stiff	-
	1.0m	62	-	Medium	-
	1.5m	18	5	Soft	Medium
	2.0m	26	-	Soft	-
	2.5m	18	-	Soft	-
	3.0m	29	8	Soft	Stiff
BH8	0.5m	107	-	Stiff	-
	1.0m	200	-	Very stiff	-
	1.5m	304	5	Very stiff	Soft
	2.0m	-	-	-	-
	2.5m	-	-	-	-
	3.0m	-	5	-	Soft
BH9	0.5m	55	-	Medium	-
	1.0m	64	-	Medium	-
	1.5m	41	3	Medium	Soft
	2.0m	59	-	Medium	-
	2.5m	152	-	Very stiff	-
	3.0m	69	5	Medium	Medium
BH10	0.5m	135	-	Stiff	-
	1.0m	284	-	Very stiff	-
	1.5m	286	5	Very stiff	Medium
	2.0m	81	-	Stiff	-
	2.5m	166	-	Very stiff	-
	3.0m	184	6	Very stiff	Medium

4.3 Rainfall Trend

Rainfall trends is addressed through descriptive analysis, data treatment processing, time series visualization, and trend assessment using the Mann-Kendall test and Sen's slope estimator.

4.3.1 Descriptive Statistic

The basic statistics for the monthly sum (MS) and monthly average (MA) of rainfall at each of the two rain gauge stations are outlined in Tables 4.4 to 4.8. These tables present a summary of the minimum, maximum, mean, median, mode, kurtosis, standard deviation, and coefficient of skewness for the rainfall data across the study areas, covering 128 months and spanning the 4 seasons. (NEM) November – February, (SWM) May – August, (IM1) September – October and (IM2) March – April.

Table 4.4
Descriptive Statistic for total 128 months rainfall.

	Bukit Berapit		**Permatang Rawa**	
Data	**Monthly Sum**	**Monthly Average**	**Monthly Sum**	**Monthly Average**
Min	2.50	0.08	0.0	0.0
Max	729.50	23.53	754.50	24.34
Mean	206.26	6.67	191.62	6.29
Median	186.80	5.94	163.25	5.35
Mode	2.50	3.69	12.0	3.29
Std. Deviation	138.45	4.59	127.79	4.2
Skewness	1.22	1.21	1.05	1.03
Kurtosis	2.18	1.94	1.89	1.68

The data in Tables 4.4 to 4.8 show key insights into the rainfall patterns at the Bukit Berapit and Permatang Pauh rain gauge stations. In Table 4.4, minimum daily rainfall values show a contrast between the two locations, with Bukit Berapit recording

2.50 mm and Permatang Pauh 0.0 mm. Additionally, Bukit Berapit exhibits higher median values, notably 186.80 mm compared to Permatang Pauh's 163.25 mm. Despite this, both locations display mean values surpassing their respective medians.

Table 4.5

Descriptive Statistic for Northeast monsoon (NEM) rainfall.

	Bukit Berapit		**Permatang Rawa**	
Data	**Monthly Sum**	**Monthly Average**	**Monthly Sum**	**Monthly Average**
Min	3.9	0.09	1.50	0.0
Max	542.8	18.09	485.50	16.18
Mean	212.41	6.37	176.37	5.33
Median	183.0	4.53	134.25	4.06
Mode	16.0	3.69	238.0	0.0
Std. Deviation	154.19	4.99	129.35	4.37
Skewness	0.56	0.84	0.65	0.83
Kurtosis	-0.75	-0.44	-0.42	-0.23

Table 4.6

Descriptive Statistic for Southwest monsoon (SWM) rainfall.

	Bukit Berapit		**Permatang Rawa**	
Data	**Monthly Sum**	**Monthly Average**	**Monthly Sum**	**Monthly Average**
Min	28.5	0.92	33.0	1.06
Max	729.5	12.58	425.0	13.71
Mean	186.16	5.70	180.82	5.88
Median	173.2	5.77	156.4	5.29
Mode	28.5	0.92	181.5	3.29
Std. Deviation	117.54	2.68	86.52	2.78
Skewness	2.39	0.35	0.87	0.85
Kurtosis	9.80	0.13	0.22	0.21

Further analysis in Tables 4.5 and 4.6 uncovers seasonal variations. During the Northeast Monsoon (NEM) and Southwest Monsoon (SWM) seasons, Bukit Berapit showcases higher maximum values (542.8 mm and 729.5 mm, respectively) compared to Permatang Rawa. However, an inverse trend emerges in Tables 4.7 and 4.8 for the Intermonsoon 1 (IM1) and Intermonsoon 2 (IM2) seasons, where Permatang Rawa records higher maximum values (754.5 mm and 453.0 mm, respectively) than Bukit Berapit.

The skewness values for all stations are positive, indicating a distribution where the tail on the right side is longer or fatter, resulting in the mean and median exceeding the mode. Notably, (Table 4.8) during the Intermonsoon 2 (IM2) season, Bukit Berapit station displays the smallest skewness value (0.39) alongside the lowest maximum total rainfall (364.5mm), suggesting a more evenly distributed rainfall pattern at this location. Syafrina et al., (2017) November to February, corresponding to the northeast monsoon period, rainfall reaches its minimum levels, with an average monthly precipitation of approximately 50 mm across all stations. Rainfall then increases, peaking between April and May with mean values ranging from 250 to 350 mm. In contrast, the present study indicates that during the second inter-monsoon period (IM2), the mean rainfall is lower compared to the northeast monsoon (NEM).

Moreover, high kurtosis signifies heavy-tailed data or the presence of outliers, while low kurtosis signals a lighter-tailed distribution with fewer outliers. Across the 128-month period and Southwest Monsoon (SWM) season, Bukit Berapit station exhibits a higher kurtosis value compared to Permatang Rawa, indicating a greater presence of outliers at Bukit Berapit station as illustrated in Table 4.4 and Table 4.6. Conversely, during the Northeast Monsoon (NEM), Intermonsoon 1 (IM1), and Intermonsoon 2 (IM2) seasons, Permatang Rawa station demonstrates higher kurtosis values, implying a higher prevalence of outliers relative to Bukit Berapit station as shown in table 4.6, table 4.7 and table 4.8.

Table 4.7

Descriptive Statistic for Intermonsoon 1 (IM1) rainfall.

	Bukit Berapit		Permatang Rawa	
Data	**Monthly Sum**	**Monthly Average**	**Monthly Sum**	**Monthly Average**
Min	121.3	3.91	122.5	4.08
Max	714.5	23.05	754.5	15.97
Mean	312.6	10.25	312.21	9.49
Median	278.7	9.14	314.7	9.67
Mode	121.3	3.91	122.5	4.08
Std. Deviation	151.65	4.97	142.98	3.25
Skewness	1.17	1.14	1.51	0.16
Kurtosis	1.46	1.26	3.78	-0.54

Table 4.8

Descriptive Statistic for Intermonsoon 2 (IM2) rainfall.

	Bukit Berapit		Permatang Rawa	
Data	**Monthly Sum**	**Monthly Average**	**Monthly Sum**	**Monthly Average**
Min	29.5	0.95	12.0	0.39
Max	364.5	12.15	453.0	15.1
Mean	168.94	5.40	162.71	5.37
Median	143.5	5.06	130.75	4.29
Mode	111.0	0.95	12.0	0.39
Std. Deviation	99.99	3.32	119.61	4.0
Skewness	0.39	0.47	0.95	0.97
Kurtosis	-0.8	-0.57	0.37	0.4

Despite being located in the same Seberang Perai Tengah district, the two rainfall stations demonstrate significant differences, particularly evident during seasonal periods. Table 4.7 mean value (312.6mm) and (312.21mm) from both rainfall station show the highest indicate it receive the highest rainfall amount among other

seasonal period. As, the main peak occurs in October, during the autumn transition period (Syafrina et al., 2017).

4.3.2 Data treatment

Initially, outlier detection is conducted using boxplot analysis with three distinct interval-setting techniques, Interquartile Range (IQR), Semi Interquartile Range (SIQR), and Robust skewness utilizing Medcouple (MC). Following outlier removal, the dataset undergoes three distinct methods for replacing missing values, Regression Imputation, Mean Method, and Linear Interpolation.

Following the approach outlined by Noor et al. (2015), the lowest Mean Absolute Error (MAE) and Root Mean Square Error (RMSE), along with the highest Coefficient of Determination (R^2) give a good performance for data replacing. The analysis on monthly sum (MS) and monthly average (MA) data spanning 128 months from two distinct rainfall stations, Bukit Berapit and Permatang Rawa.

Table 4.9
Interquartile Range (IQR) method

Monthly sum	Bukit Berapit	Lower	$(q_1 - 1.5(IQR))$	$= -133.09$
		Upper	$(q_3 + 1.5(IQR))$	$= 496.81$
	Permatang Rawa	Lower	$(q_1 - 1.5(IQR))$	$= 154.563$
		Upper	$(q_3 + 1.5(IQR))$	$= 532.74$
Monthly average	Bukit Berapit	Lower	$(q_1 - 1.5(IQR))$	$= -4.155$
		Upper	$(q_3 + 1.5(IQR))$	$= 16.354$
	Permatang Rawa	Lower	$(q_1 - 1.5(IQR))$	$= -5.523$
		Upper	$(q_3 + 1.5(IQR))$	$= 18.0775$

Table 4.10

Semi Interquartile Range

Monthly sum	Bukit Berapit	Lower	$(q_1 - 3(q_2 - q_1)$	$= -119.40$
		Upper	$(q_3 + 3(q_3 - q_2)$	$= 510.50$
	Permatang Rawa	Lower	$(q_1 - 3(q_2 - q_1))$	$= -77.05$
		Upper	$(q_3 + 3(q_3 - q_2)$	$= 610.25$
Monthly average	Bukit Berapit	Lower	$(q_1 - 3(q_2 - q_1)$	$= -3.59$
		Upper	$(q_3 + 3(q_3 - q_2)$	$= 16.92$
	Permatang Rawa	Lower	$(q_1 - 3(q_2 - q_1))$	$= -1.925$
		Upper	$(q_3 + 3(q_3 - q_2)$	$= 20.845$

Table 4.11

Robust Skewness (Medcouple)

Monthly sum	Bukit Berapit	Lower	$(q_1 - f_l(MC) * IQR$	$= 2.5$
		Upper	$(q_3 - f_u(MC) * IQR$	$= 722.833$
	Permatang Rawa	Lower	$(q_1 - f_l(MC) * IQR$	$= 0.66421$
		Upper	$(q_3 - f_u(MC) * IQR$	$= 465.071$
Monthly average	Bukit Berapit	Lower	$(q_1 - f_l(MC) * IQR$	$= 0.0842$
		Upper	$(q_3 - f_u(MC) * IQR$	$= 23.317$
	Permatang Rawa	Lower	$(q_1 - f_l(MC) * IQR$	$= 0.0235$
		Upper	$(q_3 - f_u(MC) * IQR$	$= 20.715$

Tables 4.9 to table 4.11 detail the lower and upper limits established for outlier identification using three distinct interval methods in boxplot analysis. These tables showcase a diverse range of values that influence the determination of outliers to be either retained or excluded, essential for minimizing bias in the dataset. Abnormal data can cause forecasts to be unreliable (Zhao & Yang, 2019).

In table 4.12, the quantity of missing values resulting from three different outlier detection methods is presented for both Bukit Berapit and Permatang Rawa rainfall stations. At Bukit Berapit station, the Monthly Sum (MS) and Monthly Average (MA) data exhibit lower percentages of missing values when employing the Robust skewness method, with rates of 2.3% and 1.6%, respectively. Conversely, Permatang Rawa

station demonstrates reduced missing data percentages in both data types (0.8%) through the utilization of the IQR method.

Table 4.12
Missing Value

Data	Location	Boxplot Method	Missing Value	Missing Percentage (%)
Monthly sum (MS)	Bukit Berapit	IQR	7	5.5
		SIQR	6	4.7
		Medcouple	3	2.3
	Permatang Rawa	IQR	1	0.8
		SIQR	1	0.8
		Medcouple	4	3.1
Monthly Average (MA)	Bukit Berapit	IQR	7	5.5
		SIQR	6	4.7
		Medcouple	2	1.6
	Permatang Rawa	IQR	1	0.8
		SIQR	1	0.8
		Medcouple	2	1.6

Table 4.13

Performance Indicator for Bukit Berapit (MS) and (MA) Rainfall Data

Outlier Method	Replace missing value method	Performance Indicator	MS	MA
IQR	Regression Imputation	MAE	19.80	0.6821
		RMSE	86.96	2.97
		R^2	0.626	0.616
	Mean Series	MAE	21.92	0.7277
		RMSE	96.06	3.17
		R^2	0.540	0.561
	Linear Interpolation	MAE	20.31	0.6743
		RMSE	90.94	2.99
		R^2	0.588	0.609
SIQR	Regression Imputation	MAE	18.57	0.5851
		RMSE	88.11	2.84
		R^2	0.610	0.646
	Mean Series	MAE	19.40	0.6423
		RMSE	91.58	3.02
		R^2	0.579	0.600
	Linear Interpolation	MAE	18.62	0.6153
		RMSE	88.88	2.92
		R^2	0.603	0.626
Medcouple	Regression Imputation	MAE	6.40	0.1487
		RMSE	48.46	1.41
		R^2	0.877	0.909
	Mean Series	MAE	7.26	0.1832
		RMSE	52.81	1.60
		R^2	0.853	0.882
	Linear Interpolation	MAE	5.68	0.1724
		RMSE	51.20	1.63
		R^2	0.863	0.878

Table 4.14

Performance Indicator for Permatang Rawa (MS) and (MA) Rainfall Data

Outlier Method	**Replace missing value method**	**Performance Indicator**	**MS**	**MA**
IQR	Regression	MAE	3.658	0.1157
	Imputation	RMSE	41.38	1.31
		R^2	0.896	0.903
	Mean Series	MAE	4.432	0.1421
		RMSE	50.14	1.61
		R^2	0.846	0.853
	Linear	MAE	4.709	0.1506
	Interpolation	RMSE	53.28	1.70
		R^2	0.826	0.835
SIQR	Regression	MAE	3.658	0.1157
	Imputation	RMSE	41.38	1.31
		R^2	0.896	0.903
	Mean Series	MAE	4.432	0.1421
		RMSE	50.14	1.61
		R^2	0.846	0.853
	Linear	MAE	4.709	0.1506
	Interpolation	RMSE	53.28	1.70
		R^2	0.826	0.835
Medcouple	Regression	MAE	10.826	0.1830
	Imputation	RMSE	65.50	1.48
		R^2	0.737	0.874
	Mean Series	MAE	10.556	0.1902
		RMSE	64.79	1.69
		R^2	0.745	0.836
	Linear	MAE	9.079	0.1633
	Interpolation	RMSE	62.22	1.71
		R^2	0.765	0.834

Conversely, for Permatang Rawa station, the IQR and SIQR methods demonstrate fewer outliers (0.8%) across the datasets, as indicated in Table 4.14. Similarly, Regression Imputation stands out as the preferred method for missing data replacement, boasting low MAE values of 3.658 and 0.1157, RMSE values of 41.38 and 1.31, and high R^2 values of 0.896 and 0.903. Consequently, data from Bukit Berapit (Table 4.15) station's Monthly Sum (MS) and Monthly Average (MA) will be sourced from the Robust Skewness and Regression Imputation methods due to their high performance indicators. For Permatang Rawa station, data treated from the Interquartile Range method and Regression Imputation method will be utilized for further analysis, aligning with the results obtained. As Zhao and Yang (2019) concluded, the robust skewed boxplot method is more suitable and reliable for detecting outliers in skewed rainfall distributions. However, this study employs both the Medcouple and Interquartile Range (IQR) methods for outlier identification, as combining these approaches helps reduce the risk of misclassifying data.

The analysis conducted by Noor et al., (2015), which focused on only two imputation methods, this study enhances previous research by utilising an additional imputation method for comparative analysis. The results indicate that Regression Imputation, Wang and Hu., (2022) outperforms the traditional Mean Method and Linear Interpolation, showcasing superior performance in handling missing data and enhancing the accuracy of the data treatment process.

According to Zhao and Yang (2019), the objective of employing adjusted boxplots is to diminish the number of outliers, thereby reducing the risk of misidentifying valuable data points as outliers. Analysing Table 4.12 reveals that for Bukit Berapit station, the Robust Skewness method emerges as the most suitable approach for outlier detection, showcasing fewer outliers in both the Monthly Sum (2.3%) and Monthly Average (1.6%) datasets. Regarding missing value replacement, Tables 4.15 to 4.16 highlight Regression Imputation as the recommended method due to its superior performance indicators, exhibiting lower Mean Absolute Error (MAE) values of 6.4 and 0.149, and Root Mean Square Error (RMSE) values of 48.46 and 1.41. The R^2 values, approaching unity at 0.877 and 0.909, further support the effectiveness of Regression Imputation for Bukit Berapit station.

4.3.3 Time series plot

In this section, the monthly sum rainfall time series plots for each station are visually presented in Figure 4.3 to Figure 4.7. Moreover, a comprehensive trend analysis spanning 10 years and 8 months using the Mann-Kendall (MK) and Sen's slope estimator (SSE) for the time series data was conducted and discussed. Specifically, Figure 4.3 exhibits the monthly sum rainfall time series plot for Bukit Berapit and Permatang Rawa stations from January 2014 to August 2024.

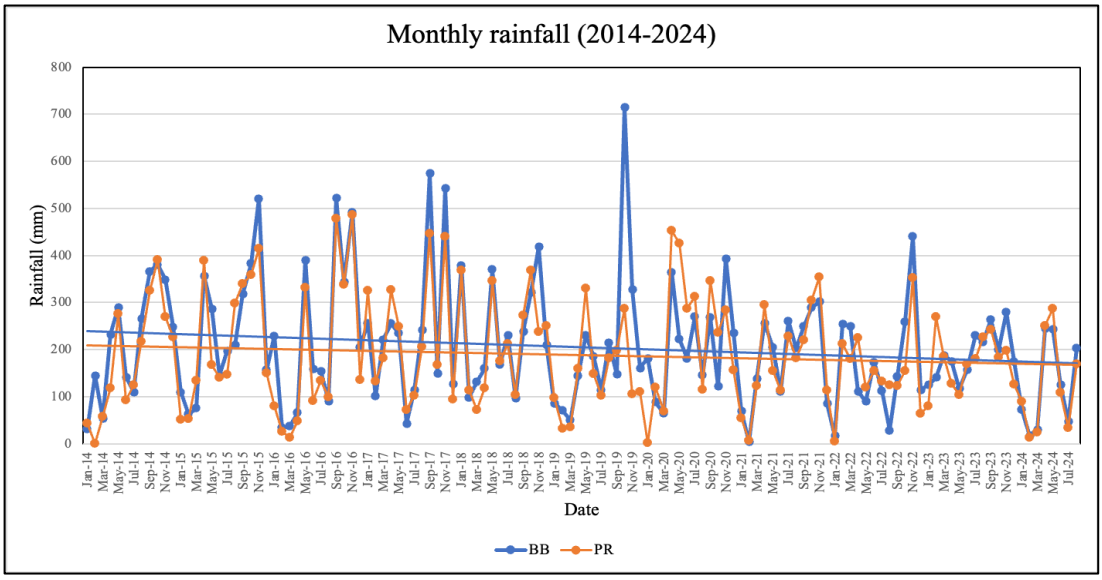

Figure 4.3 Time Series Plot for total 10 years 8 months Rainfall (monthly)

During the 10-year period, remarkable peaks in monthly sum rainfall are observed, with Permatang Rawa registering its highest value of 754.5mm in October 2019. Similarly, Bukit Berapit witnessed notable rainfall levels in May 2019 (729.5mm), October 2019 (714.5mm), and September 2017 (574.3mm). Thus support finding from Syafrina et al., (2017) as indicate during Intermonsoon 1 (Sep-Oct) recorded the highest rainfall amount at northern region especially, Pulau Pinang. Figure 4.3 showcases the time series plots and regression lines, indicating a subtle trend in monthly sum rainfall over the 128-month duration at both stations. The regression lines demonstrate a moderate negative slope, suggesting a downward trend in the monthly sum rainfall data for Bukit Berapit and Permatang Rawa. Fung et al., (2022) finding on the state of Pulau Pinang, monthly rainfall exhibited a relatively constant trend from 1988 to 2017. In

contrast, the total number of wet days showed a decreasing trend from 2008 to 2017. Fung et al. (2022) study align with the results of the present study, which, based on time series analysis from 2014 to 2024, also indicate a slight decreasing trend.

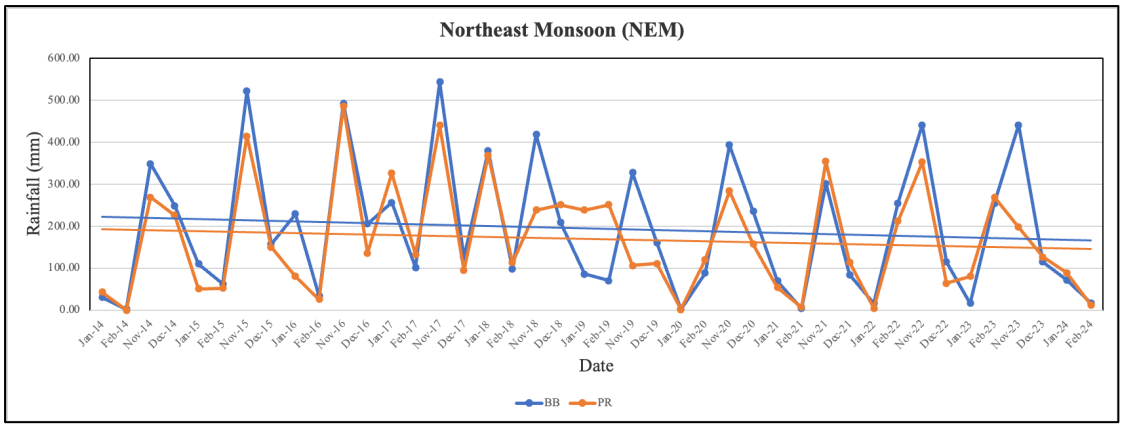

Figure 4.4 Time Series Plot for NEM

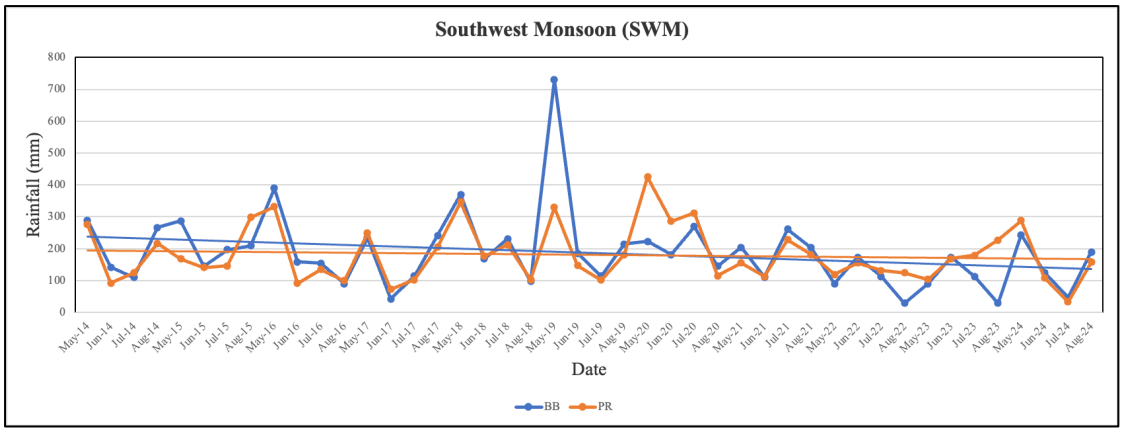

Figure 4.5 Time Series Plot for SWM

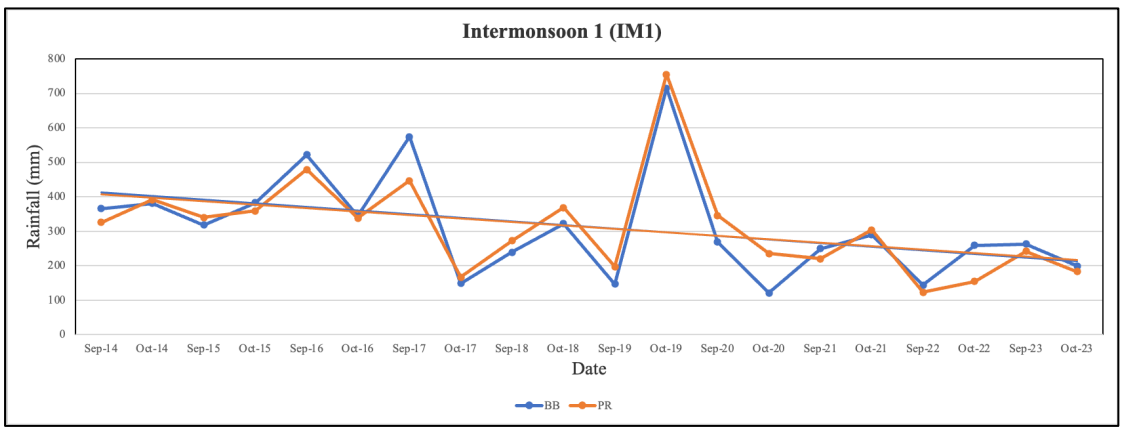

Figure 4.6 Time Series Plot for IM1

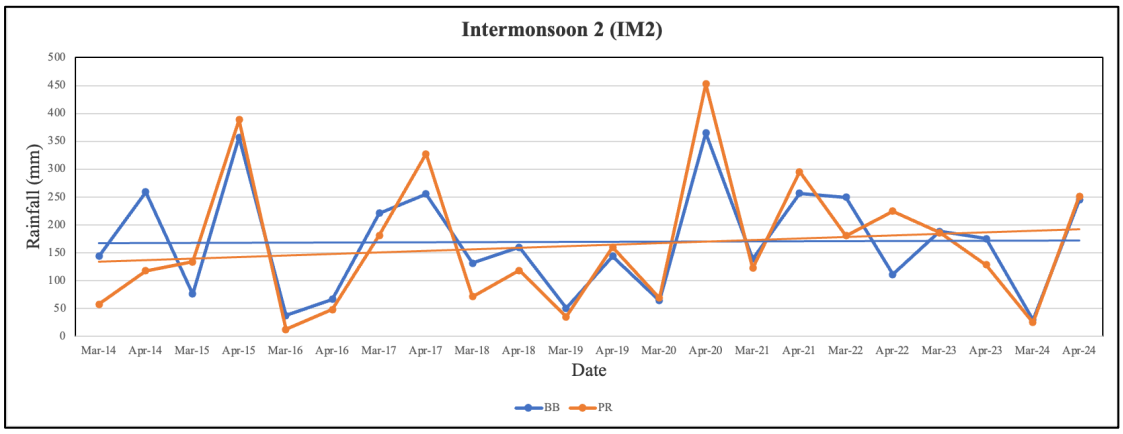

Figure 4.7 Time Series Plot for IM2

Figures 4.4 to 4.7 present the time series plots and regression lines for both stations across seasonal periods, including the Northeast Monsoon (NEM) from November to February, Southwest Monsoon (SWM) from May to August, Inter Monsoon 1 (IM1) in September and October, and Inter Monsoon 2 (IM2) in March and April. The regression lines exhibit minimal slopes, indicating a subtle trend in the monthly sum rainfall during the Northeast Monsoon period at Bukit Berapit and Permatang Rawa. Furthermore, a moderate negative slope in the regression lines suggests a downward trend in monthly sum rainfall for both stations during the Southwest Monsoon and Inter Monsoon 1 periods.

In Figure 4.7, the time series plot reveals a moderate positive slope in the regression line, signalling an upward trend in monthly sum rainfall for Permatang Rawa during the Inter Monsoon 2 (IM2) period. While, Bukit Berapit displays a minimal indication of an upward trend in the regression line during this period.

4.3.4 Trend Analysis

Table 4.15 depicts trend analysis conducted over a 10-year and 8-month period, segmented into distinct seasonal patterns. The seasonal rainfall in Malaysia is categorized into four season; Northeast Monsoon NEM (November – February), Southwest Monsoon SWM (May-August), Inter Monsoon 1 (September-October), and Inter Monsoon 2 (March-April). This study utilize the Mann-Kendall test and Sen's Slope estimator for rainfall trend analysis, methods employed in this study for comparison using Monthly Sum (MS) and Monthly Average (MA) data types.

Prior to analysis, the data undergoes a treatment process involving outlier removal and missing data replacement to reduce bias and enhance accuracy for trend analysis. R programming is utilized to ensure precise calculations, while Muhammad et al., (2024) used Python as it include trend package for reduce time consuming during calculation. R programming leveraging its functionality to compute accurate values for the Mann-Kendall test and Sen's Slope estimator, also incorporating these formulas within the 'trend' package for efficient analysis.

The outcomes of the trend analysis utilizing the Mann-Kendall (MK) and Sen's Slope Estimator (SSE) methods for both monthly sum and monthly average rainfall data are presented in Table 4.15. Consistent with the regression lines displayed in Figures 4.3 to 4.7, the trend statistics derived from the MK and SSE methods indicate positive trends for both Bukit Berapit and Permatang Rawa stations during the Inter Monsoon 2 period. Notably, a significant negative trend (p-value < 0.05) is observed in Table 4.17, where the monthly sum and monthly average rainfall at Bukit Berapit exhibit a noteworthy decline, with a significant trend (p-value = 0.003) detected during Inter Monsoon 1 (IM1). During October (IM1), previous study by Fung et., (2022) also found the total number of wet days from 1988 to 2017 exhibits a decreasing trend.

Additionally, within the Southwest Monsoon (SWM) timeframe, a significant decreasing trend is only evident in the monthly average data for Bukit Berapit. While during March (IM2), Fung et al., (2022) found the number of wet days decreased from 2008 to 2017. However, for the period 2014 to 2024, this study observed an insignificant decreasing trend based on the Mann-Kendall (MK) and Sen’s Slope Estimator (SSE) methods.

Table 4.15

Trend Analysis for Monthly Sum (MS) and Monthly Average (MA) Rainfall

Station	Seasonal Period	Data	MK	p-value	SSE	CI for SSE
Bukit Berapit	Total	MS	-1.3203	0.1867	-0.3691	(-0.9857, 0.182)
		MA	-1.5902	0.1118	-0.0157	(-0.0363, 0.0026)
	NEM	MS	-0.7373	0.4609	-1.1875	(-4.625, 1.975)
		MA	0.7153	0.4744	-0.0494	(-0.1812, 0.0620)
	SWM	MS	-1.2138	0.2248	-1.2539	(-3.280, 0.783)
		MA	-2.1448	0.0320	-0.07	(-0.13, -0.0025)
	IM1	MS	-2.1738	0.0297	-8.6167	(-18.493, -0.883)
		MA	-2.1738	0.0297	-0.2814	(-0.6164, -0.03)
	IM2	MS	0.5076	0.6118	2.1667	(-5.433, 9.3923)
		MA	0.564	0.5728	0.07	(-0.181, 0.3093)
Permatang Rawa	Total	MS	-0.5767	0.5641	-0.1673	(-0.7625, 0.3716)
		MA	-0.5458	0.5852	-0.0052	(-0.024, 0.0124)
	NEM	MS	-0.3468	0.7287	-0.9130	(-3.8833, 2.2871)
		MA	-0.3251	0.7451	-0.0238	(-0.1302, 0.0742)
	SWM	MS	-0.1821	0.8555	-0.1975	(-2.503, 1.2889)
		MA	-0.2124	0.8318	-0.0053	(-0.0796, 0.0417)
	IM1	MS	-2.7578	0.0058	-11.1988	(-17.008, -4.644)
		MA	-2.7578	0.0058	-0.3548	(-0.5675, -0.1456)
	IM2	MS	1.1279	0.2594	4.14	(-4.0769, 12.0636)
		MA	1.1279	0.2594	0.1279	(-0.1313, 0.3840)

Among the four seasons analysed, only the second inter-monsoon period (IM2), occurring from March to April, exhibited an insignificant upward trend in rainfall. Descriptive analysis indicates that this season generally experiences drier conditions compared to the others, with a daily mean rainfall of 168.94 mm. However, unprecedented changes have been observed, reflecting the impact of climate change on rainfall patterns in Pulau Pinang. As the global greenhouse effect is altering climate systems worldwide, leading to increased average temperatures and modifications in precipitation characteristics (Yahaya et al., 2015).

4.4 Correlation

4.4.1 Soil Erodibility Index

The analysis of the data (Table 4.16) highlights substantial spatial variability in soil erodibility, with distinct susceptibility patterns observed across boreholes, notably BH2 and BH7 at 1.5m depth identified as highly prone to erosion compared to less vulnerable sites like BH4. The 1.5 m and 3.0m soil depth expose erosion susceptibility. This aligns with the findings of Zhang et al. (2023), who observed that in the 0–3 m depth range, mineral particles larger than 10 μm predominated, with minimal fine particles filling pore spaces and clear signs of erosion on mineral surfaces.

A preliminary observation of the relationship between SPT values and soil erodibility indicates inconsistency. For example, soft soil conditions at BH4 and BH8 correspond to high and low soil erodibility categories, respectively. Similarly, soils classified as medium (BH1 and BH2) exhibit both moderate and critical erodibility categories, which differ significantly. Table 4.17 shows that BH1 exhibited critical soil erodibility likely due to rainwater infiltration reducing clay content. Below 0.5 m, erodibility was generally low as clay seeped deeper. BH3's erodibility decreased from moderate (2022) to low recently, while BH5 shifted from low (2022) to high erodibility in 2025. BH8 showed contrasting results. These changes highlight the significant impact of rainwater infiltration on soil properties over three years.

The migration of fine particles has also impacted the ROM Scale values, as the percentage of particle size distribution is a primary parameter in determining erodibility, with clay content serving as a key indicator (Abidin et al., 2017; Zhang et al., 2023). As shown in Figure 4.8, at the 1.5 m depth, ROM Scale values decreased for BH1 and BH3, whereas BH5 exhibited an opposite trend, reaching the "High" erodibility category, indicating increased vulnerability. This study further extends the analysis to a depth of 3.0 m, although previous researchers have generally identified erosion processes occurring between 0.5 m and 1.5 m. Results at 3.0 m depth (Figure 4.8) reveal that BH1's erodibility index increased from "Low" in 2022 to "Moderate" in 2025. These findings suggest that erosion processes may also extend to the 3.0 m depth range, consistent with observations reported by Zhang et al. (2023).

Table 4.16

Soil Erodibility Index (2022)

No. of Borehole	Depth (m)	Particle size distribution (%)			ROM scale	Soil erodibility category
		Clay	Sand	Silt		
BH1	1.5	16	64	10	2.31	Moderate
	3.0	26	52	15	1.29	Low
BH2	1.5	1	97	2	49.50	Critical
	3.0	1	98	1	49.50	Critical
BH3	1.5	23	67	9	1.65	Moderate
	3.0	20	69	9	1.95	Moderate
BH4	1.5	44	32	24	0.64	Low
	3.0	42	29	29	0.69	Low
BH5	1.5	26	63	10	1.40	Low
	3.0	23	64	10	1.61	Moderate
BH6	1.5	21	66	10	1.81	Moderate
	3.0	21.6	64.38	10	1.72	Moderate
BH7	1.5	2	81	3	21.00	Critical
	3.0	4	84	2	10.75	Very High
BH8	1.5	7	81	10	6.50	High
	3.0	55	13	32	0.41	Low
BH10	1.5	49	24	27	0.52	Low
	3.0	46	26	28	0.59	Low

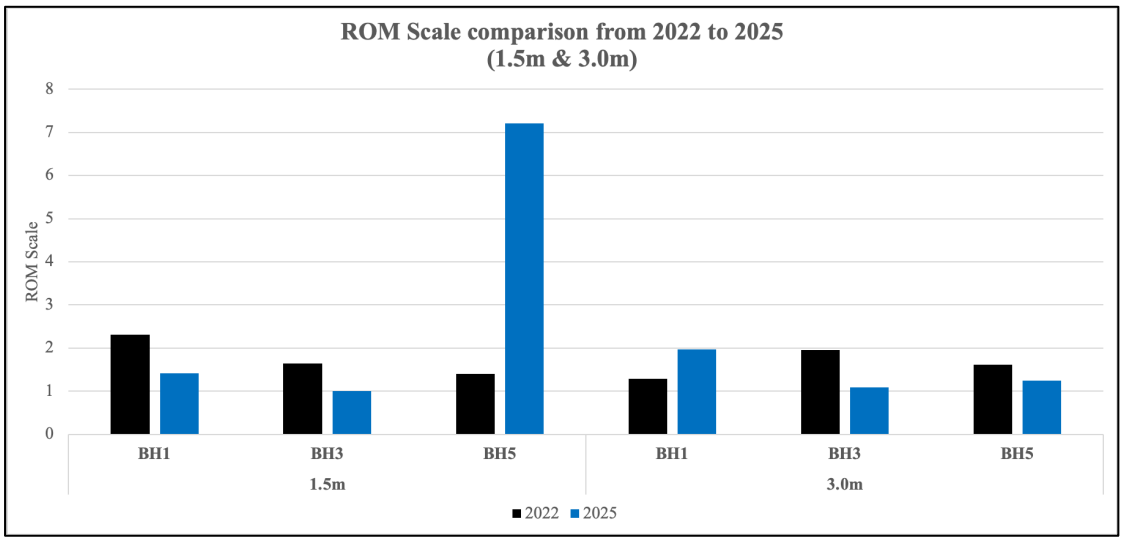

Figure 4.8 Comparison of ROM Scale (2022 to 2025)

The correlation section, which addresses Objective 3, presents a comprehensive analysis of the relationship between soil erodibility and rainfall characteristics. Initially, the study evaluates the erodibility of soil samples using data from the JKR Probe (J) in conjunction with the ROM scale, following the methodology established by Sabri et al. (2022). This approach enables a quantification of soil susceptibility to erosion based on in situ measurements.

Subsequently, the study applies the rainfall classification method proposed by Abidin and Hassan (2005), wherein days with rainfall amounts exceeding 20 mm are identified as erosive rainfall events. These events are used to characterize temporal patterns of rainfall erosivity. By compiling these data, the study produces a monthly ranking of erosive rainfall frequency.

Leveraging a decade of rainfall data, the analysis integrates the spatial distribution of soil erodibility with the temporal occurrence of erosive rainfall. This combined assessment facilitates the identification of borehole locations that are most vulnerable to landslide hazards. The integration of the erodibility index with monthly erosive rainfall rankings provides a robust framework for understanding and predicting landslide risk in the study area.

Table 4.17

Soil Erodibility Index (2025)

No. of Borehole	Depth (m)	Particle size distribution (%)			ROM Scale	Soil erodibility category
		Clay	Sand	Silt		
BH1	0.5	2.6	58.17	5.49	12.24	Critical
	1.0	33.18	51.81	6.84	0.88	Low
	1.5	22.03	51.24	10.74	1.41	Low
	2.0	25.94	56.41	7.18	1.23	Low
	2.5	21.48	54.15	6.99	1.42	Low
	3.0	16.38	61.45	2.99	1.97	Moderate
BH3	0.5	23.91	66.47	5.95	1.51	Moderate
	1.0	22.26	60.93	7.08	1.53	Moderate
	1.5	31.11	56.33	6.33	1.01	Low
	2.0	23.13	69.27	3.51	1.57	Moderate
	2.5	28.47	60.72	8.09	1.21	Low
	3.0	30.67	62.68	4.50	1.09	Low
BH5	0.5	24.91	24.66	50.43	1.51	Moderate
	1.0	18.53	68.81	12.66	2.20	Moderate
	1.5	6.49	41.34	52.22	7.21	High
	2.0	8.13	40.13	51.75	5.65	High
	2.5	12.78	30.23	56.99	3.41	Moderate
	3.0	28.61	62.93	8.46	1.25	Low
BH8	0.5	50.02	32.22	6.67	0.39	Low
	1.0	20.41	52.13	18.01	1.72	Moderate
BH9	0.5	14.35	52.61	16.05	2.39	Moderate
BH10	0.5	11.93	51.11	18.69	2.93	Moderate

Table 4.17 presents the results of sieve analysis (dry sieve and hydrometer methods) and in situ JKR probe testing. These data are used to analyze the correlation between JKR probe values and the ROM scale. This study employs the JKR probe, commonly used in Malaysia as Yusof et al., (2017) stated, in contrast to the Mackintosh probe used by Sabri et al. (2022). The erodibility data encompass measurements from

2022 and 2025, comprising a total of 39 data points, theoretically enhancing the reliability of the correlation analysis. The combined dataset allows for an assessment of the potential to estimate soil erodibility using JKR probe testing alone, thereby reducing the time and resources required for traditional soil sampling and laboratory analysis of physical properties.

4.4.2 ROM Scale and JKR Probe

The results of in situ testing conducted with the JKR Probe and erodibility index measurements using the ROM Scale are summarized in Table 4.18. The subsequent analysis will focus on establishing the correlation between these two variables. The primary objective of the correlation analysis is to determine the coefficient of determination (R^2), which will provide a measure of the strength of the relationship between the variables. This will enable an evaluation of the potential for JKR Probe testing to serve as a suitable alternative to ROM Scale analysis.

Table 4.18

Table of Erodibility Index and JKR Probe (J)

No. of Borehole	Depth (m)	Erodibility Index (EI)	JKR Probe (J)
BH1	0.5	12.24	58
	1.0	0.88	97
	1.5	2.31	134
		1.41	134
	2.0	1.23	95
	2.5	1.42	61
	3.0	1.29	93
		1.97	93
BH2	1.5	49.5	48
	3.0	49.5	85

BH3	0.5	1.51	56
	1.0	1.53	16
	1.5	1.65	17
		1.01	17
	2.0	1.57	22
	2.5	1.21	42
	3.0	1.95	134
		1.25	134
BH4	1.5	0.64	107
	3.0	0.69	181
BH5	0.5	1.51	104
	1.0	2.2	51
	1.5	1.4	24
		7.21	24
	2.0	5.65	25
	2.5	3.41	128
	3.0	1.61	136
		1.25	136
BH6	1.5	1.81	64
	3.0	1.50	51
BH7	1.5	21.0	18
	3.0	10.75	29
BH8	0.5	0.39	107
	1.0	1.72	200
	1.5	6.5	304
	3.0	0.41	-
BH9	0.5	2.39	55
BH10	0.5	2.93	135
	1.5	0.52	286
	3.0	0.59	184

Figure 4.9 illustrates an inverse relationship between JKR probe (J) count and the ROM scale, consistent with the findings of Sabri et al. (2022). However, the relatively low coefficient of determination R^2 value of 0.155 suggests a weak correlation. According to Nithiaraj et al.,(1996), an R^2 value between 0.25 and 0.55 indicates a moderately good fit. Therefore, while the data generally suggest that higher JKR blow counts correspond to lower ROM scale values, the strength of this relationship is limited. The regression line was fitted using a polynomial model, as it demonstrated the highest R^2 value compared to linear, exponential, and power regression models.

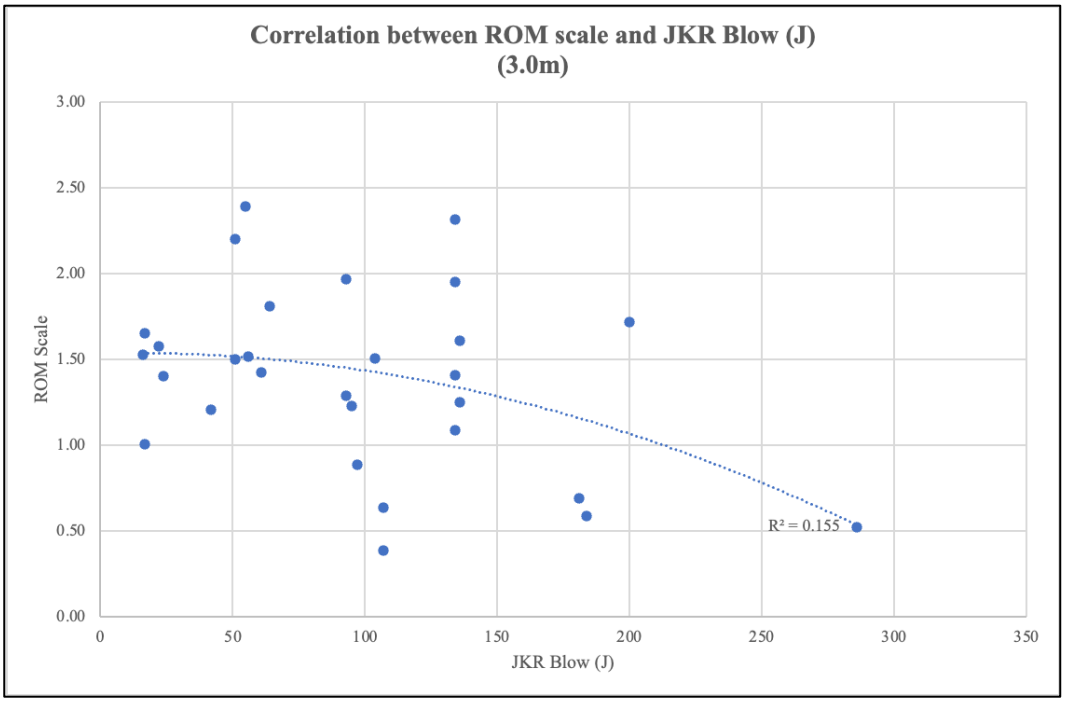

Figure 4.9 Correlation of 'ROM' Scale and JKR Blow (3.0m)

While Figure 4.10 illustrates the correlation at depths ranging from 0 m to 1.5 m, it reveals a weaker coefficient of determination (R^2) value of 0.1031. This contrasts with the findings of Sabri et al. (2022), who reported a stronger correlation ($R^2 = 0.59$) using the Mackintosh Probe. Differences in the angle of the probe cone and the weight of the hammer employed by previous researchers may have influenced their results. Theoretically, the relationship aligns with expectations, where an increase in blow count corresponds to a decrease in ROM values. However, the significant disparity in R^2 values suggests variability in methodology or site conditions between the studies.

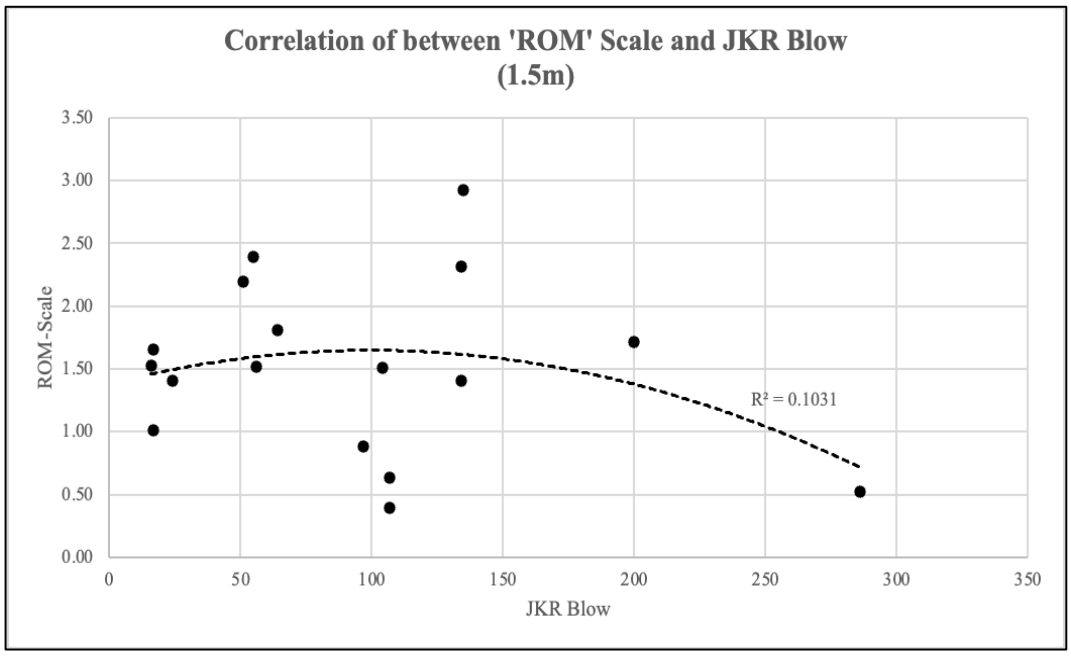

Figure 4.10 Correlation of 'ROM' Scale and JKR Blow (1.5m)

The correlation observed in this study between the number of blows and ROM Scale values differs from the results reported by Sabri et al. (2022), potentially due to variations in site selection. While both the present and previous studies were conducted at lower stream locations influenced by urbanization-related subsurface disturbances, the location used by Sabri et al. (2022), as shown in Figure 4.11a located at (latitude 2°55'52.1" and longitude 101°46'32.0") exhibited less disturbance. Trevers et al. (2025) suggest that vegetation changes can affect the level of disturbance. Specifically, the present study site (Figure 4.11b) had less vegetation cover, whereas the study by Sabri et al. (2022) had higher vegetation cover, as shown in Figure 4.11. This difference in vegetation cover may have affected the correlation strength, suggesting that the correlation found in this study may be more reliable for locations with higher levels of disturbance. To align with the conclusions presented by Sabri et al. (2022), it is recommended to utilize locations characterized by reduced disturbance. Additionally, a greater R^2 value was obtained at a 3.0m depth compared to 1.5m, suggesting that a 3.0m depth is relevant for erosion analysis, consistent with Zhang et al. (2023).

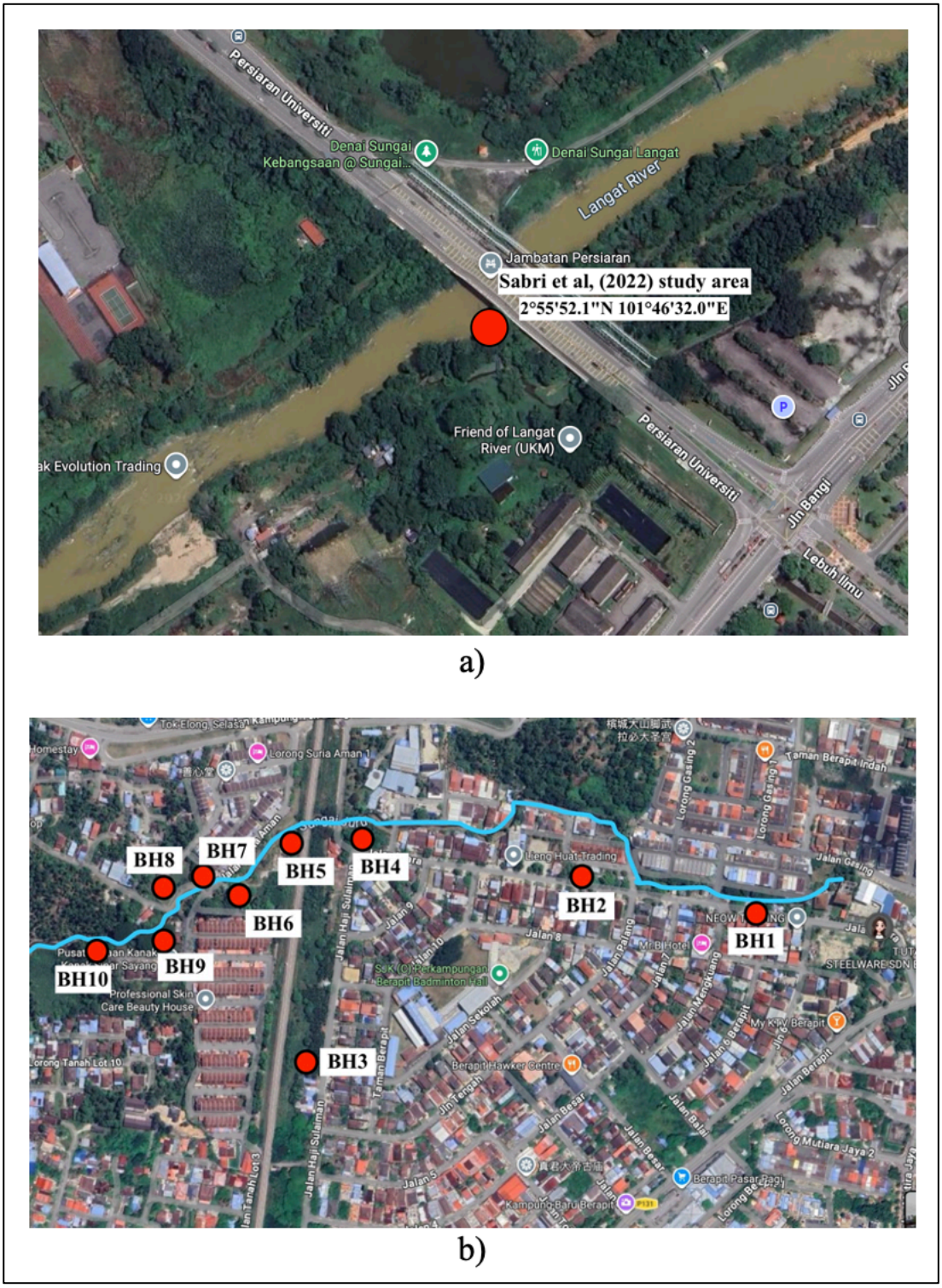

Figure 4.11 a) Previous SI location, b) Recent SI location.

4.4.3 ROM Scale and Rainfall

Daily rainfall events exceeding 20 mm have been identified as the threshold for rainfall capable of initiating soil erosion in Malaysia (Roslan and Tew, 1997). The frequency of such erosive rainfall was analysed monthly for each year over a ten-year period, allowing for the observation of annual and monthly patterns of erosive rainfall.

In Malaysia, a daily rainfall amount of at least 20 mm is considered the minimum threshold for initiating soil erosion (Abidin et al., 2017). The method of ranking erosive rainfall frequency was initially applied by Abidin et al. (2005) and later adopted and expanded upon by Derahman et al. (2025).

By correlating the timing of these potential erosive rainfall events at both study sites with the spatial probability of erosion occurrence, it is possible to derive a temporal probability for landslide risk. Consequently, months during which rainfall is classified as having a high or critical potential to cause erosion to correspond to periods with an increased likelihood of landslide events.

Table 4.19

Ranking of Erosive Rainfall according to month for the period of 2014-2023 (Bukit Berapit)

Ranking	Month	Erosive rainfall frequency
1	November	74
2	September	57
3	May	52
4	October	50
5	April	41
6	December	32
7	July	27
8	August	26
9	June	24
10	March	22
11	January	21
12	February	14

Table 4.20

Ranking of Erosive Rainfall according to month for the period of 2014-2023 (Permatang Rawa)

Ranking	Month	Erosive rainfall frequency
1	November	56
2	September	53
3	October	49
4	April	43
5	May	38
6	August	34
7	June	27
8	July	27
9	December	26
10	March	20
11	January	17
12	February	16

Tables 4.19 and 4.20 present the monthly ranking of erosive rainfall events from 2014 to 2023, based on the frequency of daily rainfall exceeding 20 mm, which is recognized as the threshold for erosive rainfall (Roslan and Tew, 1997). Analysis from two distinct rainfall stations indicates that November consistently ranks highest in terms of erosive rainfall frequency, identifying it as the most vulnerable month to erosive processes. Conversely, February registers the lowest ranking at both locations, reflecting a period of low daily rainfall intensity.

When examined according to seasonal patterns, variations in monthly rankings across the 10-year dataset reveal that the Northeast Monsoon (NEM), Southwest Monsoon (SWM), and Inter-monsoon 1 (IM1) seasons are characterized by frequent occurrences of daily rainfall exceeding 20 mm. These seasons thus represent critical periods with heightened erosive potential. Notably, borehole locations 1, 2, 7, and 9, which exhibit high and critical erodibility indices, are particularly susceptible to landslide incidents during these periods, underscoring the significance of these findings for hazard assessment.

In contrast, the Inter-monsoon 2 (IM2) season, particularly March, ranks lowest (rank 10) in terms of erosive rainfall frequency, suggesting reduced vulnerability during this month. However, April within the IM2 season emerges as an exception, ranking fourth with 43 and 50 recorded instances of daily rainfall exceeding 20 mm between 2014 and 2023. This is corroborated by Mann-Kendall (MK) and Sen's Slope Estimator (SSE) analyses, which indicate an insignificant upward trend in rainfall during IM2, whereas other seasons (NEM, SWM, IM1) exhibit decreasing trends.

In conclusion, the NEM season is identified as the most critical period for erosive rainfall and associated risks over the past decade. Meanwhile, the divergent trend observed during the IM2 season, particularly in April, highlights its potential to become increasingly significant in future erosion and landslide risk.

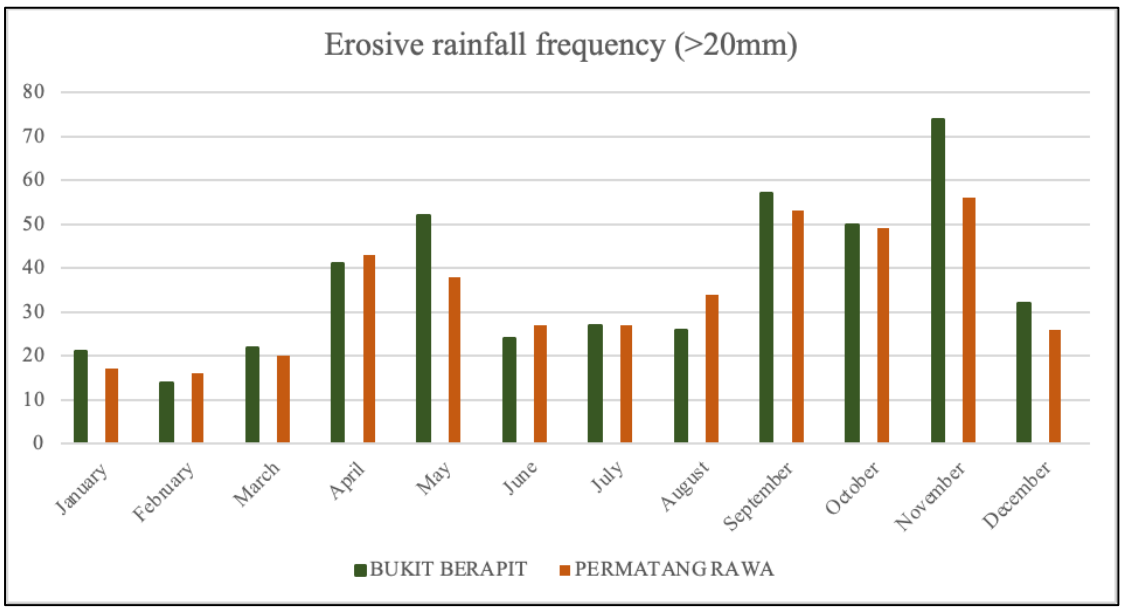

Figure 4.12 Comparison of Erosive Rainfall frequency at (Bukit Berapit and Permatang Rawa) rainfall station

Figure 4.12 illustrates a clear comparison of erosive rainfall frequency between two rainfall stations, Bukit Berapit and Permatang Rawa. The chart demonstrates that the Northeast Monsoon (NEM) plays a primary role in water resources across Peninsular Malaysia, with the highest erosive rainfall recorded at the Permatang Rawa river area, designating it as the most vulnerable period. Additionally, the following month, September (IM1), is highlighted as experiencing the highest rainfall amounts in the northern region.

CHAPTER 5
CONCLUSION AND RECOMMENDATIONS

5.1 Conclusion

This chapter presents a comprehensive review of existing literature on seasonal rainfall patterns in northern regions and their impact on soil stability. The analysis focuses on two key areas: the influence of seasonal rainfall variations and the statistical distributions of rainfall data in relation to soil stability indices. The current research analyzes ten years of rainfall data (2014-2024) from two stations: Bukit Berapit and Permatang Rawa, located in Penang, Malaysia, along the Sungai Permatang Rawa. The findings are presented as follows:

i. Analysis of soil physical properties along Sungai Permatang Rawa reveals significant spatial variability. However, across all locations and depths (0.5 m to 3.0 m), sand consistently comprised more than 50% the soil composition. Both JKR probe and SPT tests effectively predicted soil stiffness, exhibiting generally parallel results. The exception was Borehole 4, where a discrepancy may be attributed to the presence of stones or aggregates at ground level, affecting JKR probe sensitivity.
ii. Descriptive and trend analyses of rainfall data from both stations indicate maximum daily rainfall totals of 729.5 mm and 754.5 mm, respectively. The average daily rainfall (approximately 200 mm) from January 2014 to August 2024 falls below the critical threshold. Ten-year trend analysis reveals no significant downward trend for NEM, SWM, and IM1 rainfall indices. However, IM1 shows a significant downward trend, despite recording the highest daily rainfall (300 mm) at the study site during its typical period (September–October). This suggests potential water scarcity and necessitates drought hazard preparedness. Conversely, a non-significant upward trend in rainfall during IM2 may increase erodibility.

iii. The correlation analysis between JKR probe (J) values and the erodibility index (ROM scale) confirms the previously observed inverse relationship. However, the R^2 value (0.155) value differs significantly from previous studies, likely due to the increased sample size employed in this research.

iv. November records the highest frequency of erosive rainfall, making it the most erosion-prone month, while February has the lowest. Seasonal analysis shows that the Northeast Monsoon (NEM), Southwest Monsoon (SWM), and Inter-monsoon 1 (IM1) experience frequent erosive rainfall, with boreholes 1, 2, 7, and 9 exhibiting high erosion and landslide risk. In contrast, Inter-monsoon 2 (IM2), particularly March, has the lowest frequency, though April ranks fourth with a significant number of events. Trend analyses reveal a slight upward rainfall trend during IM2, while other seasons show decreasing trends. Overall, NEM remains the most critical season for erosion, with IM2's evolving trend indicating increasing future risk.

5.2 Recommendations and Limitations

This research offers several key findings applicable to practical applications. First, the comprehensive dataset of soil physical properties and rainfall patterns can be directly utilized by relevant authorities (e.g., the Department of Irrigation and Drainage Malaysia, local government agencies) to enhance mitigation and preparedness strategies for various geohazards. Specifically, the detailed characterization of soil composition and the identification of areas with high sand content can inform land-use planning and construction practices to minimize erosion risks. The observed spatial variability in soil properties highlights the need for site-specific assessments in infrastructure development.

The analysis of seasonal rainfall trends, particularly the significant downward trend observed during September-October (IM1), provides crucial information for water resource management agencies. This information can be directly incorporated into flood and drought prediction models for Seberang Perai Tengah, enabling more effective disaster preparedness and response strategies. The identification of this trend as an early indicator of potential water scarcity emphasizes the importance of proactive water conservation measures.

The established correlation between the erodibility index and in situ testing methods (JKR probe) offers a valuable tool for landslide risk assessment. This information can be used by government agencies to identify areas with high erosion susceptibility and implement preventative measures, such as slope stabilization or land-use restrictions. The efficiency and cost-effectiveness of in situ testing, as demonstrated in this study, make it a practical approach for large-scale assessments.

This study's findings highlight several areas for future research. Increasing the sample size for rainfall-erodibility analysis would improve the statistical robustness of the correlation, leading to more accurate predictions. Similarly, extending the duration of rainfall data analysis to a longer time period (e.g., 30 years) and differentiating between extreme rainfall events and prolonged rainfall would provide a more comprehensive understanding of long-term trends and their impact on erosion.

Additionally, utilizing data collected from the Permatang Rawa riverbank, geospatial analyses employing GIS software are essential for developing a comprehensive, layered understanding of the study area. Finally, integrating machine learning techniques with traditional soil sampling methods could offer a more efficient and cost-effective approach to assessing soil erodibility in future studies.

REFERENCES

Abidin, R. Z., & Abu Hassan, Z. (2005). 'ROM' Scale for Forecasting Erosion Induced Landslide Risk on Hilly Terrain. Landslides, January 2005, 197–202. https://doi.org/10.1007/3-540-28680-2_24

Abidin, R. Z., Mahamud, M. A., Kasim, M. Z. M., Abdullah, J., Yusof, M. F., Zainol, M. R. R. M. A., & Zakaria, N. A. (2022). Forecasting Erosion Induced Landslide Risk Level in Cameron Highlands Towards Environmental Sustainability. Engineering, Agriculture, Science and Technology Journal (EAST-J), 1(1), 75–82. https://doi.org/10.37698/eastj.v1i1.142

Abidin, R. Z., Sulaiman, M. S., & Yusoff, N. (2017). Erosion risk assessment: A case study of the Langat River bank in Malaysia. International Soil and Water Conservation Research, 5(1), 26–35. https://doi.org/10.1016/j.iswcr.2017.01.002

Agarwal, S., Suchithra, A. S., & Singh, S. P. (2021). Analysis and interpretation of rainfall trend using Mann-Kendall's and Sen's slope Method. Indian Journal of Ecology, 48(2), 453–457.

Ali, Z., Hamed, M. M., Nashwan, M. S., & Shahid, S. (2023). Spatiotemporal analysis of groundwater resources sustainability in South Asia and China using GLDAS data sets. Environmental Earth Sciences, 82(24). https://doi.org/10.1007/s12665-023-11282-7

Althubaiti, A. (2023). Sample size determination: A practical guide for health researchers. Journal of General and Family Medicine, 24(2), 72–78. https://doi.org/10.1002/jgf2.600

Atika, B., Kawi, B., Hamjah, R., Uni, K. K., Koichiro, K., Maznah, M., & Anand, N. (2023). Soil Erosion Risk in Relation To Rainfall Erosivity in Gunung Alab and Inobong of Crocker Range Park in Sabah, Malaysia. Journal of Sustainability Science and Management, 18(10), 220–228. https://doi.org/10.46754/jssm.2023.10.015

Azmi, Z., Shukri, A., & Ahmad, F. (2015). Rainfall erosivity estimation for Northern and Southern peninsular Malaysia using Fourneir indexes. Procedia Engineering, 125, 179–184. https://doi.org/10.1016/j.proeng.2015.11.026

Berita Harian (2015). Terkini: Banjir di Kelantan, Terengganu, Pahang tambah buruk. Online at: https://www.bharian.com.my/berita/nasional/2014/12/24876/terkini-banjir-di-kelantan-terengganu-pahang-tambah-buruk

Bellocchi, G., & Diodato, N. (2020). Rainfall erosivity in soil erosion processes. Water (Switzerland), 12(3), 10–13. https://doi.org/10.3390/w12030722

Bono, R., Arnau, J., Alarcón, R., & Blanca, M. J. (2019). Bias, precision, and accuracy of skewness and kurtosis estimators for frequently used continuous distributions. Symmetry, 12(1), 19. https://doi.org/10.3390/sym12010019

Bouyoucos, G. J. (1962). Hydrometer method improved for making particle size analysis
of soil. Agricultural Journal, 54(5), 464–465.

Bujang, M. A. (2024). An elaboration on sample size determination for correlations based on effect sizes and confidence interval width: a guide for researchers. Restorative Dentistry and Endodontics, 49(2), 1–8. https://doi.org/10.5395/rde.2024.49.e21

Chapra, S.C. and Canale, R.P., (1998) Numerical Methods for Engineers. Singapore:McGraw-Hill.

Chen, S. C. (2022). Soil–Water Conservation, Erosion and Landslide. Water (Switzerland), 14(4), 14–16. https://doi.org/10.3390/w14040665

Cheng CS, Auld H, Li Q, and Li G (2012). Possible impacts of climate change on extreme weather events at local scale in South-Central Canada. Climatic Change, 112(3-4): 963-979.

Chin, E., Maharjan, R., & Emalya, N. (2023). Navigating Soil Erosion Challenges in Malaysia: Insights, Prospects, and Solutions. Civil and Sustainable Urban Engineering, 3(2), 138–148. https://doi.org/10.53623/csue.v3i2.339

Cooksey, R. W. (2020). Descriptive statistics for summarising data (pp. 61–139). https://doi.org/10.1007/978-981-15-2537-7_5

Dale WL (1959) The rainfall of Malaya, part I. J Trop Geogr 13:23–27

Dash, C. S. K., Behera, A. K., Dehuri, S., & Ghosh, A. (2023). An outliers detection and elimination framework in classification task of data mining. Decision Analytics Journal, 6, 100164. https://doi.org/10.1016/j.dajour.2023.100164

Dekaraja, D., Mahanta, R. (2020). Riverbank Erosion and Migration Inter-linkage: With Special Focus on Assam, India. https://doi.org/10.21203/rs.3.rs-50748/v2

Department of Statistic Malaysia. (2024). Current Population Estimate. https://www.dosm.gov.my/uploads/release-content/file_20250709163825.pdf

Department of Standards Malaysia (DSM). (2006). SITE INVESTIGATIONS – CODE OF PRACTICE.

Derahman, A., Alias, R., Latib, F. W. M., Shukor, M. F., & Bachok, M. F. (2025). Prediction of Soil Erodibility Factor, ROM Scale Erodibility Index (EIROM) and ROM Scale Category using Multiple Linear Regression (MLR) and Artificial Neural Network (ANN). Jurnal Kejuruteraan, 37(3), 1307–1324. https://doi.org/10.17576/jkukm-2025-37(3)-17

Derahman, A., Bachok, M. F., Shukor, M. F., Latib, F. W. M., & Alias, R. (2022). A Review on Soil Erodibility Studies in Malaysia. Pertanika Journal of Science and Technology, 30(3), 2139–2155. https://doi.org/10.47836/pjst.30.3.22

Fung, K. F., Chew, K. S., Huang, Y. F., Ahmed, A. N., Teo, F. Y., Ng, J. L., & Elshafie, A. (2022). Evaluation of spatial interpolation methods and spatiotemporal modeling of rainfall distribution in Peninsular Malaysia. Ain Shams Engineering Journal, 13(2), 101571. https://doi.org/10.1016/j.asej.2021.09.001

Froude, M. J., & Petley, D. N. (2018). Global fatal landslide occurrence from 2004 to 2016. Natural Hazards and Earth System Sciences, 18(8), 2161–2181. https://doi.org/10.5194/nhess-18-2161-2018

Gocic, M., & Trajkovic, S. (2013). Analysis of changes in meteorological variables using Mann-Kendall and Sen's slope estimator statistical tests in Serbia. Global and Planetary Change, 100, 172–182. https://doi.org/10.1016/j.gloplacha.2012.10.014

Gofar, N., Lee, L. M., & Kassim, A. (2008). Response of suction distribution to rainfall infiltration in soil slope. Electronic Journal of Geotechnical Engineering, 13 E(June 2016).

Guo, M., Li, J., He, H., Xu, J., & Jin, Y. (2018). Detecting global vegetation changes using Mann-Kendal (MK) trend Test for 1982–2015 time period. Chinese Geographical Science, 28(6), 907–919. https://doi.org/10.1007/s11769-018-1002-2

Gupta, A., Mishra, P., Pandey, C., Singh, U., Sahu, C., & Keshri, A. (2019). Descriptive statistics and normality tests for statistical data. Annals of Cardiac Anaesthesia, 22(1), 67. https://doi.org/10.4103/aca.aca_157_18

HA Rahman and J Mapjabil. Landslides disaster in Malaysia: An overview. Health Environ. J. (2017); 8, 58-7.

Hai OS, Samah AA, Chenoli SN et al (2017) Extreme rainstorms that caused devastating flooding across the east coast of Peninsular Malaysia during November and December 2014. Weather Forecast 32:849–872. https:// doi. org/ 10. 1175/ WAF-D- 16- 0160.1

Hair, J. F., Hult, G. T. M., Ringle, C. M., and Sarstedt, M. (2017). A Primer on Partial Least Squares Structural Equation Modeling (PLS-SEM). 2nd Ed. Thousand Oaks, CA: Sage.

Hamed, M.M., Khan, N., Muhammad, M.K.I., Shahid, S., 2022a. Ranking of Empirical Evapotranspiration Models in different climate zones of Pakistan. Land 11, 2168. https://doi.org/10.3390/land11122168.

Hanif, M. F., Mustafa, M. R. U., Liaqat, M. U., Hashim, A. M., & Yusof, K. W. (2022). Evaluation of Long-Term Trends of Rainfall in Perak, Malaysia. Climate, 10(3), 1–20. https://doi.org/10.3390/cli10030044

Haron, N. A., Yusuf, B., Sulaiman, M. S., Razak, M. S. A., & Nurhidayu, S. (2022). Morphological Assessment of River Stability: Review of the Most Influential Parameters. Sustainability (Switzerland), 14(16). https://doi.org/10.3390/su141610025

Hasan, M. F. R., Susilo, A., Suryo, E. A., Agung, P. A. M., Wiyono, Pratiwie, D. L., & Dewi, N. M. (2024). Assessment and simulation of potential landslide caused by the rainfall intensity in Batu City during 2021. IOP Conference Series: Earth and Environmental Science, 1314(1). https://doi.org/10.1088/1755-1315/1314/1/012017

Hashim, M., Nayan, N., Setyowati, D. L., Said, Z. M., Mahat, H., & Saleh, Y. (2021). Analysis of Water Quality Trends Using the Mann-Kendall Test and Sen's Estimator of Slope in a Tropical River Basin. Pollution, 7(4), 933–942. https://doi.org/10.22059/POLL.2021.325794.1118

Hatem, G., Zeidan, J., Goossens, M., & Moreira, C. (2022). NORMALITY TESTING METHODS AND THE IMPORTANCE OF SKEWNESS AND KURTOSIS IN STATISTICAL ANALYSIS. BAU Journal - Science and Technology, 3(2). https://doi.org/10.54729/ktpe9512

Haydar, A. P., Mohammed, K. M., & Keya, D. R. (2024). Effect of rainfall pattern on sediment yield and runoff in different textured soils. Polytechnic Journal, 14(1). https://doi.org/10.59341/2707-7799.1747

Heeren, D. M., Mittelstet, A. R., Fox, G. A., Storm, D. E., AlMadhhachi, A. T., Midgley, T. L. Tejral, R. B. (2012). Using rapid geomorphic assessments to assess streambank stability in Oklahoma Ozark streams. Trans ASABE, 55(3), 957–968.

Institution, B. S., & Staff, B. S. I. (1990). British Standard methods of test for soils for civil engineering purposes.

Jasmin, F., Weng, F., Yip, S., Jeong Diong, Y., Dindang, A., Chang, N.K., Muhammad, Abdullah, H., Fadila, C., Fakaruddin, J., 2020. Occurrence of meridional and easterly surges and their impact on Malaysian rainfall during the northeast monsoon: a climatology study. Meteorol. Appl. 27, e1836 https://doi.org/10.1002/MET.1836.

Junninen, H., Niska, H., Tuppurrainen, K., Ruuskanen, J., Kolehmainen, M., (2002) Methods for Imputation of Missing Values in Air Quality Data Sets. Journal of Atmospheric Environment, 38, p. 2895-2907.

Kaur, P., Stoltzfus, J., & Yellapu, V. (2018). Descriptive statistics. International Journal of Academic Medicine, 4(1), 60. https://doi.org/10.4103/ijam.ijam_7_18

Kennedy, I. (2022). Sample Size Determination in Test-Retest and Cronbach Alpha Reliability Estimates. British Journal of Contemporary Education, 2(1), 17–29. https://doi.org/10.52589/bjce-fy266hk9

Khalid, N. H. N., Usman, F., & Omar, R. C. (2018). Effect of rainfall to the groundwater and soil displacement. International Journal of Engineering Research and Technology, 11(3), 439–450.

Khyber, E., Syaufina, L., & Sunkar, A. (2021). Variability and time series trend analysis of rainfall and temperature in Dramaga Sub-District, Bogor, Indonesia. IOP Conference Series: Earth and Environmental Science, 771(1). https://doi.org/10.1088/1755-1315/771/1/012016

Lu, W., Xiao, Z., Chen, Y., Sun, J., & Chen, F. (2024). Spatiotemporal Characteristics and Rainfall Thresholds of Geological Landslide Disasters in ASEAN Countries. Atmosphere, 15(5), 1–13. https://doi.org/10.3390/atmos15050599

Malay Mail, 2018. Failure to Control Water Run-Off Among Causes of Bukit Kukus Landslide. says minister | Malay Mail. https://www.malaymail.com/news/Malaysia /2018/10/25/failure-to-control-water-run-off-among-cause-of-bukit-kukus-landslide says/1686671.

Manandhar, B., Cui, S., Wang, L., & Shrestha, S. (2023). South Asia : A Review. Land. https://doi.org/10.3390/land12030627

Mohamed Yusof, M. K. T., A Rashid, A. S., Abdul Khanan, M. F., Abdul Rahman, M. Z., Abdul Manan, W. A., Kalatehjari, R., & Dehghanbanadaki, A. (2024). Assessing the impact of RCP4.5 and RCP8.5 scenarios on landslide susceptibility mapping using support vector machine: A case study of Penang Island, Malaysia. Physics and Chemistry of the Earth, 133(July 2023), 103496. https://doi.org/10.1016/j.pce.2023.103496

Mohtar, Z. A., Yahaya, A. S., Ahmad, F., Suri, S., & Halim, M. H. (2014). Trends for Daily Rainfall in Northern and Southern Region of Peninsular Malaysia. Journal of Civil Engineering Research, 4(3A), 222–227. https://doi.org/10.5923/c.jce.201402.38

Muhammad, M., Azmi, M. A. F., & Mohd Zawawi, M. A. (2024). Rainfall trend analysis using the Mann-Kendall test with pyMannKendall: a case study of Jeli, Kelantan. BIO Web of Conferences, 131. https://doi.org/10.1051/bioconf/202413105018

Muhammad, N. S., Abdullah, J., & Julien, P. Y. (2020). Characteristics of Rainfall in Peninsular Malaysia. Journal of Physics: Conference Series, 1529(5). https://doi.org/10.1088/1742-6596/1529/5/052014

Mukhlisin, M., Matlan, S. J., Ahlan, M. J., & Taha, M. R. (2015). Analysis of rainfall effect to slope stability in Ulu Klang, Malaysia. Jurnal Teknologi, 72(3), 15–21. https://doi.org/10.11113/jt.v72.4005

National Hydraulic Research Institution of Malaysia (NAHRIM) (2008). Derivation of probable maximum precipitation for design oors in Malaysia (Technical research publication No 1) Serdang, Kajang: NAHRIM.

Ng, J., Mohd Taib, A., Razali, I. H., Abd Rahman, N., Wan Mohtar, W. H. M., A. Karim, O., Mat Desa, S., Awang, S., & Mohd, M. S. F. (2022). The Effect of Extreme Rainfall Events on Riverbank Slope Behaviour. Frontiers in Environmental Science, 10(March), 1–14. https://doi.org/10.3389/fenvs.2022.859427

New Strait Time, 2025. Torrential rain sparks flooding in Seberang Perai, 1 PPS opened. https://www.nst.com.my/news/nation/2025/04/1205255/torrential-rain-sparks-flooding-seberang-perai-1-pps-opened

Nithiaraj, R., Wang, T., & Balasubramaniam, A. S. (1996). Strength parameters of residual soils and application to stability analysis of anchored slopes. Geotechnical Engineering, 27(2). http://trid.trb.org/view.aspx?id=1165969

Noor, N. M., Al Bakri Abdullah, M. M., Yahaya, A. S., & Ramli, N. A. (2015). Comparison of linear interpolation method and mean method to replace the missing values in environmental data set. Materials Science Forum, 803, 278–281. https://doi.org/10.4028/www.scientific.net/MSF.803.278

Othman, S.N., Ahmarofi, A.A., Akanmu, M.D., (2018). Predicting the occurrence of landside at Penang island , Malaysia , through artificial neural networks model. Int. J. Eng. Technol. 7 (December), 217–222. https://www.researchgate.net/publication/329556870.

Piliposyan, T. V. (2018). The Distribution of the Maximum, Minimum and Range of a Sample. Journal of Contemporary Mathematical Analysis (Armenian Academy of Sciences), 53(3), 180-186.

Pour, S. H., Wahab, A. K. A., & Shahid, S. (2020). Physical-empirical models for prediction of seasonal rainfall extremes of Peninsular Malaysia. Atmospheric Research, 233(September 2019), 104720. https://doi.org/10.1016/j.atmosres.2019.104720

Roy S (2009). A spatial analysis of extreme hourly precipitation patterns in India. International Journal of Climatology, 29(3): 345–355

Rosgen, D. L. (1994). A classification of natural rivers. Catena, 22(3), 169–199.

Roslan ZA, Mazidah M (2002) Establishment of soil erosion scale with regards to soil grading characteristic. Proc. 2nd World Engineering Congress, Sarawak, Malaysia, pp 235–239

Roslan ZA, Tew KH (1997) Rainfall analysis in relations to erosion risk frequency – case study (Cameron Highlands). Proc. 3rd International Conference on FRIEND, FRIEND 97, Postojna, Slovenia

Rosly, M. H., Mohamad, H. M., Bolong, N., & Harith, N. S. H. (2022). An Overview: Relationship of Geological Condition and Rainfall with Landslide Events at East Malaysia. Trends in Sciences, 19(8). https://doi.org/10.48048/tis.2022.3464

Sa'adi, Z., Alias, N. E., Yusop, Z., Hamed, M. M., Shukla, P., Houmsi, M. R., Mohamad, N. A., Shiru, M. S., Sa'adi, N., Muhammad, M. K. I., Iqbal, Z., & Banday, U. J. (2024). Characterization of the future northeast monsoon rainfall based on the clustered climate zone under CMIP6 in Peninsular Malaysia. Atmospheric Research, 304(April), 107407. https://doi.org/10.1016/j.atmosres.2024.107407

Saad, M. H. M., Kamarudin, M. K. A., Toriman, M. E., Wahab, N. A., Ata, F. M., Samah, M. A. A., Saudi, A. S. M., & Manoktong, S. N. (2023). Analysis of the Flash Flood Event and Rainfall Distribution Pattern on Relau River Basin Development, Penang, Malaysia. Planning Malaysia, 21(1), 58–71. https://doi.org/10.21837/PM.V21I25.1224

Saadatkhah, N., Kassim, A., Lee, L. M., & Rahnamarad, J. (2015). Spatiotemporal regional modeling of rainfall-induced slope failure in Hulu Kelang, Malaysia. Environmental Earth Sciences, 73(12), 8425–8441. https://doi.org/10.1007/s12665-014-4002-2

Sabri, N. F. A., Rahman, N. A., Taib, A. M., Mohtar, W. H. M. W., Karim, O. A., Desa, S. M., Awang, S., & Mohd, M. S. F. (2022). Erosion risk index: Correlation of ROM-scale and Mackintosh Probe at Sungai Langat tributary. E3S Web of Conferences, 347, 1–12. https://doi.org/10.1051/e3sconf/202234703009

Sabtan, A. A., & Shehata, W. M. (1994). Mackintosh probe as an exploration tool. Bulletin of the International Association of Engineering Geology, 50(1), 89–94. https://doi.org/10.1007/bf02594960

Safiah Yusmah, M. Y., Bracken, L. J., Sahdan, Z., Norhaslina, H., Melasutra, M. D., Ghaffarianhoseini, A., Sumiliana, S., & Shereen Farisha, A. S. (2020). Understanding urban flood vulnerability and resilience: a case study of Kuantan, Pahang, Malaysia. Natural Hazards, 101(2), 551–571. https://doi.org/10.1007/s11069-020-03885-1

Saimi, F. M., Hamzah, F. M., Toriman, M. E., Jaafar, O., & Tajudin, H. (2020). Trend and linearity analysis of meteorological parameters in peninsular Malaysia. Sustainability (Switzerland), 12(22), 1–19. https://doi.org/10.3390/su12229533

Sarkar, G., Siddiqua, S., Banik, R., & Rokonuzzaman, M. (2015). Prediction of soil type and standard penetration test (SPT) value in Khulna City, Bangladesh using general regression neural network. Quarterly Journal of Engineering Geology and Hydrogeology, 48(3–4), 190–203. https://doi.org/10.1144/qjegh2014-108

Shankar, A., Kumar, A., Chandra Sahana, B., & Sinha, V. (2023). A Case Study of Heavy Rainfall Events and Resultant Flooding During the Summer Monsoon Season 2020 Over the River Catchments of North Bihar, India. VayuMandal, 48(2), 2022.

Sholagberu, A. T., Ul Mustafa, M. R., Wan Yusof, K., & Ahmad, M. H. (2016). Evaluation of rainfall-runoff erosivity factor for cameron highlands, Pahang, Malaysia. Journal of Ecological Engineering, 17(3), 1–8. https://doi.org/10.12911/22998993/63338

Singh, N. B., Jibanchand, N., & Devi, K. R. (2017). Applicability of standard penetration tests to estimate undrained shear strength of soils of Imphal. International Journal of Engineering Technology Science and Research, 4(3), 250–255.

Sivrikaya, O., & Toğrol, E. (2006). Determination of undrained strength of fine-grained soils by means of SPT and its application in Turkey. Engineering Geology, 86(1), 52–69. https://doi.org/10.1016/j.enggeo.2006.05.002

Suhaila, J., Deni, S. M., Zin, W. Z. W., & Jemain, A. A. (2010). Spatial patterns and trends of daily rainfall regime in Peninsular Malaysia during the southwest and northeast monsoons: 1975-2004. Meteorology and Atmospheric Physics, 110(1), 1–18. https://doi.org/10.1007/s00703-010-0108-6

Syafrina, A. H., Zalina, M. D., & Juneng, L. (2015). Historical trend of hourly extreme rainfall in Peninsular Malaysia. Theoretical and Applied Climatology, 120(1–2), 259–285. https://doi.org/10.1007/s00704-014-1145-8

Syafrina, et al. (2017). Rainfall analysis in the northern region of Peninsular Malaysia. International Journal of ADVANCED AND APPLIED SCIENCES, 4(11), 11–16. https://doi.org/10.21833/ijaas.2017.011.002

Syafrina, A. H., Zalina, M. D., & Juneng, L. (2015). Historical trend of hourly extreme rainfall in Peninsular Malaysia. Theoretical and Applied Climatology, 120(1–2), 259–285. https://doi.org/10.1007/s00704-014-1145-8

Tan, J. J., & Ramli, H. (2023). Effect of Standard Penetration Test Corrections on the Estimation of Undrained Shear Strength. Journal of Civil Engineering and Management, 29(6), 501–515. https://doi.org/10.3846/jcem.2023.18441

Tan, K. C. (2018). Trends of rainfall regime in Peninsular Malaysia during northeast and southwest monsoons. Journal of Physics: Conference Series, 995(1). https://doi.org/10.1088/1742-6596/995/1/012122

The Sun Daily, 2017. Tanjung Bungah Landslide a Man-Made Tragedy, Says Commission of Inquiry. https://www.thesundaily.my/local/tanjung-bungah-landslide-a-man- made-tragedy-says-commission-of-inquiry-DB1311207.

Toriman, M. E., & Gasim, M. B. (2014). Floods in Malaysia: Historical reviews, causes, effects and mitigations approach. International Journal of Interdisciplinary Research and Innovations. International Journal of Interdisciplinary Research and Innovation, 2(4), 59–65.

Travers, S. K., Woodward, R., Slavich, E., McAllister, D., Chu, N., Lawrie, K., & Gorrod, E. (2025). Interacting contemporary and legacy disturbances affect management of floodplain forest vegetation. Basic and Applied Ecology, 90, 99–108. https://doi.org/10.1016/j.baae.2025.12.008

Trigo R. M., Zeˆzere J.L., Rodriguez M.L., Trigo I.F. 2005. The influence of the north Atlantic oscillation on rainfall triggering of landslides near Lisbon. Nat Hazards 36: 331–353.

UN. (2024). Progress towards the Sustainable Development Goals, Report of the Secretary-General. Assembly, 64782(May), 14.

Varikoden, H., Preethi, B., Samah, A. A., & Babu, C. A. (2011). Seasonal variation of rainfall characteristics in different intensity classes over Peninsular Malaysia. Journal of Hydrology, 404(1–2), 99–108. https://doi.org/10.1016/j.jhydrol.2011.04.021

Vincent, T., & Yusoff, N. (2022). Trends In Peninsular Malaysia Rainfall During The Southwest Monsoon Using Degree Of Rainfall Amount (DORA). International Journal of Infrastructure Research and Management, 10(2), 66–73. https://iukl.edu.my/rmc/publications/ijirm/

Wang, S., & Hu, H. (2022). Impute the missing data using retrieved dropouts. BMC Medical Research Methodology, 22(1), 1–15. https://doi.org/10.1186/s12874-022-01509-9

Wazoh, H. N. and M. S. J. (2014). Standard Penetration Test in Engineering Geological Site Investigations-A Review. The International Journal Of Engineering And Science, 3(7), 40–48. www.theijes.com

Wong, C. L., Yusop, Z., & Ismail, T. (2018). Trend Of daily rainfall and temperature in Peninsular Malaysia based on gridded data set. International Journal of GEOMATE, 14(44), 65–72. https://doi.org/10.21660/2018.44.3707

Yahaya, A. S., Ahmad, F., Mohtar, Z. A., & Suri, S. (2015). Determination of rainfall erosivity in Penang. 15th Asian Regional Conference on Soil Mechanics and Geotechnical Engineering, ARC 2015: New Innovations and Sustainability, January, 1132–1136. https://doi.org/10.3208/jgssp.ATC1-3-05

Yik, D.J., Yip, W.S., MatAdam, M.K., Chang, N.K., Yunus, F., Abdullah, M.H., (2015). The definitions of the southwest monsoon climatological onset and withdrawal over Malaysian region. Malaysian Meteorol. Dep. 3, 1–30.

Yusof, M. K. T. M., Rashid, A. S. A., Khanan, M. F. A., Rahman, M. Z. A., Manan, W. a. A., Kalatehjari, R., & Dehghanbanadaki, A. (2023). Assessing the impact of RCP4.5 and RCP8.5 scenarios on landslide susceptibility mapping using support vector machine: A case study of Penang Island, Malaysia. Physics and Chemistry of the Earth Parts a/B/C, 133, 103496. https://doi.org/10.1016/j.pce.2023.103496

Yusof, M. F., Abd Khalid, M. N. F., Ahmad Tajudin, S. A., Madun, A., & Zainal Abidin, M. H. (2017). Correlation of JKR Probe with Undrained Shear Strength. MATEC Web of Conferences, 103, 2–7. https://doi.org/10.1051/matecconf/201710307009

Yusof, N. Q. A. M., & Zabidi, H. (2018). Reliability of Using Standard Penetration Test (SPT) in Predicting Properties of Soil. Journal of Physics: Conference Series, 1082(1). https://doi.org/10.1088/1742-6596/1082/1/012094

Zhang, Z., Zeng, R., Meng, X., Zhao, S., Wang, S., Ma, J., & Wang, H. (2023). Effects of changes in soil properties caused by progressive infiltration of rainwater on rainfall-induced landslides. Catena, 233(August), 107475. https://doi.org/10.1016/j.catena.2023.107475

Zhao, C., & Yang, J. (2019). A Robust Skewed Boxplot for Detecting Outliers in Rainfall Observations in Real-Time Flood Forecasting. Advances in Meteorology, 2019, 1–7. https://doi.org/10.1155/2019/1795673

APPENDICES

APPENDIX A

Medcouple Boxplot Result

Monthly sum (Bukit Berapit)

```
> > # Create an adjusted boxplot
> adjbox(Rainfall_Data$`SUM (BB)`, main = "Adjusted Boxplot", medcouple = mc)
> > cat("Medcouple:", mc, "\n")
Medcouple: 0.07616361
> > q_alpha <- quantile(Rainfall_Data$`SUM (BB)`, probs = 0.0035)
> print(q_alpha)
0.35%
  2.5
> q_beta <- quantile(Rainfall_Data$`SUM (BB)`, probs = 0.9965)
> print(q_beta)
  99.65%
722.8325
```

Monthly sum (Permatang Rawa)

```
> > # Calculate Medcouple_SUM(PR)
> mc <- mc(Rainfall_Data$`SUM (PR)`)
> > # Create an adjusted boxplot
> adjbox(Rainfall_Data$`SUM (PR)`, main = "Adjusted Boxplot", medcouple = mc)
> > cat("Medcouple:", mc, "\n")
Medcouple: 0.255627
> > q_alpha <- quantile(Rainfall_Data$`SUM (PR)`, probs = 0.0035)
> print(q_alpha)
  0.35%
0.66675
> q_beta <- quantile(Rainfall_Data$`SUM (PR)`, probs = 0.9965)
> print(q_beta)
  99.65%
634.9295
```

Monthly mean (Bukit Berapit)

```
> # Create an adjusted boxplot
> adjbox(Rainfall_Data$`MEAN (BB) R`, main = "Adjusted Boxplot", medcouple = mc)
>
> cat("Medcouple:", mc, "\n")
Medcouple: 0.1219512
>
> q_alpha <- quantile(Rainfall_Data$`MEAN (BB) R`, probs = 0.0035)
> print(q_alpha)
   0.35%
0.084445
> q_beta <- quantile(Rainfall_Data$`MEAN (BB) R`, probs = 0.9965)
> print(q_beta)
  99.65%
23.31664
```

Monthly mean (Permatang Rawa)

```
> # Create an adjusted boxplot
> adjbox(Rainfall_Data$`MEAN (PR) R`, main = "Adjusted Boxplot", medcouple = mc)
>
> cat("Medcouple:", mc, "\n")
Medcouple: 0.2541176
>
> q_alpha <- quantile(Rainfall_Data$`MEAN (PR) R`, probs = 0.0035)
> print(q_alpha)
   0.35%
0.022225
> q_beta <- quantile(Rainfall_Data$`MEAN (PR) R`, probs = 0.9965)
> print(q_beta)
  99.65%
20.71288
```

APPENDIX B

Trend Analysis Result

Mann Kendall test result for Monthly Sum and Monthly Mean at Bukit Berapit and Permatang Rawa (10 years)

```
> mk.test(Rainfall_Data$`SUM (BB)`)

        Mann-Kendall trend test

data:  Rainfall_Data$`SUM (BB)`
z = -1.3203, n = 128, p-value = 0.1867
alternative hypothesis: true S is not equal to 0
sample estimates:
            S          varS           tau
-6.420000e+02  2.357080e+05 -7.900566e-02

> mk.test(Rainfall_Data$`SUM (PR)`)

        Mann-Kendall trend test

data:  Rainfall_Data$`SUM (PR)`
z = -0.57673, n = 128, p-value = 0.5641
alternative hypothesis: true S is not equal to 0
sample estimates:
            S          varS           tau
-2.810000e+02  2.357050e+05 -3.458675e-02
```

```
> mk.test(Rainfall_Data$`MEAN (BB)`)

        Mann-Kendall trend test

data:  Rainfall_Data$`MEAN (BB)`
z = -1.5902, n = 128, p-value = 0.1118
alternative hypothesis: true S is not equal to 0
sample estimates:
            S          varS           tau
-7.730000e+02  2.356943e+05 -9.520296e-02

> mk.test(Rainfall_Data$`MEAN (PR)`)

        Mann-Kendall trend test

data:  Rainfall_Data$`MEAN (PR)`
z = -0.54583, n = 128, p-value = 0.5852
alternative hypothesis: true S is not equal to 0
sample estimates:
            S          varS           tau
-2.660000e+02  2.357060e+05 -3.273846e-02
```

Sen's Slope estimator result for Monthly Sum and Monthly Mean at Bukit Berapit and Permatang Rawa (10 years)

```
> sens.slope(Rainfall_Data$`SUM (BB)`)

        Sen's slope

data:  Rainfall_Data$`SUM (BB)`
z = -1.3203, n = 128, p-value = 0.1867
alternative hypothesis: true z is not equal to 0
95 percent confidence interval:
 -0.9857143  0.1820000
sample estimates:
Sen's slope
 -0.3690476

> sens.slope(Rainfall_Data$`SUM (PR)`)

        Sen's slope

data:  Rainfall_Data$`SUM (PR)`
z = -0.57673, n = 128, p-value = 0.5641
alternative hypothesis: true z is not equal to 0
95 percent confidence interval:
 -0.7625000  0.3716049
sample estimates:
Sen's slope
 -0.1673333
```

```
> sens.slope(Rainfall_Data$`MEAN (BB)`)

        Sen's slope

data:  Rainfall_Data$`MEAN (BB)`
z = -1.5902, n = 128, p-value = 0.1118
alternative hypothesis: true z is not equal to 0
95 percent confidence interval:
 -0.036250000  0.002619048
sample estimates:
Sen's slope
-0.01573214

> sens.slope(Rainfall_Data$`MEAN (PR)`)

        Sen's slope

data:  Rainfall_Data$`MEAN (PR)`
z = -0.54583, n = 128, p-value = 0.5852
alternative hypothesis: true z is not equal to 0
95 percent confidence interval:
 -0.02400000  0.01243243
sample estimates:
 Sen's slope
-0.005240942
```

Mann Kendall test result for Monthly Sum and Monthly Mean at Bukit Berapit and Permatang Rawa (NEM)

```
> library(trend)
> mk.test(Rainfall_Data$`NEM (BB) SUM`)

        Mann-Kendall trend test

data:  Rainfall_Data$`NEM (BB) SUM`
z = -0.73729, n = 42, p-value = 0.4609
alternative hypothesis: true S is not equal to 0
sample estimates:
           S         varS          tau
 -69.0000000 8506.3333333   -0.0805143

> mk.test(Rainfall_Data$`NEM (PR) SUM`)

        Mann-Kendall trend test

data:  Rainfall_Data$`NEM (PR) SUM`
z = -0.3468, n = 42, p-value = 0.7287
alternative hypothesis: true S is not equal to 0
sample estimates:
            S          varS           tau
 -33.00000000 8514.33333333   -0.03832753
```


```
> library(trend)
> mk.test(Rainfall_Data$`NEM (BB) SUM`)

        Mann-Kendall trend test

data:  Rainfall_Data$`NEM (BB) SUM`
z = -0.73729, n = 42, p-value = 0.4609
alternative hypothesis: true S is not equal to 0
sample estimates:
           S         varS          tau
 -69.0000000 8506.3333333   -0.0805143

> mk.test(Rainfall_Data$`NEM (PR) SUM`)

        Mann-Kendall trend test

data:  Rainfall_Data$`NEM (PR) SUM`
z = -0.3468, n = 42, p-value = 0.7287
alternative hypothesis: true S is not equal to 0
sample estimates:
            S          varS           tau
 -33.00000000 8514.33333333   -0.03832753
```


Sen's Slope estimator result for Monthly Sum and Monthly Mean at Bukit Berapit and Permatang Rawa (NEM)

```
> sens.slope(Rainfall_Data$`NEM (BB) SUM`)

        Sen's slope

data:  Rainfall_Data$`NEM (BB) SUM`
z = -0.73729, n = 42, p-value = 0.4609
alternative hypothesis: true z is not equal to 0
95 percent confidence interval:
 -4.625  1.975
sample estimates:
Sen's slope
    -1.1875

> sens.slope(Rainfall_Data$`NEM (PR) SUM`)

        Sen's slope

data:  Rainfall_Data$`NEM (PR) SUM`
z = -0.3468, n = 42, p-value = 0.7287
alternative hypothesis: true z is not equal to 0
95 percent confidence interval:
 -3.883333  2.287097
sample estimates:
Sen's slope
 -0.9130435
```

```
> sens.slope(Rainfall_Data$`NEM (BB) MEAN`)

        Sen's slope

data:  Rainfall_Data$`NEM (BB) MEAN`
z = -0.71527, n = 42, p-value = 0.4744
alternative hypothesis: true z is not equal to 0
95 percent confidence interval:
 -0.1812  0.0620
sample estimates:
Sen's slope
  -0.049375

> sens.slope(Rainfall_Data$`NEM (PR) MEAN`)

        Sen's slope

data:  Rainfall_Data$`NEM (PR) MEAN`
z = -0.32512, n = 42, p-value = 0.7451
alternative hypothesis: true z is not equal to 0
95 percent confidence interval:
 -0.13029412  0.07428571
sample estimates:
Sen's slope
   -0.02375
```

Mann Kendall test result for Monthly Sum and Monthly Mean at Bukit Berapit and Permatang Rawa (SWM)

```
> mk.test(Rainfall_Data$`SWM (BB) SUM`)

        Mann-Kendall trend test

data:  Rainfall_Data$`SWM (BB) SUM`
z = -1.2138, n = 44, p-value = 0.2248
alternative hypothesis: true S is not equal to 0
sample estimates:
           S         varS          tau
-121.0000000 9774.3333333   -0.1279746

> mk.test(Rainfall_Data$`SWM (PR) SUM`)

        Mann-Kendall trend test

data:  Rainfall_Data$`SWM (PR) SUM`
z = -0.18207, n = 44, p-value = 0.8555
alternative hypothesis: true S is not equal to 0
sample estimates:
            S          varS           tau
 -19.00000000 9774.33333333   -0.02009519
```

```
> mk.test(Rainfall_Data$`SWM (BB) MEAN`)

        Mann-Kendall trend test

data:  Rainfall_Data$`SWM (BB) MEAN`
z = -2.1448, n = 44, p-value = 0.03197
alternative hypothesis: true S is not equal to 0
sample estimates:
          S        varS         tau
-213.000000 9770.333333   -0.225756

> mk.test(Rainfall_Data$`SWM (PR) MEAN`)

        Mann-Kendall trend test

data:  Rainfall_Data$`SWM (PR) MEAN`
z = -0.21242, n = 44, p-value = 0.8318
alternative hypothesis: true S is not equal to 0
sample estimates:
            S          varS           tau
 -22.00000000 9773.33333333   -0.02328044
```

Sen's Slope estimator result for Monthly Sum and Monthly Mean at Bukit Berapit and Permatang Rawa (SWM)

```
> sens.slope(Rainfall_Data$`SWM (BB) SUM`)

        Sen's slope

data:  Rainfall_Data$`SWM (BB) SUM`
z = -1.2138, n = 44, p-value = 0.2248
alternative hypothesis: true z is not equal to 0
95 percent confidence interval:
 -3.2800000  0.7529412
sample estimates:
Sen's slope
  -1.253934

> sens.slope(Rainfall_Data$`SWM (PR) SUM`)

        Sen's slope

data:  Rainfall_Data$`SWM (PR) SUM`
z = -0.18207, n = 44, p-value = 0.8555
alternative hypothesis: true z is not equal to 0
95 percent confidence interval:
 -2.503256  1.288889
sample estimates:
Sen's slope
    -0.1975
```

```
> sens.slope(Rainfall_Data$`SWM (BB) MEAN`)

        Sen's slope

data:  Rainfall_Data$`SWM (BB) MEAN`
z = -2.1448, n = 44, p-value = 0.03197
alternative hypothesis: true z is not equal to 0
95 percent confidence interval:
 -0.1300 -0.0025
sample estimates:
Sen's slope
      -0.07

> sens.slope(Rainfall_Data$`SWM (PR) MEAN`)

        Sen's slope

data:  Rainfall_Data$`SWM (PR) MEAN`
z = -0.21242, n = 44, p-value = 0.8318
alternative hypothesis: true z is not equal to 0
95 percent confidence interval:
 -0.07960000  0.04166667
sample estimates:
 Sen's slope
-0.005333333
```

Mann Kendall test result for Monthly Sum and Monthly Mean at Bukit Berapit and Permatang Rawa (IM1)

```
> mk.test(Rainfall_Data$`INTER1 (BB) SUM`)

        Mann-Kendall trend test

data:  Rainfall_Data$`INTER1 (BB) SUM`
z = -2.1738, n = 20, p-value = 0.02972
alternative hypothesis: true S is not equal to 0
sample estimates:
          S        varS         tau
-68.0000000 950.0000000  -0.3578947

> mk.test(Rainfall_Data$`INTER1 (PR) SUM`)

        Mann-Kendall trend test

data:  Rainfall_Data$`INTER1 (PR) SUM`
z = -2.7578, n = 20, p-value = 0.00582
alternative hypothesis: true S is not equal to 0
sample estimates:
          S        varS         tau
-86.0000000 950.0000000  -0.4526316
```

```
> mk.test(Rainfall_Data$`INTER1 (BB) MEAN`)

        Mann-Kendall trend test

data:  Rainfall_Data$`INTER1 (BB) MEAN`
z = -2.1738, n = 20, p-value = 0.02972
alternative hypothesis: true S is not equal to 0
sample estimates:
          S        varS         tau
-68.0000000 950.0000000  -0.3578947

> mk.test(Rainfall_Data$`INTER1 (PR) MEAN`)

        Mann-Kendall trend test

data:  Rainfall_Data$`INTER1 (PR) MEAN`
z = -2.7578, n = 20, p-value = 0.00582
alternative hypothesis: true S is not equal to 0
sample estimates:
          S        varS         tau
-86.0000000 950.0000000  -0.4526316
```

Sen's Slope estimator result for Monthly Sum and Monthly Mean at Bukit Berapit and Permatang Rawa (IM1)

```
> sens.slope(Rainfall_Data$`INTER1 (BB) SUM`)

        Sen's slope

data:  Rainfall_Data$`INTER1 (BB) SUM`
z = -2.1738, n = 20, p-value = 0.02972
alternative hypothesis: true z is not equal to 0
95 percent confidence interval:
 -18.4928571  -0.8833333
sample estimates:
Sen's slope
  -8.616667

> sens.slope(Rainfall_Data$`INTER1 (PR) SUM`)

        Sen's slope

data:  Rainfall_Data$`INTER1 (PR) SUM`
z = -2.7578, n = 20, p-value = 0.00582
alternative hypothesis: true z is not equal to 0
95 percent confidence interval:
 -17.008333  -4.644444
sample estimates:
Sen's slope
  -11.19881
```

```
> sens.slope(Rainfall_Data$`INTER1 (BB) MEAN`)

        Sen's slope

data:  Rainfall_Data$`INTER1 (BB) MEAN`
z = -2.1738, n = 20, p-value = 0.02972
alternative hypothesis: true z is not equal to 0
95 percent confidence interval:
 -0.6164286 -0.0300000
sample estimates:
Sen's slope
 -0.2814286

> sens.slope(Rainfall_Data$`INTER1 (PR) MEAN`)

        Sen's slope

data:  Rainfall_Data$`INTER1 (PR) MEAN`
z = -2.7578, n = 20, p-value = 0.00582
alternative hypothesis: true z is not equal to 0
95 percent confidence interval:
 -0.5675000 -0.1455556
sample estimates:
Sen's slope
 -0.3547768
```

Mann Kendall test result for Monthly Sum and Monthly Mean at Bukit Berapit and Permatang Rawa (IM2)

```
> mk.test(Rainfall_Data$`INTER2 (BB) SUM`)

        Mann-Kendall trend test

data:  Rainfall_Data$`INTER2 (BB) SUM`
z = 0.50756, n = 22, p-value = 0.6118
alternative hypothesis: true S is not equal to 0
sample estimates:
           S         varS          tau
1.900000e+01 1.257667e+03 8.225108e-02

> mk.test(Rainfall_Data$`INTER2 (PR) SUM`)

        Mann-Kendall trend test

data:  Rainfall_Data$`INTER2 (PR) SUM`
z = 1.1279, n = 22, p-value = 0.2594
alternative hypothesis: true S is not equal to 0
sample estimates:
           S         varS          tau
  41.0000000 1257.6666667    0.1774892
```

```
> mk.test(Rainfall_Data$`INTER2 (BB) MEAN`)

        Mann-Kendall trend test

data:  Rainfall_Data$`INTER2 (BB) MEAN`
z = 0.56396, n = 22, p-value = 0.5728
alternative hypothesis: true S is not equal to 0
sample estimates:
           S         varS          tau
2.100000e+01 1.257667e+03 9.090909e-02

> mk.test(Rainfall_Data$`INTER2 (PR) MEAN`)

        Mann-Kendall trend test

data:  Rainfall_Data$`INTER2 (PR) MEAN`
z = 1.1279, n = 22, p-value = 0.2594
alternative hypothesis: true S is not equal to 0
sample estimates:
           S         varS          tau
  41.0000000 1257.6666667    0.1774892
```

Sen's Slope estimator result for Monthly Sum and Monthly Mean at Bukit Berapit and Permatang Rawa (IM2)

```
> sens.slope(Rainfall_Data$`INTER2 (BB) SUM`)

        Sen's slope

data:  Rainfall_Data$`INTER2 (BB) SUM`
z = 0.50756, n = 22, p-value = 0.6118
alternative hypothesis: true z is not equal to 0
95 percent confidence interval:
 -5.433333  9.392308
sample estimates:
Sen's slope
   2.166667

> sens.slope(Rainfall_Data$`INTER2 (PR) SUM`)

        Sen's slope

data:  Rainfall_Data$`INTER2 (PR) SUM`
z = 1.1279, n = 22, p-value = 0.2594
alternative hypothesis: true z is not equal to 0
95 percent confidence interval:
 -4.076923 12.063636
sample estimates:
Sen's slope
       4.14
```

```
> sens.slope(Rainfall_Data$`INTER2 (BB) MEAN`)

        Sen's slope

data:  Rainfall_Data$`INTER2 (BB) MEAN`
z = 0.56396, n = 22, p-value = 0.5728
alternative hypothesis: true z is not equal to 0
95 percent confidence interval:
 -0.1816667  0.3093333
sample estimates:
Sen's slope
       0.07

> sens.slope(Rainfall_Data$`INTER2 (PR) MEAN`)

        Sen's slope

data:  Rainfall_Data$`INTER2 (PR) MEAN`
z = 1.1279, n = 22, p-value = 0.2594
alternative hypothesis: true z is not equal to 0
95 percent confidence interval:
 -0.13125  0.38400
sample estimates:
Sen's slope
  0.1278947
```

AUTHOR'S PROFILE



Muhammad Fahmi Bin Muhammad Iskandar completed his MSc in Civil Engineering at the Faculty of Civil Engineering, Universiti Teknologi MARA. He received his MSc. in Civil Engineering at the Faculty of Civil Engineering, Universiti Teknologi MARA. He was a research assistant for NAHRIM funded project from 2024-2026.

LIST OF PUBLICATIONS

Fahmi, M., Iskandar, M., Ibrahim, A., Mohtar, Z. A., Faizal, M., Mohamed, P., & Yahaya, N. K. E. M. (2025). *Assessing rainfall trends and variability in a climate change*. https://doi.org/10.24191/esteem.v21iMarch.4892.g